Multiple point interactions in lattice gas models far from equilibrium

Dissertation

zur

Erlangung des Doktorgrades (Dr. rer. nat.)

der

Mathematisch-Naturwissenschaftlichen Fakultät

der

Rheinischen Friedrich-Wilhelms-Universität Bonn

vorgelegt

von

Matthias Paeßens

aus

Moers

2004

Anfertigung mit Genehmigung der Mathematisch-Naturwissenschaftlichen Fakultät der Rheinischen Friedrich-Wilhelms-Universität Bonn.

1. Referent: PD Dr. G. M. Schütz
2. Referent: Prof. Dr. U.–G. Meißner

Tag der Promotion:

Contents

1 Introduction **3**
- 1.1 Models far from equilibrium 4
- 1.2 Outline 6

2 Kinetic spherical model **8**
- 2.1 Introduction 9
- 2.2 Model and formalism 12
- 2.3 Spherical model in a magnetic field 15
  - 2.3.1 Solution of the constraint 16
  - 2.3.2 Single-time observables 18
  - 2.3.3 Two-time observables 22
- 2.4 Scaling of the linear response 25
  - 2.4.1 Crossover of the thermoremanent magnetization 26
  - 2.4.2 Scaling of the susceptibility 29
- 2.5 Dynamics in an oscillating field 36
  - 2.5.1 Behavior of the magnetization 37
  - 2.5.2 Behavior of the Lagrange multiplier 40
- 2.6 Conclusions 43
- 2.7 Appendix: Numerical method 46

3 Bosonic PCPD **48**
- 3.1 Introduction 49
- 3.2 Model 51
- 3.3 Contact process with diffusion, $m = 1$ 54
- 3.4 Pair contact process with diffusion, $m = 2$ 55
- 3.5 Spatial correlations 60
- 3.6 Phase transitions of the 3^{rd} moment 62
- 3.7 Activity spreading 64
  - 3.7.1 Analytical calculation 65
  - 3.7.2 Hyperscaling relation 68
- 3.8 Conclusions 76

3.9 Appendix: Calculation of the spatial dependence 77

4 Hysteresis in driven diffusive systems **83**
4.1 Introduction 84
4.1.1 Driven diffusive systems 85
4.1.2 Coupling to a bulk reservoir 87
4.2 Method 88
4.3 Criterion for ergodicity breaking 90
4.4 Model 92
4.5 Phase diagram 94
4.6 First passage times 98
4.7 Simulations 99
4.7.1 Hysteresis 101
4.7.2 Random transitions 102
4.8 Conclusions 104

5 Reaction fronts **106**
5.1 Introduction 107
5.2 Formalism 109
5.3 Product– and shock–measures 110
5.4 Classification of models 113
5.4.1 Shocks from $\rho_1 = 0$ to $\rho_2 = 1$ 114
5.4.2 Shocks from $\rho_1 \in (0;1)$ to $\rho_2 \in (0;1)$ 114
5.4.3 Shocks from $\rho_1 = 0$ to $\rho_2 \in (0;1)$ 116
5.5 Reactions of domain walls 121
5.6 Conclusions 125
5.7 Appendix: $P \wedge T$ models 126

Summary / Zusammenfassung **142**

Chapter 1

Introduction

1.1 Models far from equilibrium

In this work non–equilibrium phenomena are examined in statistical models with more than nearest neighbor interactions. Investigating non–equilibrium systems is a current problem in recent research. Although many systems tend toward equilibrium one should bring to mind that the most prominent phenomena are based on non–equilibrium dynamics. As an example taken from everyday life one may consider what is colloquially called energy "consumption", a term which originates from the irreversibility of the processes. Another example are all mechanisms including any kind of a net transport which is absent in an equilibrium system. Lastly, well–known in statistical physics, it should be mentioned that a phase–transition in one–dimensional systems is solely possible far from equilibrium.

For treating equilibrium systems a general concept has established – the minimal principle of the free energy, whereas for non–equilibrium systems a universal method still lacks. For some subareas solution techniques have been developed but a generally valid principle could not be found up to now.

This constitutes the importance of model systems. As they are definitively simpler and easier to control than real systems, it might be possible to determine what are the underlying mechanisms leading to the observed phenomena. Exactly solvable models are of special interest as one is able to extract the mathematical origins and is additionally not faced with the problems of numerical inaccuracy. Unfortunately exact solutions are more the exception than the rule and thus although this work is focused on exact calculations in some cases numerical methods have to be used. One should of course not lose manifest reality out of sight, but the purpose of this work is to understand qualitatively the principles rather than to reproduce empirical observations on a quantitative level. although some of the models to be presented in what follows might be considered for explaining experiments, their interest here is on a much more basic level.

There are three different situations of systems out of equilibrium. First there are systems which possess an equilibrium state in general, but they are prepared in a non–equilibrium initial state such that the system will tend to relax to equilibrium. Under certain conditions however the relaxation times diverge and equilibrium is never reached. A typical example is a magnetic system after a quench from the disordered phase to a temperature below the Curie point. One then observes a time dependence of measured quantities, this is the so called aging. Second the existence of absorbing states, i.e. states for which transitions into but not out of them are possible, prohibits the possibility of equilibrium in an other class of systems. These are described in the theory of absorbing phase transitions which among other things roots

in the investigations of epidemic spreading. Third there are systems which do not have an equilibrium state at all – for all times a net current is present, which violates the condition of detailed balance for equilibrium systems. This can be observed in heat conduction problems between reservoirs of different temperatures. Typical model systems of this class are driven lattice gases where the particles have an intrinsic hopping bias.

The most prominent models of these three categories are nearest neighbor interaction models. The magnetic model par excellence is the Ising model where only nearest neighbor spins interact. In the theory of absorbing phase transitions a widely investigated model is the contact process whose kinetics comprises two lattice sites. The simplest driven diffusive system is the asymmetric exclusion process where particles are hopping by only one lattice site.

The scope of this work is the investigation of models with a larger range of interactions. Various models are considered: The spherical model, a model for magnetism, where a constraint results in an effective long ranged interaction. In this model temperature quenches in the presence of an external magnetic field are investigated. In the bosonic pair contact process with diffusion, a diffusive system with three point interaction reaction kinetics, absorbing phase transitions are examined. While in this system no constraint for the particle number on a lattice site is present, also exclusion models are used where each lattice site may be occupied by at most one particle. One of these models is the totally asymmetric exclusion process equipped with a non–conservative three point reaction kinetics for which ergodicity breaking and hysteresis are demonstrated. And finally for reaction diffusion systems with an exclusion rule the emergence of sharp domain walls is investigated in the most general case of three point interactions.

Although the origins of these models are different, their investigations show more parallels than might be expected on first sight. Interestingly it is particularly the spherical model – the only model considered here which is not a lattice gas – which is linked to each of the other models by certain means. First, although the link to the bosonic pair contact process is least apparent, it turns out that both systems can be treated by the same formalism and that even a phase transition in the bosonic pair contact process with diffusion follows exactly the dynamics of the one observed in the spherical model. Thus the link between the two model is of rather technical nature, in contrast to, second, the link to the totally asymmetric exclusion process equipped with reaction kinetics which is on a phenomenologically level: Hysteresis is a phenomenon exemplary for magnetism and it is directly connected to the problem of reversal dynamics also investigated for the spherical model. In this context the investigation of shocks has to be seen as it is known that

reversal dynamics and aging are based on the phenomenon of domain growth. The movements of shocks in driven lattice gases is put in this part onto a more general basis. Thus we see that in spite of the different nature of the models a more or less comprehensive connection exists.

1.2 Outline

The outline of this work is as follows. In chapter 2 the kinetic mean spherical model with an external magnetic field is investigated. After giving a general introduction into the problem of aging the definition of the spherical model is recalled. The exact solution of the problem is presented by establishing an integral equation which contains all the information needed for describing the system completely. It is then applied to the magnetization reversal transition from a metastable state to equilibrium. The behavior of the linear response function is also discussed in detail. Finally the behavior of the system in an oscillating external field is examined and the question addressed whether there exists a dynamical phase transition in the kinetic spherical model. The work presented in this chapter was done in collaboration with M. Henkel and M. Pleimling, the results are published in Refs. [1, 2, 3].

In chapter 3 the variance of the bosonic pair contact process with diffusion is calculated. To this end partial differential equations resulting from the bosonic description of this problem are solved. It is shown that for appropriate parameters the correlation function shows a phase transition leading to unusual behavior of the system. Both the temporal and the spatial dependence of the correlation function are calculated exactly. It is shown that also the 3^{rd} moment of the probability distribution exhibits a phase transition. As at least some of the critical exponents can be determined exactly a hyperscaling relation can be tested. To this end additional information is needed which is extracted from numerical simulations. Parts of the results presented in this chapter are published in Ref. [4].

In chapter 4 ergodicity breaking and hysteresis in a one–dimensional reaction diffusion system are demonstrated. The general necessary conditions for observing this phenomenon are derived and then used to build up a system as an example. For this system, the asymmetric exclusion process coupled to non–conserving reaction kinetics, the exact phase diagram is calculated showing five distinct phases. The underlying dynamical mode is revealed, i.e. an equilibrium random walker in a space dependent potential which reduces the originally many particle model to an effective one particle problem. Monte Carlo simulations are used to confirm this picture and to illustrate the phenomenon of hysteresis. The work of this chapter was done in collaboration

with A. Rákos and the results are published in Ref. [5].

Finally in chapter 5 the movement of reaction fronts in reaction diffusion systems is addressed. For this purpose it is investigated which three point interaction models show exact shock measures. It is shown that these models give rise to aspects not seen in nearest neighbor models, like double shocks or additional symmetries. A general solution of the problem can not be given as the number of degrees of freedom is too large. Instead a complete classification of the systems by their symmetries is given. The link of domain wall motion and a free fermion description is also discussed.

Chapter 2

Kinetic spherical model

2.1 Introduction

In this chapter aging in a specific magnetic system, the kinetic spherical model in a magnetic field, is investigated. This work was done in collaboration with Malte Henkel and Michel Pleimling. The results are published in Ref. [1, 2, 3].

Aging is a non–equilibrium phenomenon which in general is defined by the fact that two–time quantities depend on both times instead of only the time difference. Assume that the correlation $C(t, t+\tau)$ of a quantity at time t and $t+\tau$ is calculated. In equilibrium we expect $C(t, t+\tau) \equiv C(\tau)$ while in a system which undergoes aging the correlation function will always depend as well on t, i.e. the *age* of the system plays a role.

Aging was first investigated in glassy systems, for a review see Ref. [6]. The glassy state is reached by under-cooling a liquid by a temperature quench from a high temperature T_1 to a temperature T_2 below the melting temperature $T_m > T_2$. If the liquid is cooled down slowly the system is able to equilibrate for each temperature and will end up in the equilibrium state at T_2, the crystal. But as the viscosity of the system strongly depends on the temperature – variations of 10 orders of magnitude are possible – the dynamics slow down and the relaxation times increase considerably. The time scales the system needs to reach equilibrium can occur to be much larger than accessible in experiments. An example taken from every day life is the glass used in windows – although the system is not in the equilibrium state the transition to equilibrium takes several hundred years. In theoretical models for glassy systems, like the spin–glasses, the transition times diverge with system size, thus equilibrium is never reached.

In a magnetic system aging is observed when it is quenched from a high temperature T_1 above the critical temperature T_c to a temperature $T_2 < T_c$. At T_1 the equilibrium state is a disordered one, i.e. correlations persist only on small scales, and the net magnetization is zero. At T_2 below the critical temperature there exist two equilibrium states corresponding to positive and negative net magnetization, i.e. symmetry is broken. Thus after a quench the system is in an unstable state and it tends to reach an equilibrium state. The transition to equilibrium takes place by phase–ordering kinetics; domains of a time–dependent typical size $L(t) \sim t^{1/z}$ form and grow, where z is the dynamical exponent. In a mean–field investigation of phase–ordering kinetics one generally finds $z = 2$ for non–conserved order parameters and $z = 3$ for conserved order parameters [7]. Consequently the transition time to equilibrium is $\tau \propto L_0^z$ (L_0 is the edge length of the system) which is the time needed for a cluster to span the whole system. It diverges for systems of infinite size and thus the system remains out of equilibrium.

Another way to prepare a system in a non–equilibrium state is to start from a magnetically ordered state below T_c and then turn on a magnetic field H oriented anti-parallel with respect to the magnetic order parameter. Then the system will find itself in a metastable state and a magnetization reversal transition toward the stable ground state will take place.

The effect of aging is revealed through the study of *two-time* quantities, such as the two-time autocorrelation function $C(t,s)$ and the autoresponse function $R(t,s)$

$$C(t,s) = \langle \phi(t)\phi(s) \rangle \quad , \quad R(t,s) = \left. \frac{\delta \langle \phi(t) \rangle}{\delta h(s)} \right|_{h=0} \tag{2.1}$$

where ϕ is the order parameter, h the conjugate magnetic field, t is called the observation time and s the waiting time. Aging occurs in the regime when s and $\tau = t - s > 0$ are simultaneously much larger than any microscopic time scale $\tau_{\rm micro}$. In many systems, one finds in the aging regime a scaling behavior, see Refs. [8, 9]

$$C(t,s) = s^{-b} f_C(t/s) \quad , \quad R(t,s) = s^{-1-a} f_R(t/s) \tag{2.2}$$

where a and b are non-equilibrium exponents. For $T < T_c$, $b = 0$ while a depends on whether there are short-ranged or long-ranged correlations in the equilibrium state. For short-ranged correlations, $a = 1/z$, whereas for long-ranged correlations $a = (d - 2 + \eta)/z$ [2]. The scaling functions behave for large arguments $x = t/s \gg 1$ asymptotically as

$$f_C(x) \sim x^{-\lambda_C/z} \quad , \quad f_R(x) \sim x^{-\lambda_R/z} \tag{2.3}$$

where λ_C and λ_R are the autocorrelation [10, 11] and autoresponse [12] exponents, respectively. For the usually studied case of an initial state without long–range correlations, it is generally accepted that $\lambda_C = \lambda_R = \lambda$. Combinations of rigorous results and of heuristic scaling arguments were used to derive the bounds $d/2 \leq \lambda \lesssim d$ [10, 13].

It has been proposed recently that one might be able to go beyond mere dynamical scale invariance as expressed by eq. (2.2) to a group of *local* scale transformations related to conformal transformations in time [14]. If that hypothesis applies, the form of the scaling function

$$f_R(x) = r_0 \, x^{1+a-\lambda_R/z} (x-1)^{-1-a} \tag{2.4}$$

is completely fixed (r_0 is a normalization constant). Eq. (2.4) has been confirmed in several models, especially, through extensive simulations, in the $2D$ and $3D$ Glauber-Ising models [15].

Another central questions in this context is how to characterize when under the conditions just described the system reaches thermodynamic equilibrium. It is convenient to consider the fluctuation-dissipation ratio [16, 17]

$$X(t,s) = TR(t,s)\left(\frac{\partial C(t,s)}{\partial s}\right)^{-1}. \tag{2.5}$$

At equilibrium, the fluctuation-dissipation theorem states that $X(t,s) = 1$. The breaking of the fluctuation-dissipation theorem has been investigated intensively both theoretically (see e.g. Refs. [6, 8, 9, 18, 19]) and experimentally [20, 21, 22].

The spherical model is one of the very few models which can be solved exactly in a great variety of circumstances and has been studied in detail in the past, either in the context of continuum field theories [23, 24, 25, 26, 27, 28, 29, 30, 31, 32] or else in the form of a lattice model [12, 33, 34, 35, 36, 37, 38, 39]. It is known that in $d < 4$ dimensions, the spherical model yields results distinct from mean–field theory and therefore permits the study of fluctuation effects. In addition, recall that experimental results of the magnetization reversal [40, 41] are usually described in terms of an anisotropic Heisenberg model. The spherical model shares the following *equilibrium* properties with the O(3) Heisenberg model and which distinguishes it from the often-used Ising model:

- it has a continuous symmetry (O(n) in the $n \to \infty$ limit),
- there is no equilibrium phase-transition in $2D$,
- the equilibrium specific heat exponent $\alpha < 0$ in $3D$.

These similarities might suggest that qualitatively the kinetics of spherical and the O(3) Heisenberg models should be closer to each other than either is to the kinetics of the Ising model. Still, the spherical model should be considered a toy model certainly not meant to be physically realistic.

This chapter is organized as follows. In section 2.2 the model is defined and the exact solution outlined. In section 2.3 the magnetization reversal transition from the metastable to the equilibrium state is investigated. In section 2.4 the scaling of the linear response function will be investigated in detail. It is argued that extracting information from integrated response has to be done carefully. In section 2.5 the time dependent response to an oscillating magnetic field is addressed and it is studied whether there exists a dynamic phase transition at a finite and non vanishing value of the period of the field.

2.2 Model and formalism

Here, the definition of the kinetic mean spherical model is recalled, using the formalism as exposed in Refs. [12, 34, 35, 37]. Consider a system of time-dependent classical spin variables $S_{\boldsymbol{x}}(t)$ located on the sites $\boldsymbol{x}$ of a d-dimensional hypercubic lattice. They may take arbitrary real values subject only to the mean spherical constraint

$$\sum_{\boldsymbol{x}} \left\langle S_{\boldsymbol{x}}(t)^2 \right\rangle = \mathcal{N} \tag{2.6}$$

where $\mathcal{N}$ is the number of sites of the lattice. The role of imposing the spherical constraint either microscopically or rather in the mean (which is the only case where the dynamics can be solved) has been carefully studied recently [32]. Provided the infinite-volume limit is taken *before* the long-time limit, either way of treating the spherical constraint leads to the same results.

The spherical model Hamiltonian reads

$$\mathcal{H} = -J \sum_{<\boldsymbol{x},\boldsymbol{y}>} S_{\boldsymbol{x}}(t) S_{\boldsymbol{y}}(t) - \sum_{\boldsymbol{x}} H_{\boldsymbol{x}}(t) S_{\boldsymbol{x}}(t) \tag{2.7}$$

where $H_{\boldsymbol{x}}(t)$ is the space- and time-dependent external magnetic field. The first sum extends over nearest-neighbor pairs only and the second sum over the entire lattice. Units are chosen such that $J = 1$. The system is supposed to be translation-invariant in all directions. The kinetics is assumed to be described in terms of a Langevin equation

$$\frac{\mathrm{d}S_{\boldsymbol{x}}(t)}{\mathrm{d}t} = \sum_{\boldsymbol{y}(\boldsymbol{x})} S_{\boldsymbol{y}}(t) - (2d + \mathfrak{z}(t)) S_{\boldsymbol{x}}(t) + H_{\boldsymbol{x}}(t) + \eta_{\boldsymbol{x}}(t) \tag{2.8}$$

where the sum over $\boldsymbol{y}$ extends over the nearest neighbors of $\boldsymbol{x}$. The Gaussian noise $\eta_{\boldsymbol{x}}(t)$ describes that the model is in contact with a heat bath. It is characterized by a vanishing ensemble-average and the second moment

$$\langle \eta_{\boldsymbol{x}}(t) \eta_{\boldsymbol{y}}(t') \rangle = 2T \, \delta_{\boldsymbol{x},\boldsymbol{y}} \delta(t - t'). \tag{2.9}$$

Finally, the function $\mathfrak{z}(t)$ is fixed by the mean spherical constraint (2.6) and has to be determined.

By a Fourier transformation

$$\widetilde{f}(\boldsymbol{q}) = \sum_{\boldsymbol{r}} f_{\boldsymbol{r}} e^{-\mathrm{i}\boldsymbol{q}\cdot\boldsymbol{r}} \quad , \quad f_{\boldsymbol{r}} = (2\pi)^{-d} \int_{\mathcal{B}} \mathrm{d}\boldsymbol{q} \, \widetilde{f}(\boldsymbol{q}) e^{\mathrm{i}\boldsymbol{q}\cdot\boldsymbol{r}} \tag{2.10}$$

where the integral is taken over the first Brillouin zone $\mathcal{B}$, the Fourier-transformed spin variable $\widetilde{S}(\boldsymbol{q},t)$ becomes

$$\widetilde{S}(\boldsymbol{q},t)=\frac{e^{-\omega(\boldsymbol{q})t}}{\sqrt{g(t)}}\left[\widetilde{S}(\boldsymbol{q},0)+\int_0^t \mathrm{d}t'\; e^{\omega(\boldsymbol{q})t'}\sqrt{g(t')}\;\left[\widetilde{H}(\boldsymbol{q},t')+\widetilde{\eta}(\boldsymbol{q},t')\right]\right] \tag{2.11}$$

with the dispersion relation

$$\omega(\boldsymbol{q})=2\sum_{i=1}^{d}\left(1-\cos(q_i)\right) \tag{2.12}$$

and the definition

$$g(t)=\exp\left(2\int_0^t \mathrm{d}t'\;\mathfrak{z}(t')\right). \tag{2.13}$$

Clearly, the time-dependence of $\widetilde{S}(\boldsymbol{q},t)$ and any correlators will be given in terms of the function $g=g(t)$.

We now derive the expressions for the correlators and response functions for an arbitrary external field $H_{\boldsymbol{x}}(t)$ and general initial conditions. Consider the two-time spin-spin correlation function

$$\begin{aligned} C_{\boldsymbol{x},\boldsymbol{y}}(t,s) &= C_{\boldsymbol{x}-\boldsymbol{y}}(t,s)=\langle S_{\boldsymbol{x}}(t)S_{\boldsymbol{y}}(s)\rangle \\ &= (2\pi)^{-2d}\int_{\mathcal{B}^2}\mathrm{d}\boldsymbol{q}\,\mathrm{d}\boldsymbol{q}'\;e^{\mathrm{i}(\boldsymbol{q}\cdot\boldsymbol{x}+\boldsymbol{q}'\cdot\boldsymbol{y})}\;\langle\widetilde{S}(\boldsymbol{q},t)\widetilde{S}(\boldsymbol{q}',s)\rangle. \end{aligned} \tag{2.14}$$

A straightforward calculation gives

$$\begin{aligned} \widetilde{C}(\boldsymbol{q},\boldsymbol{q}';t,s) &= \langle\widetilde{S}(\boldsymbol{q},t)\widetilde{S}(\boldsymbol{q}',s)\rangle \\ &= \frac{e^{-\omega(\boldsymbol{q})t-\omega(\boldsymbol{q}')s}}{\sqrt{g(t)g(s)}}\times \\ &\quad\times\left[(2\pi)^d\delta^d(\boldsymbol{q}+\boldsymbol{q}')\left(\widetilde{C}(\boldsymbol{q},t)+2T\int_0^t \mathrm{d}t'\;e^{2\omega(\boldsymbol{q})t'}g(t')\right)\right. \\ &\quad+\langle\widetilde{S}(\boldsymbol{q}',0)\rangle\int_0^t \mathrm{d}t'\;e^{\omega(\boldsymbol{q})t'}\sqrt{g(t')}\;\widetilde{H}(\boldsymbol{q},t') \\ &\quad+\langle\widetilde{S}(\boldsymbol{q},0)\rangle\int_0^s \mathrm{d}s'\;e^{\omega(\boldsymbol{q}')s'}\sqrt{g(s')}\;\widetilde{H}(\boldsymbol{q}',s') \\ &\quad+\int_0^t \mathrm{d}t'\;e^{\omega(\boldsymbol{q})t'}\sqrt{g(t')}\;\widetilde{H}(\boldsymbol{q},t')\times \\ &\quad\left.\times\int_0^s \mathrm{d}s'\;e^{\omega(\boldsymbol{q}')s'}\sqrt{g(s')}\;\widetilde{H}(\boldsymbol{q}',s')\right] \end{aligned} \tag{2.15}$$

where $\widetilde{C}(\boldsymbol{q},t)$ is the single-time correlator. Here the average was carried out over the noise and the initial conditions $S_{\boldsymbol{x}}(0)$ such that

$$\langle \widetilde{S}(\boldsymbol{q},0)\rangle = \sum_{\boldsymbol{x}} \langle S_{\boldsymbol{x}}(0)\rangle e^{-\mathrm{i}\boldsymbol{q}\cdot\boldsymbol{x}} = (2\pi)^d \delta^d(\boldsymbol{q})\, S_0. \tag{2.16}$$

In direct space, the two-time autocorrelator becomes

$$\begin{aligned} C_{\boldsymbol{x},\boldsymbol{x}}(t,s) &= (2\pi)^{-2d} \int_{\mathcal{B}^2} \mathrm{d}\boldsymbol{q}\, \mathrm{d}\boldsymbol{q}'\, e^{\mathrm{i}(\boldsymbol{q}+\boldsymbol{q}')\cdot\boldsymbol{x}}\, \widetilde{C}(\boldsymbol{q},\boldsymbol{q}';t,s) \\ &= \frac{1}{\sqrt{g(t)g(s)}} \left[A\left(\frac{t+s}{2}\right) + 2T \int_0^s \mathrm{d}u\, f\left(\frac{t+s}{2}-u\right) g(u) \right. \\ &\quad + S_0 \int_0^t \mathrm{d}t' B_{\boldsymbol{x}}(t') \sqrt{g(t')} + S_0 \int_0^s \mathrm{d}s' B_{\boldsymbol{x}}(s') \sqrt{g(s')} \\ &\quad \left. + \int_0^t \mathrm{d}t' B_{\boldsymbol{x}}(t') \sqrt{g(t')} \int_0^s \mathrm{d}s' B_{\boldsymbol{x}}(s') \sqrt{g(s')} \right] \end{aligned} \tag{2.17}$$

with the definition

$$\begin{aligned} f(t) &= (2\pi)^{-d} \int_{\mathcal{B}} \mathrm{d}\boldsymbol{q}\, e^{-2\omega(\boldsymbol{q})t} = \left(e^{-4t} I_0(4t)\right)^d \\ A(t) &= (2\pi)^{-d} \int_{\mathcal{B}} \mathrm{d}\boldsymbol{q}\, e^{-2\omega(\boldsymbol{q})t}\, \widetilde{C}(\boldsymbol{q},0) \\ B_{\boldsymbol{x}}(t) &= (2\pi)^{-d} \int_{\mathcal{B}} \mathrm{d}\boldsymbol{q}\, e^{\omega(\boldsymbol{q})t + \mathrm{i}\boldsymbol{q}\cdot\boldsymbol{x}}\, \widetilde{H}(\boldsymbol{q},t) \end{aligned} \tag{2.18}$$

and I_0 is a modified Bessel function [42]. We see explicitly how the initial magnetization S_0 and the initial correlator $C_{\boldsymbol{x}}(0)$ affect the dynamics of the system.

It remains to determine the function $g(t)$. Because of the spherical constraint (2.7) and spatial translation invariance, the equal-time autocorrelator must satisfy

$$C_{\boldsymbol{0}}(t,t) = \int_{\mathcal{B}} \mathrm{d}\boldsymbol{q}\, \widetilde{C}(\boldsymbol{q},t) = \langle S_{\boldsymbol{x}}(t)^2\rangle = 1. \tag{2.19}$$

This in turn fixes $\mathfrak{z}(t)$ or via (2.13) the function $g(t)$ as the solution of a nonlinear Volterra integral equation

$$\begin{aligned} g(t) &= A(t) + 2T \int_0^t \mathrm{d}t'\, f(t-t') g(t') + 2S_0 \int_0^t \mathrm{d}t'\, B_{\boldsymbol{x}}(t') \sqrt{g(t')} \\ &\quad + \left(\int_0^t \mathrm{d}t'\, B_{\boldsymbol{x}}(t') \sqrt{g(t')} \right)^2 . \end{aligned} \tag{2.20}$$

For $S_0 = 0$ and $T = 0$, Eqs. (2.17,2.20) had been derived before for the spherical spin-glass [35]. Besides on time, $g(t)$ also depends on the temperature T and the initial conditions parametrized by S_0 and $C_{\boldsymbol{x}}(0)$.

The expressions for $A(t)$ and $B_{\boldsymbol{x}}(t)$ simplify in certain cases. For uncorrelated initial conditions

$$C_{\boldsymbol{x},\boldsymbol{y}}(0) = \left(1 - S_0^2\right) \delta_{\boldsymbol{x},\boldsymbol{y}} + S_0^2. \tag{2.21}$$

Then $\widetilde{C}(\boldsymbol{q}, 0) = 1 - S_0^2 + (2\pi)^d \delta^d(\boldsymbol{q}) S_0^2$ and

$$A(t) = \left(1 - S_0^2\right) f(t) + S_0^2. \tag{2.22}$$

For a spatially uniform magnetic field $H_{\boldsymbol{x}}(t) = H(t)$ we have

$$B_{\boldsymbol{x}}(t) = H(t). \tag{2.23}$$

These two conditions and consequently Eqs. (2.22,2.23) will be used throughout this chapter.

When $S_0 \neq 0$, it will be useful to consider besides $C(t, s)$ also the connected two-time autocorrelator (see Ref. [12] for an analogous situation in the $1D$ Glauber-Ising model)

$$\Gamma(t, s) = \langle S_{\boldsymbol{x}}(t) S_{\boldsymbol{x}}(s) \rangle - \langle S_{\boldsymbol{x}}(t) \rangle \langle S_{\boldsymbol{x}}(s) \rangle. \tag{2.24}$$

Finally, the response function is obtained in the usual way [12, 25, 26, 34, 35, 37] by considering the linear response to the magnetic field. It is easy to see that in Fourier space

$$\widetilde{R}(\boldsymbol{q}, t, s) = \left. \frac{\delta \langle \widetilde{S}(\boldsymbol{q}, t) \rangle}{\delta \widetilde{h}(\boldsymbol{q}, s)} \right|_{h_{\boldsymbol{r}} = 0} = e^{-\omega(\boldsymbol{q})(t-s)} \sqrt{\frac{g(s)}{g(t)}}. \tag{2.25}$$

From these expressions, the autocorrelation function $C(t, s) = C_{\boldsymbol{0}}(t, s)$ and the autoresponse function $R(t, s) = R_{\boldsymbol{0}}(t, s)$ can be obtained by integrating over the momentum $\boldsymbol{q}$.

Summarizing, the physically interesting correlation and response functions are given by Eqs. (2.17,2.24,2.25) together with the constraint Eq. (2.20). This constitutes the main result of the general formalism.

2.3 Spherical model in a magnetic field

The non–equilibrium behavior associated with the magnetization-reversal transition from the metastable to the equilibrium state is investigated. This

problem has also received intense attention, both experimentally (e.g. Refs. [40, 41, 43]) and theoretically, see Refs. [44, 45, 46, 47, 48, 49, 50].

Compared to the case without an external magnetic field, the solution of the equations is difficult since the underlying Volterra equation (2.20) is nonlinear. The mathematical theory of nonlinear Volterra equations is still being developed [51]. In a few cases, explicit analytic solutions can be found. Otherwise, it shall be turned to numerical methods.

2.3.1 Solution of the constraint

It is the peculiar feature of the kinetic spherical model that a complicated many-body problem can be exactly reduced to the solution of a single equation. First the exact late-time asymptotic behavior of the solution $g(t)$ of Eq. (2.20) is derived for a constant field $H(t) = H$, that is for times $t \gg 1$. Afterward, the use of asymptotic expansions for the calculation of physical observables is commented.

It is convenient to consider first the initial condition $S_0 = 0$ which is easier to handle. As we shall see, the system actually looses its memory of the initial state quite rapidly.

A first condition on the late-time asymptotics comes from the known fact $|C_{\boldsymbol{x},\boldsymbol{x}}| \leq 1$. Together with Eq. (2.17), it is easy to see that the power-law dependence of $g(t)$ on t as found [37] for the special case $H = 0$ and $T < T_c$ is incompatible with that condition in the case at hand.

It is therefore worth to try, for late times $t \gg 1$, an asymptotic exponential ansatz

$$g(t) = a\, e^{t/\tau}, \tag{2.26}$$

where a and τ are constants to be determined. Indeed Eq. (2.17) now shows that $|C_{\boldsymbol{x},\boldsymbol{x}}|$ is bounded if $\tau > 0$. To see this, observe that because of the ansatz (2.26) the main contribution to the terms in Eq. (2.17) which depend on the magnetic field comes from the upper limit of integration. Consequently, the quadratic term in $B_{\boldsymbol{x}}(t)$ dominates over the terms linear in $B_{\boldsymbol{x}}(t)$ and also over those terms which do not contain $B_{\boldsymbol{x}}(t)$ at all. For large times t, s we have asymptotically

$$\lim_{t,s\to\infty} C_{\boldsymbol{x},\boldsymbol{x}}(t,s) = 4H^2\tau^2, \tag{2.27}$$

where the limit is taken for a constant time difference $\sigma = t - s \geq 0$. Inserting Eq. (2.26) into Eq. (2.20) yields for $S_0 = 0$, along the same lines

$$g(t) = A(t) + 2T\int_0^t \mathrm{d}t'\; f(t-t')g(t') + 4H^2\tau^2 g(t) \tag{2.28}$$

with $f(t) = (e^{-4t} I_0(4t))^d$ from Eq. (2.18). Using the Laplace transformation

$$\overline{f}(p) = \int_0^\infty \mathrm{d}t\, f(t)\, e^{-pt} \tag{2.29}$$

we find from (2.28)

$$\overline{g}(p) = \frac{\overline{A}(p)}{1 - 2T\overline{f}(p) - 4H^2\tau^2}. \tag{2.30}$$

This must be consistent with the Laplace-transformed ansatz of Eq. (2.26)

$$\overline{g}(p) = \frac{a}{p - \tau^{-1}}. \tag{2.31}$$

These two expressions can only be compatible if the denominator in Eq. (2.30) vanishes at $p = \tau^{-1}$, i.e.

$$1 - 2T\overline{f}(\tau^{-1}) = 4H^2\tau^2 \tag{2.32}$$

and this must be a simple intersection (from Eq. (2.22) we know that $A(t) > 0$, therefore $\overline{A}(p) > 0$ can be related to a). Eq. (2.32) is an implicit equation for τ and now it is shown that there is always a unique solution, provided $H \neq 0$.

First, consider the case $\tau \to 0$. From the definition of $\overline{f}(p)$ and $f(t) > 0$, we have $\overline{f}(p) > 0$. Similarly, $f(t) \leq 1$ for $t \geq 0$ implies $\overline{f}(p) \leq p^{-1}$. Therefore

$$\lim_{\tau \to 0} \left(1 - 2T\overline{f}(\tau^{-1})\right) = 1. \tag{2.33}$$

Second, consider the case $\tau \to \infty$. From the results of Ref. [37] on $\overline{f}(p)$ one has

$$\lim_{\tau \to \infty} \left(1 - 2T\overline{f}(\tau^{-1})\right) = 1 - \frac{T}{T_c}. \tag{2.34}$$

It is well-known that the Laplace transformation $\overline{f}(p)$ of a positive function $f(t)$ decreases monotonously with p [42]. Therefore, the left-hand-side of Eq. (2.32) decreases monotonously from 1 to $1 - T/T_c$ as τ increases from 0 to ∞, while the right-hand-side $\sim \tau^2$ increases monotonously for $H \neq 0$. This establishes the existence of a simple intersection and therefore of a unique τ which describes the late-time asymptotics of $g(t)$ for $H \neq 0$, see Eq. (2.26). For $|H| \to 0$ and $T \leq T_c$ we find $\tau \to \infty$, while for $H = 0$ a solution for τ only exists if $T > T_c$. This reproduces the well-known result that for $H = 0$, $g(t)$ only has an exponential behavior for $T > T_c$ [12, 37]. The fact that in the case $H \neq 0$ we find an exponential behavior for all temperatures T shows

that the system relaxes to an equilibrium state after the finite time τ [35] and neither critical behavior nor aging is expected for late times. It is now clear that adding the extra terms coming in for $S_0 \neq 0$ will merely generate sub-leading corrections and the asymptotic solution Eq. (2.26) will not be affected.

In conclusion, it is established: *the leading long-time asymptotic behavior of $g(t)$ is given by Eq. (2.26) where τ is the unique solution of Eq. (2.32) and with $a = -\overline{A}(1/\tau)/(2T\overline{f}'(1/\tau))$, for any value $H \neq 0$ of the constant magnetic field and any given mean initial magnetization S_0.*

For finite times, there is no analytical solution of Eq. (2.20) available. Instead, as described in the appendix, sec. 2.7, $g(t)$ is determined numerically. Although the two–time observables are the relevant quantities for the study of aging phenomena, it is still useful to consider single–time observables like the average magnetization $S(t)$ given by

$$S(t) = \langle S_{\boldsymbol{x}}(t) \rangle = \frac{1}{\sqrt{g(t)}} \left[S_0 + \int_0^t \mathrm{d}t' H(t') \sqrt{g(t')} \right] . \tag{2.35}$$

In practice, care is required in using asymptotic solutions of $g(t)$ for the prediction of the time-dependence of observables such as $S(t)$. This is illustrated in figure 2.1, where $g(t)$ and the distance of the magnetization to its equilibrium value $S_\infty - S(t)$ are shown as a function of time. We see in figure 2.1a that after an initial fall-off, $g(t)$ quickly reaches the asymptotic regime of exponential growth. In figure 2.1b, however, the mean magnetization $S(t)$ as found from the exact numerical solution $g(t)$ (see appendix, sec. 2.7) is compared with the one obtained from an asymptotic fit of the form

$$g(t) \simeq e^{t/\tau} \sum_{\ell=0}^{\ell_{\max}} a_\ell (t - t_0)^{-\ell} \tag{2.36}$$

where $\ell_{\max} = 5$ is used. Although that the asymptotic fit for $g(t)$ cannot be distinguished from the exact numerical result in figure 2.1a, the deviation in $S(t)$ is considerable.

In the rest of this chapter, the direct numerical solution of Eq. (2.20) is used.

2.3.2 Single-time observables

Our first applications consider single-time observables, which are the ones most commonly studied.

An instructive example on the importance of fluctuation effects is constructed as follows. For a given external magnetic field H, one may easily

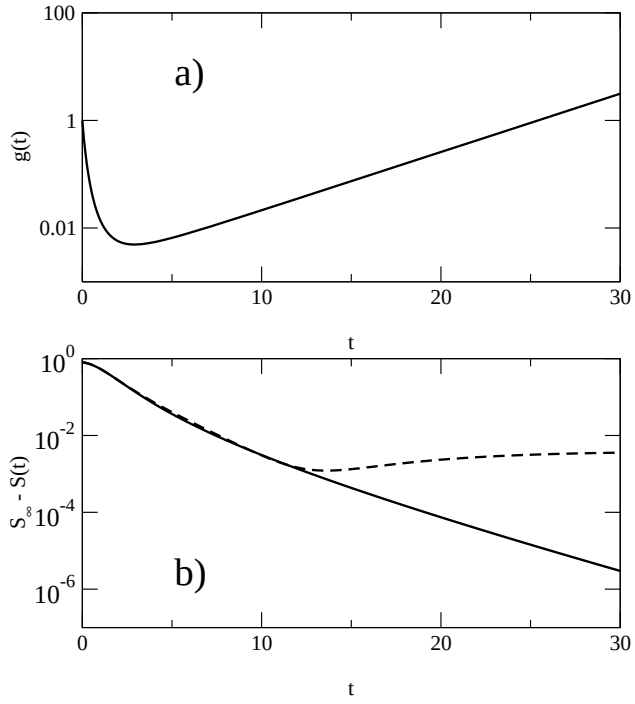

Figure 2.1: The function $g(t)$ (a) and the distance of the magnetization to its equilibrium value (b) for $d = 3.5$, $T = 2$ $(T_c \approx 5.27)$, $H = 0.1$ and $S_0 = 0$. The full curve shows the results for the direct numerical calculation, the dashed line shows the results for the 5th order fit which coincides with the full curve in (a).

calculate the equilibrium magnetization $M_{\rm eq}$. Now prepare the system such that the spins have a mean magnetization $M_{\rm eq}$ but such that spins on different sites are uncorrelated. The time evolution of $S(t)$ is shown in figure 2.2. While a mean–field description would have predicted a constant $S(t)$, we see that the magnetization is not constant but increases toward a peak before it falls back to the equilibrium value $M_{\rm eq}$. Intuitively, we would expect that the individual spins tend to align with the local magnetic field provided by their neighbors. Since initially $S_0 = M_{\rm eq} > 0$, one orientation is preferred with respect to the other one and domains oriented parallel to $M_{\rm eq}$ will grow preferentially. When the domains have grown large enough the influence of this effect decreases and the system approaches quickly the equilibrium state and the magnetization decreases again. This picture, although close in spirit to the Ising model with its discrete spin variables, also works in the spherical model, in spite of the fact that the interaction can be reduced to a free–field theory. The remnant interaction between different spins provided by the

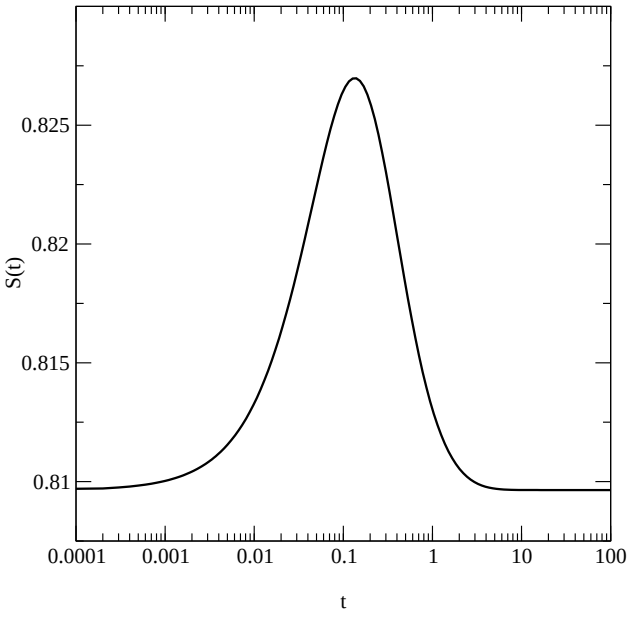

Figure 2.2: The magnetization of the system evolving from $S_0 = S_\infty$ calculated for $d = 3.5$, $T = 2(< T_c)$, $H = 0.2$ and $S_0 \approx 0.810$.

spherical constraint is sufficient to achieve non-trivial correlations between different spins.

We have seen in the previous section that for $H \neq 0$ and very late times the system relaxes back to its unique equilibrium state. For a vanishing magnetic field, the equilibrium free energy would have a double-well structure with two equivalent minima, corresponding to the two possible orientations of the mean magnetization. Turning on a magnetic field, this potential is tilted and the depth of the two local minima is no longer the same. The lower minimum becomes the unique equilibrium state, the other one corresponds to a metastable state. It is clear that if the system is initially prepared in the well corresponding to the equilibrium state, it will relax rapidly toward that state. Here the question is addressed how the transition from the metastable state toward the equilibrium state occurs.

Therefore, the system is prepared with an initial magnetization antiparallel to the given external field. In figure 2.3a the time evolution of the mean magnetization is shown. After a short time the system reaches the metastable state, independently of the absolute value of the initial magnetization S_0, and where $S(t)$ stays practically constant. The system remains in the metastable state for several decades until the magnetization is reversed quite rapidly (although one should not be misled by the logarithmic time-

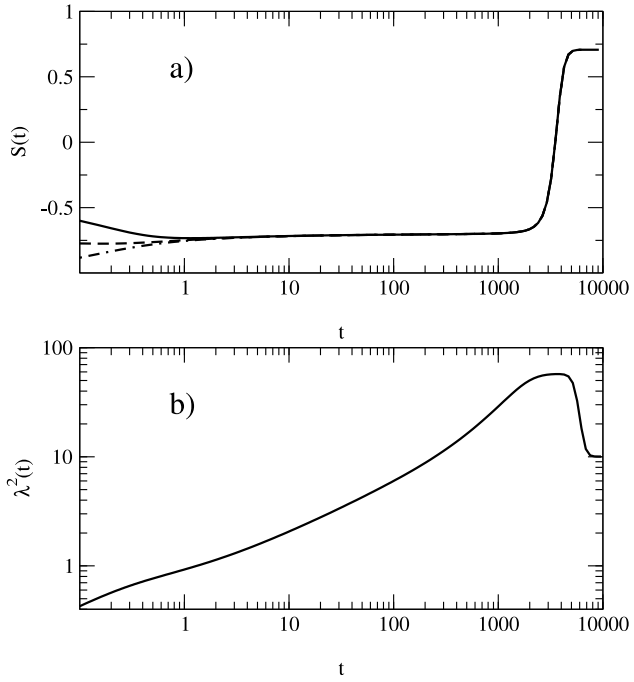

Figure 2.3: (a) Average magnetization $S(t)$ for $d = 3$, $T = 2$ ($< T_c \simeq 3.96$), $H = 10^{-3}$ and $S_0 = -0.5$ (full curve), $S_0 = -0.75$ (dashed curve) and $S_0 = -1$ (dash-dotted curve). (b) Squared correlation length $\lambda(t)^2$ of fluctuations for $S_0 = -0.5$, where the other parameters are as in (a).

scale in this figure which makes the changeover to appear be very fast). In order to understand better what is going on a characteristic length $\lambda(t)$ of the *fluctuations* is defined:

$$\lambda(t)^2 = \sum_{\boldsymbol{r}\in\Lambda} \boldsymbol{r}^2 \left(C_{\boldsymbol{r}}(t,t) - S(t)^2\right), \tag{2.37}$$

where $\boldsymbol{r}$ runs over all sites of the lattice $\Lambda \subset \mathbb{Z}^d$ and $C_{\boldsymbol{r}}(t,s)$ is the spin–spin correlation function (2.14). The time evolution of $\lambda(t)$ is shown in figure 2.3b. Starting from a very small initial value, $\lambda(t)$ increases toward a maximum value which is reached at the time when $S(t)$ starts to deviate perceptively from its value in the metastable state. While $S(t)$ changes its sign, $\lambda(t)$ remains approximately constant at its maximal values before it relaxes toward the equilibrium correlation length, with a typical value of a few lattice spacings. The coincidence of the times of the reversal of $S(t)$ and the peak in $\lambda(t)$ shows that whole domains rather than single uncorrelated spins are flipping.

2.3.3 Two-time observables

Having seen that the magnetization reversal passes via an intermediate state with highly correlated fluctuations, in this section it is discussed how this manifests itself in the behavior of the two-time quantities. An important quantity is the time ϑ after which the magnetization reverses itself. Evidently, $\vartheta = \vartheta(H, T, d)$, but we have not investigated in detail how ϑ depends on these parameters in detail. For illustration purposes, in this section the same choice of parameter values as in figure 2.3 shall be used, then $\vartheta \approx 3000$. For finite values of t, $g(t)$ can be readily found from Eq. (2.20) using the numerical methods described in the appendix, sec. 2.7. It shall be focused on the metastable state by restricting to waiting times s in the intermediate time regime $s \leq \vartheta$. A magnetization reversal is seen if the initial magnetization is chosen antiparallel to the external field.

Our choice of initially uncorrelated spin with a mean magnetization S_0 can be considered as a special case of initially correlated spins. The case of spatial long-range correlations of the form $C_{\rm ini}(\boldsymbol{r}) \sim |\boldsymbol{r}|^{-d-\alpha}$ in the initial state was studied in detail before [12, 25]. Formally, this reduces to an initial state with a constant mean magnetization in the limit $\alpha \to -d$. Using the exact results of Ref. [12] for $T < T_c$, we have

$$\begin{aligned} C(t,s) &= 1 - \frac{T}{T_c} = M_{\rm eq}^2 \\ R(t,s) &= [4\pi(t-s)]^{-d/2}\,, \end{aligned} \tag{2.38}$$

where $M_{\rm eq}$ is the equilibrium magnetization.

In figure 2.4a the correlation function $C(t,s)$ is plotted versus the time difference $t - s$ for several values of the waiting times s which are chosen to be in the metastable state, that is $s \leq \vartheta$ (compare figure 2.3a). After a short time the curves reach a plateau, with a value very close to the equilibrium value $C(t,s) = M_{\rm eq}^2$ (a small contribution of the magnetic field can be neglected here). $C(t,s)$ maintains itself at this value for approximatively three decades, independently of the waiting time s. When the observation time t becomes larger than the magnetization reversal time ϑ, the correlation function $C(t,s)$ changes its sign because the spins at time s before the reversal are anticorrelated to the spins at time t after the reversal. However, it should be pointed out that the changeover takes more time when the waiting time s is increased. The curves rapidly approach the expected value $-M_{\rm eq}^2$ because spins of the metastable state are compared to the stable state. So we conclude that the correlation function $C(t,s)$ is mainly determined by the value of magnetization.

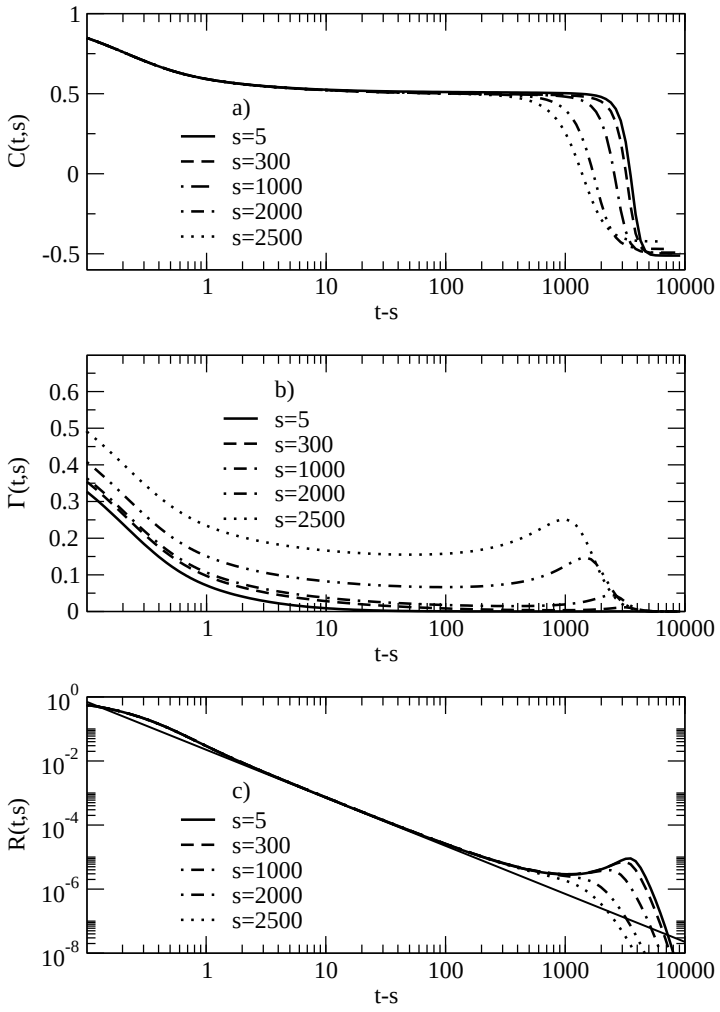

Figure 2.4: The two–time autocorrelation function $C(t,s)$ (a), the correlation of fluctuations $\Gamma(t,s)$ (b) and the response function $R(t,s)$ (c) plotted vs. the time difference $t-s$ for waiting times $s = \{5; 300; 1000; 2000; 2500\}$; the data were calculated for $d = 3$, $T = 2$ and $H = 10^{-3}$. In (c) the straight line shows the formula $[4\pi(t-s)]^{-d/2}$.

While $C(t,s)$ measures the time-dependence of the autocorrelation of a given spin, $\Gamma(t,s)$, see Eq. (2.24), measures the fluctuations. This is shown in figure 2.4b. It can be seen that for waiting times $s \leq 1000$, $\Gamma(t,s)$ decreases fairly rapidly as a function of the time difference $t-s$. In addition, a small peak is observed in the region $t \approx \vartheta$. But for waiting times closer to the magnetization reversal time ϑ (here for $s = 2000$ and $s = 2500$), the fluctuations have become quite substantial and show a larger peak around $(t-s)+s \approx \vartheta$. This may be viewed as another hint for the existence of correlated domains: as the spins inside of a domain are highly correlated a fluctuation of a spin within such a domain will cause other spins in the domain to follow this fluctuation. In turn, a side-effect of the enhanced correlations is a longer lifetime of a spin fluctuation. After the magnetization reversal, $\Gamma(t,s)$ rapidly falls to zero.

Finally, in figure 2.4c the response function $R(t,s)$ is shown. First, we observe that for a time region of at least two decades we recover Eq. (2.38), which was derived in Ref. [12] for the case without an external field. In this region translation invariance holds and hence no aging occurs. The system behaves as if it were in equilibrium although it is only in a metastable state. Second, for observation times t getting closer to the reversal time ϑ, the response function begins to deviate from this simple behavior. It should be pointed out that the curves for all waiting times s still collapse onto each other and that this deviation occurs although $C(t,s)$ still has not appreciably changed away from M_{eq}^2. Third, for times $t \gtrsim \vartheta$ the dependence on the waiting times becomes obvious before the response curves decrease very fast. This can be explained by considering that the memory of perturbations is lost during the reversal from the metastable to the stable state.

In order to decide whether the system is in equilibrium or not the zero–field–cooled (ZFC) magnetization shall be investigated now which is defined by

$$M_{\mathrm{ZFC}} = HT \int_s^t \mathrm{d}u\, R(t,u). \tag{2.39}$$

This quantity may be related to the fluctuation-dissipation ratio using Eq. (2.5). Because of the non-vanishing initial magnetization S_0 and the presence of an external magnetic field, the quantities $C(t,s)$ and $\Gamma(t,s)$ are different and a fluctuation-dissipation ratio is better defined using $\Gamma(t,s)$, namely $X(t,s) = TR(t,s)\left(\partial\Gamma(t,s)/\partial s\right)^{-1}$. This had been checked explicitly in the $1D$ Glauber-Ising model [12] and in certain simple model of glassy behavior [52]. In spin glasses, it had been shown [16, 17] from mean–field theory that $X = X(C(t,s))$ although that is not necessarily so beyond mean–field or in simple ferromagnets [37, 53, 54]. Nevertheless, this assumption is of good

heuristic value. In the spirit of the enterprise, let us consider the case where here $X = X(\Gamma(t,s))$. This amounts to saying that Γ serves as a clock for the evolution of the system. Then

$$M_{\rm ZFC}/H = \int_{\Gamma(t,s)}^{\Gamma(t,t)} {\rm d}\Gamma\, X(\Gamma). \tag{2.40}$$

Consequently, when plotting $M_{\rm ZFC}(t,s)/H$ versus $\Gamma(t,s)$ for fixed s (see figure 2.5) the slope of the curve corresponds to the value of X – provided of course that the assumptions leading to (2.40) are valid.[1] Rather, we find in figure 2.5 that with increasing waiting time s the curves move from the lower right to the upper left. On the other hand, for a given value of s, the system starts in the lower right corner and moves rapidly along a curve $M_{\rm ZFC}(\Gamma) = \Gamma_0 - \Gamma$ until the metastable value $M_{\rm ZFC}/H = 1 - M_{\rm meta} \simeq 1 - M_{\rm eq}$ is reached. The slope of unity of this curve is the same as would be found for an equilibrium system. Surprisingly, while it undergoes the magnetization reversal, the system then passes through a loop, which corresponds to the peak in $\Gamma(t,s)$, before it reaches a horizontal line, of height $1 - M_{\rm eq}$. The movement along the horizontal line is a behavior typical of the low-temperature phase, indeed through the magnetization reversal the system behaves as if the quasiequilibrium branch close to the metastable state had to be joined with the low-temperature behavior after the magnetization reversal. All in all, this behavior is quite analogous to the one observed for $M_{\rm ZFC}$ as a function of $C(t,s)$ for systems brought into the two-phase region by a temperature quench [56].

Of course, all the results in this section depend on having taken $s \leq \vartheta$. If we take instead $s > \vartheta$, the system quickly relaxes to its unique equilibrium state.

2.4 Scaling of the linear response

Only few magnetic systems can be solved analytically. Consequently, in most of the cases one has to revert to numerical methods, like Monte–Carlo simulations, and for the determination of exponents power–law fits are used. Consequently, the results depend on both accuracy and simulation times, which gives rise to different interpretations. In this section we focus on the scaling of the linear response, whose behavior has been debated [2, 15, 57]. In this context, the spherical model is of special interest, as its solution is

[1] For metastable systems with detailed balance and for time-scales shorter than the nucleation time, a fluctuation-dissipation relation is discussed in Ref. [55].

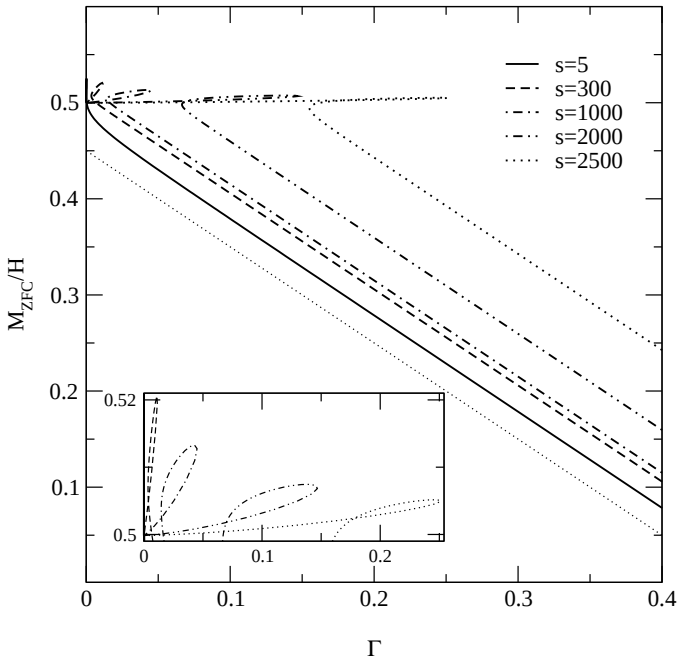

Figure 2.5: $M_{\rm ZFC}/H$ vs. Γ, where the parameters are as in figure 2.4. For reference, the gray line gives the curve $M_{\rm ZFC}/H = 1\Gamma$. In the inset the region of the loops is shown in more detail.

not based on simulations. General concepts can be tested using analytical methods.

2.4.1 Crossover of the thermoremanent magnetization

In this section the value of the non–equilibrium exponent a of the response function (2.2) is investigated. It is shown that in the spherical model the thermoremanent magnetization shows a crossover which is generic for any magnetic model. Due to this crossover the determination of the non–equilibrium exponent a in numerical calculations may be misleading when too short times are considered.

In quite a few models, values of a were obtained, see Ref. [9] for a review, but no clear picture has yet emerged. In the exactly solved $1D$ Glauber-Ising model, one has $a = 0$ [58, 59]. However, the value of a in the $2D$ and $3D$ kinetic Glauber-Ising models and the kinetic spherical models has been debated recently. In the $2D$ and $3D$ Glauber-Ising model, analytical [60] and numerical [15] results indicate $a = 1/2$. In the exactly solvable spherical model, one reads off $a = d/2 - 1$ for all spatial dimensions $d > 2$ from the

exact result for $R(t,s)$ [12, 34, 36, 37, 39].

In Ref. [2] it is discussed that one should distinguish between those systems (called *class S*) with a short-ranged (exponential) decay of the equilibrium connected spin-spin correlator in the ordered phase and those (called *class L*) for which there remain long-range (algebraic) correlations in the ordered phase. The Glauber-Ising model in $d > 1$ belongs to class S while the spherical model and the $2D$ XY-model are members of class L [2]. Then

$$a = \begin{cases} 1/z & ; \text{class S} \\ (d-2+\eta)/z & ; \text{class L} \end{cases} \tag{2.41}$$

where η is a well-known equilibrium critical exponent. Since for the Glauber-Ising model $z = 2$ [7], one recovers the well-known $a = 1/2$ for class S in all dimensions $d > 1$. These results are derived by comparing the scaling form of the dissipative part χ'' of the non-equilibrium susceptibility with heuristic expectations which for class S amount to the generally accepted idea that the aging comes from the movement of the domain walls which separate the ordered domains [7, 8, 60]. In addition, a more complete scaling form for the thermoremanent magnetization $M_{\rm TRM}(t,s)$ in the limit of large waiting times $s \gg 1$ can be derived [2],

$$M_{\rm TRM}(t,s)/h = \int_0^s \mathrm{d}u\, R(t,u) = s^{-a} f_M(t/s) + s^{-\lambda_R/z} g_M(t/s) \tag{2.42}$$

provided the system was initially prepared at infinite temperature. Eq. (2.42) implies that the behavior of $M_{\rm TRM}$ will be one of a cross-over between two distinct regimes [36, 61]. In practice, the cross-over region may well be large. If local scale invariance [14] holds, the scaling functions can be found from Eq. (2.4) and read explicitly ($r_{0,1}$ are non-universal constants)

$$\begin{aligned} f_M(x) =& r_0\, x^{-\lambda_R/z}\, {}_2F_1\left(1+a, \frac{\lambda_R}{z} - a; \frac{\lambda_R}{z} - a + 1; x^{-1}\right) \quad , \\ g_M(x) \approx& r_1\, x^{-\lambda_R/z}. \end{aligned} \tag{2.43}$$

This scaling form can be verified using the numerical method presented in the previous sections. In figure 2.6 we show the thermoremanent magnetization $M_{\rm TRM}$ obtained from numerically integrating the Langevin equation, at a temperature $T < T_c$ (recall that for $d = 3$, $T_c \simeq 3.96$ and for $d = 3.5$, $T_c \simeq 5.27$). As an initial state, we used uncorrelated spins with either a mean magnetization $S_0 = 0$ (figure 2.6a) or else $S_0 = 0.5$ (figure 2.6b and

[2] The kinetics of the $1D$ Glauber-Ising model is very peculiar since its critical temperature is $T_c = 0$. It appears to fit into class L rather than class S.

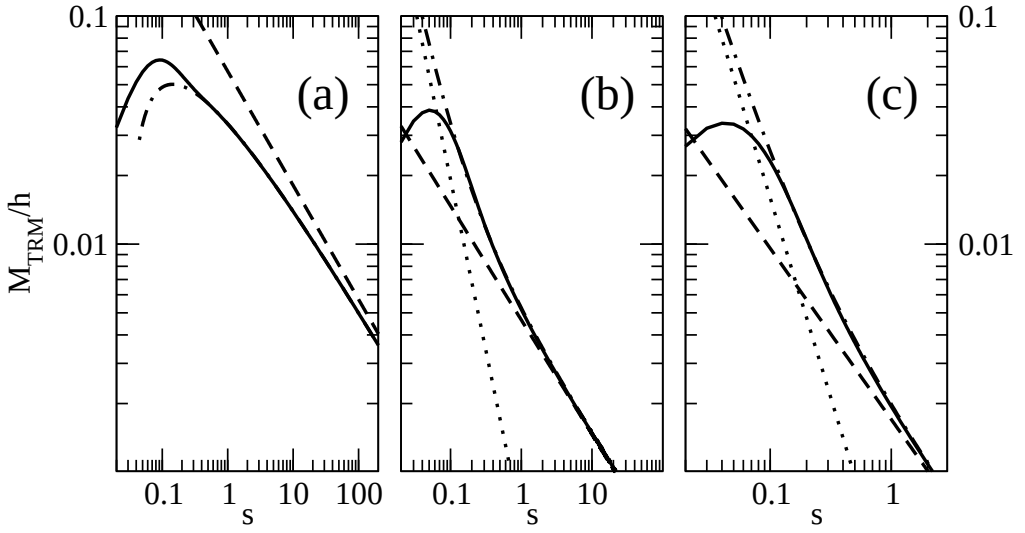

Figure 2.6: Scaling of the thermoremanent magnetization $M_{\rm TRM}(t,s)$ (full curve) at $T=2$ as a function of the waiting time s in the spherical model for $x=t/s=5$. (a) $d=3$ and $S_0=0$, (b) $d=3$ and $S_0=0.5$, (c) $d=3.5$ and $S_0=0.5$. The dashed and dotted lines show the leading contributions $\sim s^{-a}$ and $\sim s^{-\lambda_R/z}$, respectively, whereas the dash-dotted lines give their sum.

2.6c). Then the exponents $z=2$, $a=d/2-1$ and $\lambda_R=d/2$ for $S_0=0$ or $\lambda_R=d$ for $S_0=0.5$, respectively, are expected [12]. The leading term $\sim s^{-a}$ and the sum of the two leading contributions to $M_{\rm TRM}$ according to Eq. (2.42) are shown and are compared with the numerical solution of the Langevin equation [3]. For $S_0=0.5$, the cross-over between the two regimes is evident. On the other hand, for $S_0=0$, we observe that although the slope of $\ln M_{\rm TRM}$ versus $\ln s$ appears to be fairly constant, the second term expected from Eq. (2.42) produces a sizable correction. Finally, we see that down to values of s as small as $s\sim 1$, the time-dependence of $M_{\rm TRM}$ is well described by Eq. (2.42). We observed a similar behavior, and in quantitative agreement with the scaling functions (2.43), for other values of x.

The scaling of the thermoremanent magnetization and the predicted values of a can also be confirmed in the 2D Ising model as shown in Ref. [2].

[3] In figure 2.6, we have (a) $r_0\simeq 0.057$, $r_1\simeq -0.0235$, (b) $r_0\simeq 0.0047$, $r_1\simeq 0.00061$, (c) $r_0\simeq 0.0017$, $r_1\simeq 0.00028$.

2.4.2 Scaling of the susceptibility

In this section the behavior of the field–cooled susceptibility $\chi_{\rm FC}$ after a temperature quench is investigated. The hypothesis is verified that the scaling follows $\chi_{\rm FC}(t)-\chi_0 \propto t^{-A}$ where χ_0 is related to the equilibrium magnetization and the exponent A is related to the time–dependent scaling of the interface width between ordered domains. The same effect also dominates the scaling of the zero–field–cooled susceptibility $\chi_{\rm ZFC}(t,s)$, but does not enter into the thermoremanent susceptibility $\rho_{\rm TRM(t,s)}$. An important conceptual point on the interpretation of the scaling behavior of several commonly used observables related to $R(t,s)$ obtained by numerical investigations is addressed. It should be mentioned that these findings stand in contrast to the methods used in Refs. [39, 57, 61, 62].

General concept

Numerical information on $R(t,s)$ can be obtained using a by now standard method devised by Barrat [63]. One perturbs the system by a *random* magnetic field h_i with zero mean $\bar{h_i}=0$. Instead of measuring $R(t,s)$ directly, two common procedures run as follows. Either one quenches the system and turns on the magnetic field after the waiting time s has elapsed and then works with the zero–field–cooled susceptibility $\chi_{\rm ZFC}(t,s)$. Alternatively, one may also keep the random field until the waiting time s when it is turned off and then has the thermoremanent susceptibility $\rho_{\rm TRM}(t,s)$. These are related to $R(t,s)$ as follows

$$\chi_{\rm ZFC}(t,s) \;=\; \chi(t,s) = \int_s^t {\rm d}u\, R(t,u) \stackrel{?}{=} s^{-a} f_\chi(t/s) \tag{2.44}$$

$$\rho_{\rm TRM}(t,s) \;=\; \rho(t,s) = \int_0^s {\rm d}u\, R(t,u) \stackrel{?}{=} s^{-a} f_M(t/s) \tag{2.45}$$

Here, we straightforwardly used the scaling forms (2.2) *without paying attention to the conditions of validity* of these and in particular *did not pay any attention as to whether* $t-s \gg t_{\rm micro}$ *holds true or not*. As we shall show, however, careful consideration of these conditions is crucial in order to obtain valid scaling forms for the integrated responses $\chi_{\rm ZFC}(t,s)$ and $\rho_{\rm TRM}(t,s)$.

On a discrete lattice $\Lambda \subset \mathbb{Z}^d$, the integrated responses (2.44,2.45) are obtained by measuring the time-dependent magnetization [63]

$$M = \frac{1}{|\Lambda|\, h} \overline{\left\langle \sum_{\boldsymbol{i}\in\Lambda} \phi_{\boldsymbol{i}}(t) h_{\boldsymbol{i}} \right\rangle} \tag{2.46}$$

where $|\Lambda|$ is the number of sites of the lattice Λ. Depending on whether one works in the zero-field-cooled or the thermoremanent protocol, one obtains $\chi_{\rm ZFC} = M_{\rm ZFC}/h$ or $\rho_{\rm TRM} = M_{\rm TRM}/h$, respectively.

In order to extract the aging behavior from the integrated response function correctly, one has to consider the following [3]:

1. Consider the field-cooled susceptibility

$$\chi_{\rm FC}(t) = \chi_{\rm ZFC}(t,s) + \rho_{\rm TRM}(t,s) = \int_0^t {\rm d}u\, R(t,u). \tag{2.47}$$

   For ferromagnets of class S, one has $\chi_{\rm FC}(t) - \chi_0 \sim t^{-A}$, [3]. Here $T\,\chi_0 = 1 - m_{\rm eq}^2$ is given by the mean equilibrium magnetization. The exponent A is a new exponent without a direct relationship to aging, rather it is related to the roughness of the interface between ordered domains. We stress that since the power-law behavior of $\chi_{\rm FC}(t)$ is *independent* of the waiting time s it has no relation with a possible aging behavior. In particular, $A = 1/4$ for the $2D$ Glauber-Ising model with $T < T_c$ [3]. Furthermore, for a fixed scaling variable $x = t/s$ one has, with the scaling function $g(x) \sim x^{-A}$

$$\chi_{\rm ZFC}(t,s) = \chi_{\rm FC}(t) - \rho_{\rm TRM}(t,s) \sim \chi_0 + s^{-A} g(x) + {\rm O}(s^{-a}). \tag{2.48}$$

   Here we anticipate an important result of Ref. [3], namely that $\rho_{\rm TRM}(t,s) \sim s^{-a}$, see also Eq. (2.49) below. Since for rough interfaces one has $A - a = A - 1/z < 0$, it follows that (2.44) cannot be used. The leading scaling of $\chi_{\rm FC}$ with the waiting time s is unrelated to the aging behavior of the model as described by (2.2). Indeed, the terms describing aging only occur as subleading terms in $\chi_{\rm ZFC}(t,s)$ and are therefore difficult to extract. In particular, the exponent A cannot be identified with the aging exponent a. An example is provided by the $2D$ Glauber-Ising model, where $a = 1/z = 1/2$ but $A = 1/4$.

2. For ferromagnets of class L, like the spherical model, we shall show that $A = 0$. We shall explicitly test this in the kinetic mean spherical model for any $T \leq T_c$.

3. Eq. (2.48) shows that aging effects merely provide a finite-time correction to the scaling of $\chi_{\rm ZFC}$. On the other hand, aging terms are leading in the thermoremanent magnetization which scales more precisely as [2]

$$\rho_{\rm TRM}(t,s) = s^{-a} f_M(t/s) + s^{-\lambda_R/z} g_M(t/s) \tag{2.49}$$

where the scaling functions $f_M(x)$ and $g_M(x)$ are related to the response function $R(t,s)$. For example, for a system in class S with an uncorrelated initial state, one has $\lambda_C = \lambda_R \geq d/2$ [13] and since $a = 1/z$, these two terms may be of almost the same order and a simple log-log plot may not be sufficient to yield a precise value of a for times accessible in present simulations. Indeed, this situation occurs in the $2D$ and $3D$ Glauber-Ising model. However, subtracting the leading correction according to Eq. (2.49) allows to reliably determine a and the scaling function $f_M(x)$ [2, 3, 64].

The heuristic argument why the scaling form

$$\chi_{\mathrm{FC}}(t) \propto t^{-A} \tag{2.50}$$

is to be expected and where the value of A comes from is the following [3]. Consider a simple ferromagnet in $d > 1$ dimensions which is quenched at time $t = 0$ from an infinite-temperature initial state to a final temperature $T < T_c$. The dynamics is assumed to be purely relaxational, i.e. without any conservation law. Microscopically, it is well-known that the configurations of the system consist of fully ordered domains of spins, of a typical size $L(t) \sim t^{1/z}$ with $z = 2$. We now perturb with a random field of zero mean $\overline{h_{\boldsymbol{i}}} = 0$ and wish to obtain the susceptibility $\chi_{\mathrm{FC}} = M_{\mathrm{FC}}/h$. First consider the case when $T = 0$. Then, because the spins deep inside the cluster are ordered, the only non-vanishing contribution to χ_{FC} comes from the spins from near the interfaces between the ordered clusters. We denote the interface density by $\rho_{\mathrm{I}}(t)$ and have $\rho_{\mathrm{I}}(t) \sim L(t)^{-1}$, see Refs. [6, 8, 60]. If $w(t)$ is the interface width, we have

$$\chi_{\mathrm{FC}}(t) = \frac{1}{|\Lambda|\, h^2} \overline{\left\langle \sum_{\boldsymbol{i}\in\Lambda} \sigma_{\boldsymbol{i}}(t) h_{\boldsymbol{i}} \right\rangle} = \frac{1}{|\Lambda|\, h^2} \overline{\left\langle \sum_{\boldsymbol{i}\in \text{ interfaces}} \sigma_{\boldsymbol{i}}(t) h_{\boldsymbol{i}} \right\rangle} \sim L(t)^{-1} w(t). \tag{2.51}$$

For a finite temperature $T > 0$, the order deep inside the clusters is not perfect and there remains a residual contribution to the susceptibility. We then have, for large times

$$\chi_{\mathrm{FC}}(t) \simeq \chi_0 + L(t)^{-1} w(t) \ \ , \ \ T\chi_0 = 1 - m_{\mathrm{eq}}^2 \tag{2.52}$$

where m_{eq} is the equilibrium magnetization (for the $2D$ Ising model, $m_{\mathrm{eq}} = (1 - \sinh(2/T)^{-4})^{1/8}$, see e.g. Ref. [65]).

Test in the spherical model

We now test the heuristic discussion of the scaling of χ_{FC} in the spherical model which belongs to class L. This is the contribution of the author to

Ref. [3]. There also a discussion for class S systems, like the 2D Ising model, and a numerical verification of the hypothesis can be found.

Indeed, the main physical difference with respect to systems of class S is that although correlated clusters of size $L(t) \sim t^{1/z}$ form, fluctuations do persist in the interior of these clusters on all length scales up to $L(t)$. This means that one should consider an 'interface width' scaling as $w(t) \sim L(t)$. This in turn leads to $\chi_{\mathrm{FC}}(t) \sim$ const. and $A = 0$ (on the other hand, since the clusters should have no 'inside', we do not expect a term χ_0 to occur).

We now test this heuristic idea in the exactly solvable mean spherical model by adding a random magnetic field $h_{\boldsymbol{x}}$. The equations of motion read

$$\frac{\mathrm{d}}{\mathrm{d}t} S_{\boldsymbol{x}}(t) = \sum_{\boldsymbol{y}(\boldsymbol{x})} S_{\boldsymbol{y}}(t) - (2d - \mathfrak{z}(t)) S_{\boldsymbol{x}}(t) + h_{\boldsymbol{x}} + \eta_{\boldsymbol{x}}(t) \tag{2.53}$$

where the noise and the random field have zero average $\langle \eta_{\boldsymbol{x}} \rangle = \overline{h_{\boldsymbol{x}}} = 0$ and the correlators

$$\langle \eta_{\boldsymbol{x}}(t) \eta_{\boldsymbol{y}}(t') \rangle = 2T\, \delta_{\boldsymbol{x},\boldsymbol{y}}\, \delta(t - t') \quad , \quad \overline{h_{\boldsymbol{x}} h_{\boldsymbol{y}}} = 2\Gamma\, \delta_{\boldsymbol{x},\boldsymbol{y}} \tag{2.54}$$

where the temperature T and the width Γ are constants and $\mathfrak{z}(t)$ is a Lagrange multiplier to be determined below. In addition, the noise and the field are assumed independent, i.e. $\overline{\langle \eta_{\boldsymbol{x}}(t) h_{\boldsymbol{y}} \rangle} = 0$, and in addition the initial state is uncorrelated in the sense that $\overline{\langle S_{\boldsymbol{x}}(0) h_{\boldsymbol{y}} \rangle} = 0$. Here and in the following the average $\langle \mathfrak{X} \rangle$ is always taken over the initial conditions and the noise, while the average $\overline{\mathfrak{X}}$ is over the random field. These equations are solved straightforward with the methods presented in section 2.2. Taking Fourier transforms, the solution of Eq. (2.53) is

$$\widetilde{S}(\boldsymbol{q}, t) = \frac{\exp(-\omega(\boldsymbol{q}) t)}{\sqrt{g(t)}} \left[\widetilde{S}(\boldsymbol{q}, 0) + \int_0^t \mathrm{d}t'\, e^{\omega(\boldsymbol{q}) t'} \sqrt{g(t')} \left(\widetilde{h}(\boldsymbol{q}) + \widetilde{\eta}(\boldsymbol{q}, t') \right) \right] \tag{2.55}$$

with the dispersion relation $\omega(\boldsymbol{q}) = 2 \sum_{i=1}^{d} (1 - \cos q_i)$ and

$$g(t) = \exp(2 \int_0^t \mathrm{d}t' \mathfrak{z}(t')). \tag{2.56}$$

The spin-spin correlator $\widetilde{C}(\boldsymbol{q}, \boldsymbol{q}'; t, s) = \overline{\left\langle \widetilde{S}(\boldsymbol{q}, t) \widetilde{S}(\boldsymbol{q}', s) \right\rangle}$ is readily found and

we have in direct space the autocorrelator

$$\begin{aligned} C(t,s) = C_{\boldsymbol{x},\boldsymbol{x}}(t,s) &= \frac{1}{(2\pi)^{2d}} \int_{\mathcal{B}^2} \mathrm{d}\boldsymbol{q}\mathrm{d}\boldsymbol{q}'\, e^{\mathrm{i}(\boldsymbol{q}+\boldsymbol{q}')\cdot\boldsymbol{x}}\, \widetilde{C}(\boldsymbol{q},\boldsymbol{q}';t,s) \\ &= \frac{1}{\sqrt{g(t)g(s)}} \left[A\left(\frac{t+s}{2}\right) + 2T \int_0^s \mathrm{d}u\, f\left(\frac{t+s}{2}-u\right) g(u) \right. \\ &\quad \left. +2\Gamma \int_0^t \mathrm{d}t' \int_0^s \mathrm{d}s'\, f\left(\frac{t+s-t'-s'}{2}\right) \sqrt{g(t')g(s')} \right] \end{aligned} \tag{2.57}$$

where $\mathcal{B}$ is the Brillouin zone and with the definitions

$$A(t) = (2\pi)^{-d} \int_{\mathcal{B}} \mathrm{d}\boldsymbol{q}\, e^{-2\omega(\boldsymbol{q})t} \widetilde{C}(\boldsymbol{q},0) \tag{2.58}$$

$$f(t) = (2\pi)^{-d} \int_{\mathcal{B}} \mathrm{d}\boldsymbol{q}\, e^{-2\omega(\boldsymbol{q})t} = \left(e^{-4t} I_0(4t)\right)^d \tag{2.59}$$

and where I_0 is a modified Bessel function. For infinite-temperature initial conditions $A(t) = f(t)$. The mean spherical constraint (2.6) gives $C(t,t) = 1$ and this leads to the following generalized Volterra integral equation

$$\begin{aligned} g(t) =& A(t) + 2T \int_0^t \mathrm{d}u\, f(t-u) g(u) \\ &+ 2\Gamma \int_0^t \mathrm{d}u' \int_0^t \mathrm{d}u''\, f\left(t - \frac{u'+u''}{2}\right) \sqrt{g(u')g(u'')} \end{aligned} \tag{2.60}$$

which determines $g(t)$. Finally, the response function is given by the usual equation $R(t,s) = f((t-s)/2)\sqrt{g(s)/g(t)}$. At zero temperature $T = 0$, eqs. (2.58,2.60) are identical to those found for the spherical spin-glass [35, 66].

The field-cooled susceptibility is given by

$$\chi_{\mathrm{FC}}(t) = \int_0^t \mathrm{d}u\, R(t,u) = \int_0^t \mathrm{d}u\, f\left(\frac{t-u}{2}\right) \sqrt{\frac{g(u)}{g(t)}}\,. \tag{2.61}$$

At this point, it is instructive to re-derive the equivalence between the definition (2.61) and Eq. (2.46), originally proposed in Ref. [63] for the Glauber-Ising model, in the context of the mean kinetic spherical model. Indeed, we

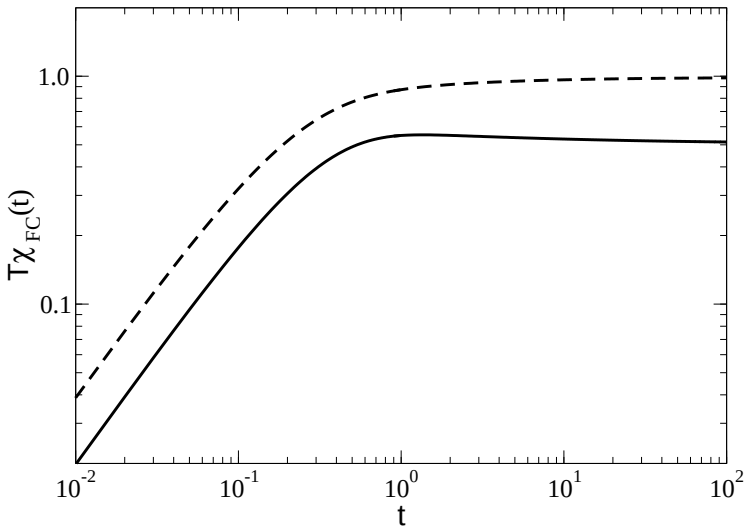

Figure 2.7: Field-cooled susceptibility $\chi_{\rm FC}(t)$ for the $3D$ kinetic mean spherical model in a Gaussian random magnetic field of width $\Gamma = 0.01$ at $T = 2 < T_c$ (full curve) and at $T = T_c \simeq 3.96$ (dashed curve).

have ($|\Lambda|$ denotes the number of sites of the lattice Λ)

$$\begin{aligned}
\frac{1}{|\Lambda|}\overline{\left\langle \sum_{\boldsymbol{x}\in\Lambda} S_{\boldsymbol{x}}(t) h_{\boldsymbol{x}} \right\rangle} &= \frac{(2\pi)^{-2d}}{|\Lambda|} \sum_{\boldsymbol{x}\in\Lambda} \int_{\mathcal{B}^2} \mathrm{d}\boldsymbol{q}\mathrm{d}\boldsymbol{q}'\, e^{\mathrm{i}(\boldsymbol{q}+\boldsymbol{q}')\cdot\boldsymbol{x}}\, \overline{\left\langle \widetilde{S}(\boldsymbol{q},t)\widetilde{h}(\boldsymbol{q}') \right\rangle} \\
&= \frac{(2\pi)^{-2d}}{|\Lambda|} \sum_{\boldsymbol{x}\in\Lambda} \int_{\mathcal{B}^2} \mathrm{d}\boldsymbol{q}\mathrm{d}\boldsymbol{q}'\, e^{\mathrm{i}(\boldsymbol{q}+\boldsymbol{q}')\cdot\boldsymbol{x}} \int_0^t \mathrm{d}t'\, e^{\omega(\boldsymbol{q})(t'-t)} \sqrt{\frac{g(t')}{g(t)}}\, \cdot \\
&\qquad\qquad \cdot\overline{\widetilde{h}(\boldsymbol{q})\widetilde{h}(\boldsymbol{q}')} \\
&= (2\pi)^{-d}\, 2\Gamma \int_0^t \mathrm{d}t' \int_{\mathcal{B}} \mathrm{d}\boldsymbol{q}\, e^{-\omega(\boldsymbol{q})(t-t')} \sqrt{\frac{g(t')}{g(t)}} \\
&= 2\Gamma\chi_{\rm FC}(t)
\end{aligned} \tag{2.62}$$

as asserted, and where we used in the second line Eq. (2.55) and in the third line the field correlator (2.54).

After these preparations we can test the heuristic picture. Using the techniques described in the previous sections, we obtain $g(t)$ by solving Eq. (2.60) numerically. In figure 2.7 we show $\chi_{\rm FC}(t)$ for the three–dimensional case, starting from an infinite-temperature initial state. We clearly see that $\chi_{\rm FC}(t)$ saturates rapidly. Consequently, $A = 0$ for all temperatures $T \leq T_c$. Similar tests can be performed for other values of d as well.

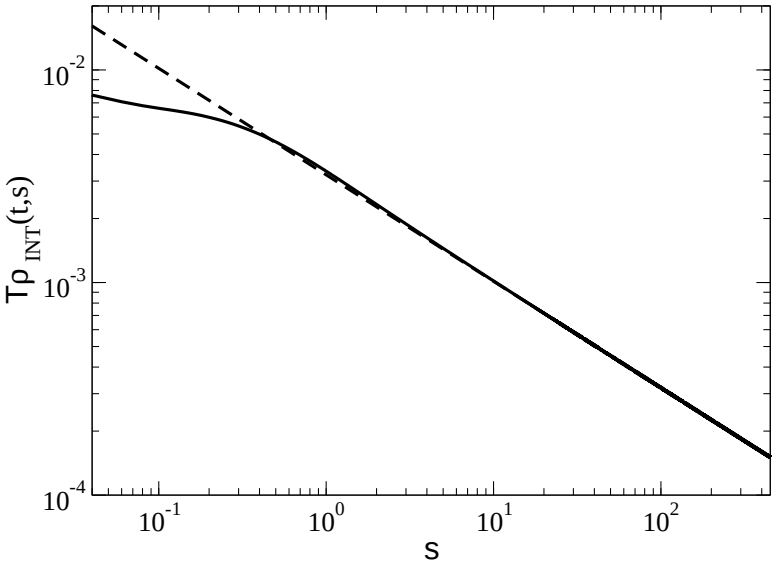

Figure 2.8: Integrated linear response $\rho_{\rm INT}(t,s)$ according to the intermediate protocol for the $3D$ mean spherical model with $T=2$, an infinite-temperature initial state and $x=20$. The full curve is the exact solution, the dashed line is a power-law fit $\sim s^{-0.5}$.

If $\Gamma = 0$, solution of the spherical constraint gives for $T < T_c$ the well-known exact result, valid for all values of d and in the aging regime $s \gg 1$ and $t - s \gg 1$ is, see Refs. [12, 15, 36, 37, 39, 57, 61, 62]

$$R(t,s) = r_0' \left(\frac{t}{s}\right)^{d/4} (t-s)^{-d/2} \tag{2.63}$$

with $r_0' = (4\pi)^{-d/2}$. From (2.2), we read off $a = (d-2)/2$ and $\lambda_R/z = d/4$. This exact result for a is in contradiction with the claim raised in Refs. [39, 57, 61, 62]. Furthermore, we see that the exact result Eq. (2.63) has precisely the form (2.4) predicted by local scale invariance [14, 15]. A similar test can be performed for $T = T_c$ [12, 15], or even in a spherical model with spatially long-ranged interactions [38]. It is important to note that the local scale invariance prediction (2.4) applies to the full response function $R(t,s)$ and not to the part remaining after subtraction of a 'stationary' term, as suggested in Ref. [57].

In summary we have argued that for ferromagnetic systems in class L, one should find saturation for the field-cooled susceptibility, viz. $\chi_{\rm FC}(t) \sim {\rm O}(1)$. While from the scaling form (2.2), one might have expected a simple scaling $\chi(t,s) \sim s^{-a}$ of the integrated response, we have shown that matters are

more complicated. Conceptually, the issue can be clarified by studying the scaling of the *field-cooled* susceptibility $\chi_{\rm FC}(t)$ and we have seen that two broad classes of systems must be distinguished, which are called classes S and L, according to whether their equilibrium spin-spin correlator shows short-ranged or long-ranged spatial decay, respectively [2].

If questions of simulational efficiency play no role, it might be technically easier to avoid both the ZFC and the TRM protocol, as already suggested in Ref. [57], for example, by using the 'intermediate' protocol [3], which runs as follows: quench the system at $t = 0$ without a magnetic field and fix a waiting time s. At time $s/2$, turn on a random magnetic field and keep it on until the waiting time s. Then turn the field off again and measure the magnetization at the observation time $t > s$. The *intermediate integrated response* is

$$\rho_{\rm INT}(t,s) = M_{\rm INT}(t,s)/h := \int_{s/2}^{s} {\rm d}u\, R(t,u) = s^{-a} f_{\rm INT}(t/s)\left(1 + {\rm o}(s^{-\lambda_R/z})\right) \tag{2.64}$$

and should be free of the leading term coming from the interface roughness as well as the finite-time correction of order $\mathrm{O}(s^{-\lambda_R/z})$. We illustrate this for the mean spherical model in figure 2.8, where it can be seen that already for short times much shorter than those in figure 2.6a), the the *linear* response (2.61) obtained from the exact solution of the Langevin equation (with $\Gamma = 0$) converges to the expected power law, with $a = 0.5$ in $3D$.

2.5 Dynamics in an oscillating field

Additional insight in the magnetization reversal transitions may be obtained by studying the system's response to a time-dependent, e.g. oscillating, magnetic field and the question is studied whether there exists a dynamic phase-transition at a finite and non-vanishing value of the period P of the field [67, 68]. Surprisingly, there is *no* such transition in the spherical model, although it is known to occur e.g. in the $2D$ Ising model.

The response of the system to a time-dependent external field $H = H(t)$ allows us to study hysteresis effects – related to the easily measured Barkhausen noise – and has been studied for a long time, see Refs. [69, 70] for reviews. From mean–field descriptions [67, 68, 71], one finds evidence that depending on the amplitude and the period P of $H(t)$, the time-dependent (and periodic) magnetization $S(t) = S(t + P)$ changes between two different forms. First, there is a single symmetric solution (corresponding to the

paramagnetic phase) such that

$$S(t + P/2) = -S(t). \tag{2.65}$$

Second, there may exist a pair of non-symmetric solutions in the ferromagnetic phase where (2.65) does not hold. Indeed, the existence of a dynamical phase transition was established beyond mean–field theory through simulations in the $2D$ Ising model with Glauber dynamics [45, 46, 47]. The order parameter of this transition is the period–averaged magnetization $Q = Q(t)$ defined as

$$Q(t) = \frac{1}{P} \int_{t-P}^{t} \mathrm{d}t' S(t'), \tag{2.66}$$

where P is the period of $H(t)$. In the Ising model for sufficiently strong fields and/or low frequencies $Q = 0$ and $S(t)$ oscillates around zero, but Q remains finite for smaller fields and higher frequencies and $S(t)$ then oscillates around one of the two values of the equilibrium magnetization. Detailed finite-size scaling analysis has shown that the exponents of $Q(t)$ and also of the associated susceptibility agree with those of the *equilibrium* phase transition of the $2D$ Ising model [45, 46, 49]. This was further backed up by showing that the equation of motion of the order parameter reduces to the ϕ^4-theory with noise [71] (similar studies were also performed on the equation of motion of the anisotropic XY model [72, 73]).

Still, this kind of non-equilibrium phase transition needs not generically to exist. It is therefore of interest to explore the role of the topology of the phase space further by considering a model in a different equilibrium universality class.

2.5.1 Behavior of the magnetization

Consider the spatially constant but time-dependent external field

$$H(t) = H_0 \sin\left(\frac{2\pi}{P} t\right). \tag{2.67}$$

The calculation of the observables follows the same lines as in the case of the constant field although a larger numerical effort is required. By inserting Eq. (2.35) into Eq. (2.66) the period-averaged magnetization $Q(t)$ is readily obtained. In figure 2.9a a typical example for $Q(t)$ is shown but the behavior seen in this case turns out to be generic. Taking the Ising model as a guide, a heuristic argument [68] suggests that a dynamic phase-transition should occur at least for all temperatures and field amplitudes H_0 for which a metastable state exists. Therefore the same values for T as before are used.

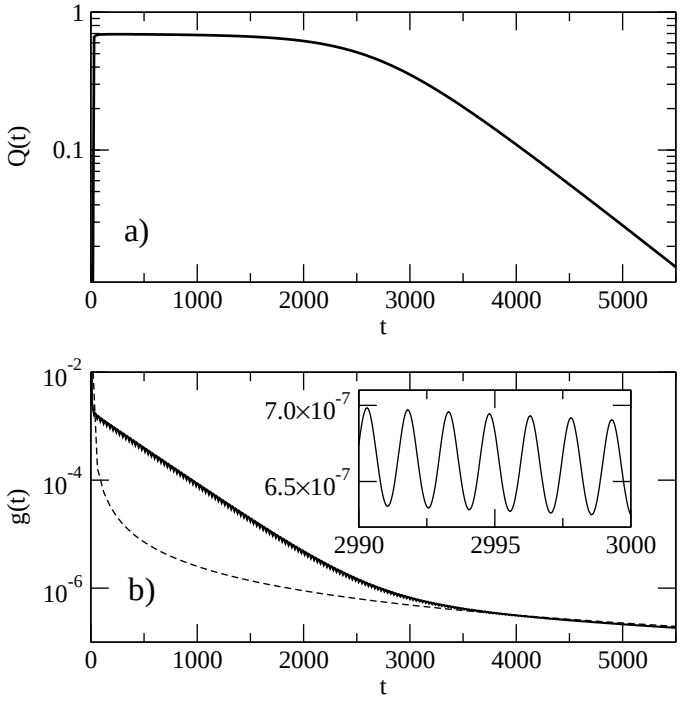

Figure 2.9: (a) The period-averaged magnetization $Q(t)$ for $d = 3$, $T = 2$, $S_0 = 0$, a sinusoidal external field with period $P = 1.5$ and amplitude $H_0 = 0.2$. (b) The Lagrange multiplier $g(t)$. On this scale only the behavior of the bounds can be seen between which oscillations take place; these oscillations are shown in the inset. The dashed line shows a power law $g(t) = 0.1\, t^{-1.54} \approx c\, t^{-d/2}$.

However, in the spherical model it is found that for small times $Q(t)$ takes a plateau value before it decays exponentially for later times. In principle, and in analogy with the Ising model, one might try to find the dynamic phase transition by measuring the time $\tau = \tau(P, H_0)$ when the transition between the plateau and the decay occurs. Following the practical experience of the Ising model either the scale of H or P can be normalized away, see Refs. [45, 46, 47]. It should therefore be enough to vary the period P (or the frequency) but keep the amplitude H_0 constant and map out $\tau(P, H_0)$. If there is a dynamic phase transition at some critical period P_c, the cross-over time should diverge $\tau(P_c, H_0) = \infty$. In practice, however, this method is quite slow, because the calculations have to be done for increasingly larger time-scales.

It is a lot more efficient to study the Lagrange multiplier $g(t)$ which is

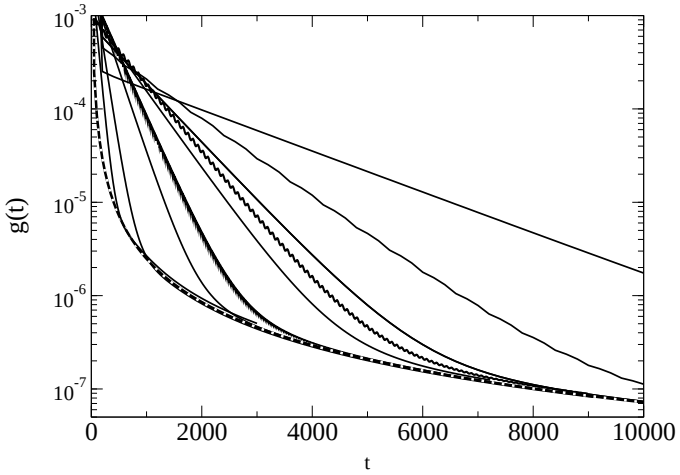

Figure 2.10: $g(t)$ for $d = 3$, $T = 2$ and a sinusoidal external field with $H_0 = 0.2$; the periods are $P = \{0.4; 0.6; 0.8; 0.9; 1; 1.5; 2; 5; 10\}$ (from top to bottom). The dashed line shows a function $g_{\rm mas}(t) = 0.1\, t^{-1.54} \approx c \cdot t^{-d/2}$

shown in figure 2.9b. We observe that the value of $g(t)$ oscillates between two bounds and the temporal behavior of the bounds correlates with the time-dependence of $Q(t)$. Namely, when $Q(t)$ displays a plateau, the bounds for $g(t)$ decay exponentially with time while in the region of the exponential decay of $Q(t)$ the bounds of $g(t)$ decay according to a power law. Therefore, the cross-over time $\tau(P, H_0)$ can be found by determining the intersection of the two regimes for the bounds for $g(t)$.

In figure 2.10 a typical behavior of $g(t)$ is displayed for several values of the period P. We observe the cross-over from a roughly exponential behavior $g_{\rm exp}(t) \approx \exp(-t/\mathfrak{t})$ with a relaxation time $\mathfrak{t}$ toward a master curve $g_{\rm mas}(t) \sim t^{-1.54}$ which is reached for all given values of P for sufficiently long times. In principle, one might try to estimate the time of cross-over between these two regimes by looking for the intersection of $g_{\rm exp}(t)$ and $g_{\rm mas}(t)$ and then further ask when this cross-over time will diverge in order to find the critical period P_c. Since for finite $\mathfrak{t}$ this intersection will always occur, a more reliable estimate of P_c will be given by the condition $\mathfrak{t}^{-1}(P_c, H_0) = 0$.

In figure 2.11 $\mathfrak{t}(P, H_0)$ is shown for $d = 3$ and $d = 5$, that is below and above the upper critical dimension of the equilibrium critical behavior. In all curves, we see that $\mathfrak{t}(P)$ remains finite for all values of P which have been considered. Phenomenologically, $\mathfrak{t} \sim 1/P^v$ for P small enough and some exponent $v > 0$ ($v \approx 1.4$ in $3D$; $v \simeq 1.95$ in $5D$). The fact that $\mathfrak{t}$ only diverges as $P \to 0$ is evidence that there is *no DPT* in the spherical model in

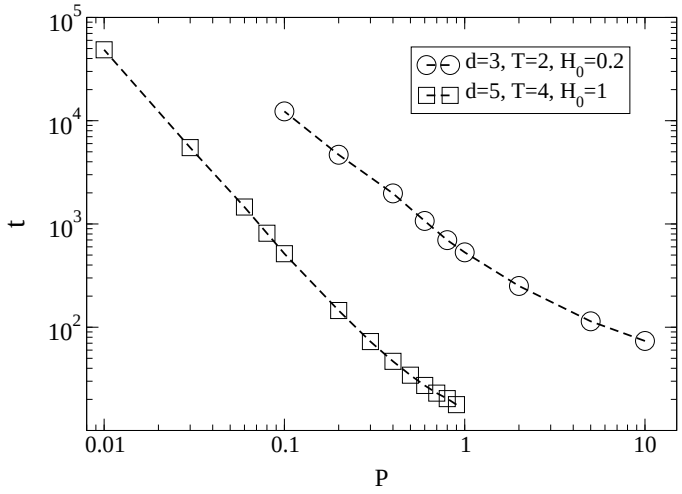

Figure 2.11: $\mathfrak{t}(P, H_0)$ for $d = 3$ and $d = 5$ as read off from $g_{\rm exp}(t)$, see text.

an oscillating magnetic field, in contrast to established results [45, 46, 47, 49] in the 2D Ising model and also with results on the $n \to \infty$ limit of the O(n) model [74, 75]. We also see from figure 2.11 that the absence of the DPT is not related to whether or not the equilibrium phase transition of the spherical model is in the mean–field regime.

2.5.2 Behavior of the Lagrange multiplier

By fitting $g_{\rm mas}(t)$ for $d = 3$ and $d = 5$ exponents of $w = 1.52 \pm 0.01$ and $w = 2.51 \pm 0.01$ respectively are found. From these observations, we conjecture that for sufficiently long times, the Lagrange multiplier $g(t)$ satisfies the bounds

$$C_1 \leq t^w g(t) \leq C_2 \tag{2.68}$$

with an exponent $w = d/2$ and some constants $C_{1,2}$. Indeed, we have also checked that these bounds hold not only for sinusoidal fields $H(t)$, but for triangular and rectangular oscillating fields as well. Remarkably, the conjectured exponent $w = d/2$ of the power-law bounds Eq. (2.68) coincides with the same value found for the kinetic spherical model *without* a magnetic field [37] ! We have checked this for several values of the dimension d and temperatures $T > 0$. In Ref. [1], the bounds (2.68) are derived analytically and especially the exponent $w = d/2$ in the $P \to 0$ limit and for $T = 0$, under mild additional conditions. A fully disordered initial state simplifies the calculations but the result remains the same for any short-ranged initial correlators. Therefore, the relaxation time $\mathfrak{t}(P, H_0)$ is formally infinite for

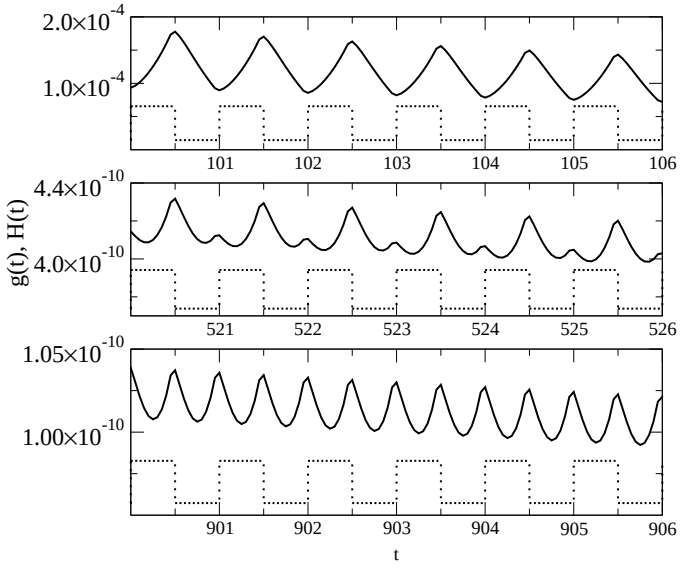

Figure 2.12: $g(t)$ (full line) compared to $H(t)$ (dotted line, scaled and shifted) for different times. These calculations were done for $d = 5$, $T = 4$, $S_0 = 0$ and a rectangular external field with amplitude $H_0 = 0.6$ and with period $P = 1$.

$P \ll 1$ and $T = 0$. Thus the *absence of a DPT is shown in the physical situation where it would have been expected to be seen first.* In this respect, the spherical model behaves in quite a different way than the Ising model. The rigorous derivation of Eq. (2.68) is left as an open mathematical problem.

The absence of a dynamical phase transition is further illustrated in figure 2.12. There $g(t)$ is compared with a rectangular field $H(t)$ (scaled and shifted for convenience). While for small times, $g(t)$ oscillates with the driving period P, we see that with t increasing, an additional peak builds up until $g(t)$ oscillates with half the period of the driving field at late times. The fact that $g(t)$ oscillates with half the external period P is an indication that the system is described by the symmetric solution, see Eq. (2.65). The same kind of period-halving is also found for triangular and sinusoidal fields.

This phenomenon is easily understood: since for small times the magnetization oscillates around a non-vanishing value, the global symmetry is broken and the two half-periods of the external field affect the system in two qualitatively different ways. However, for later times the magnetization oscillates around zero and there is no qualitative difference of the response of the system between the two half-periods of the external field any more. This fact is reflected by $g(t)$ actually becoming periodic with period $P/2$,

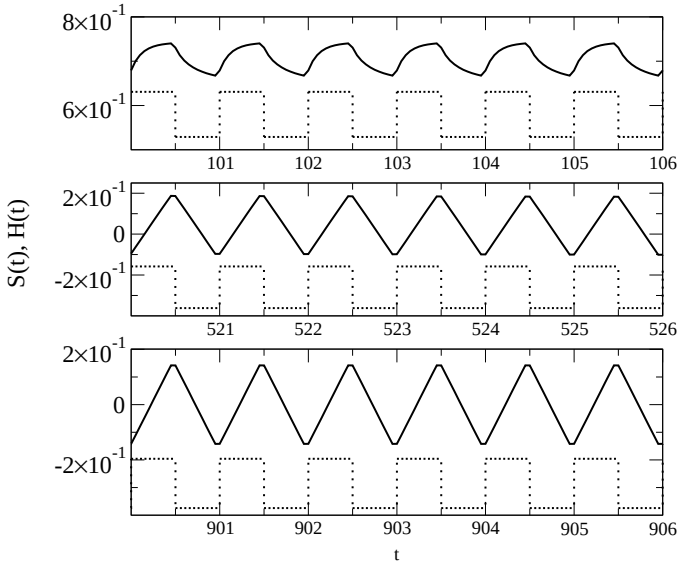

Figure 2.13: Time evolution of the mean magnetization $S(t)$ (full line) compared to the one of a rectangular magnetic field $H(t)$ (dotted line, scaled and shifted) for different time regimes; the parameters are as in fig. 2.12.

viz. $g(t + P/2) = g(t)$.

The behavior of $S(t)$ is illustrated in figures 2.13, 2.14, and 2.15. For relatively small times (upper panel), $S(t)$ oscillates around the positive equilibrium value and is periodic with period P. It is interesting to note that the qualitative shape of $S(t)$ for the rectangular oscillating external field in this regime matches closely the one observed in the dynamically ordered phase of the $2D$ Ising model, see Ref. [46, figure 2(b)]. For larger times, the dynamic order parameter $Q(t)$ decreases until $S(t)$ oscillates around zero. The slow cross-over toward a solution which satisfies Eq. (2.65) is illustrated in the middle panels of figures 2.13-2.15 and in the lowest panels, a situation near to (2.65) is reached, where $S(t)$ becomes *anti*periodic with period $P/2$. In the case of a rectangular field shown in figure 2.13 the external magnetic-field amplitude is still rather small which results in a linear increase and decrease of the magnetization. For stronger fields the magnetization reaches saturation during one half–period and the behavior of $S(t)$ deviates from piecewise linearity. The comparison to the sinusoidal and triangular oscillating external field shows that in all three cases the magnetization follows the integrated external field for not too large amplitudes.

The main result of this section is surprising: in spite of the fact that for $T < T_c$ there are just two equilibrium states for both the Ising and

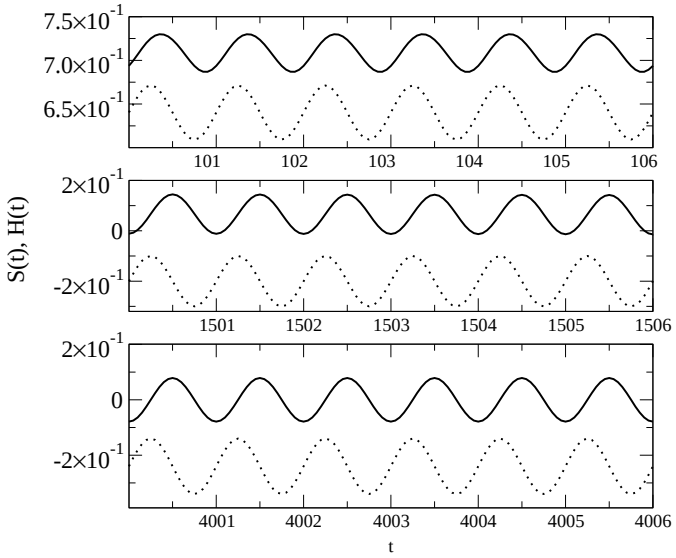

Figure 2.14: Time evolution of the mean magnetization $S(t)$ (full line) compared to the one of a sinusoidal magnetic field $H(t)$ with amplitude $H_0 = 0.5$ (dotted line, scaled and shifted) for different time regimes; the other parameters are as in fig. 2.12.

the spherical models in a (sufficiently small) constant magnetic field, the well-established dynamic phase-transition of the Ising model in a temporally oscillating magnetic field is apparently *absent in the spherical model*.

2.6 Conclusions

In this chapter we have investigated the non-equilibrium behavior of the spherical model in an external magnetic field. The model's dynamics is described in terms of a Langevin equation and all quantities of physical interest can be expressed exactly in terms of the solution of a non-linear Volterra integral equation. In few especially simple cases this Volterra equation can be solved exactly, but we have in general used numerical methods.

First, we studied the magnetization reversal transition, in a temporally constant magnetic field, which occurs if the system is initially prepared near to the metastable state from which it relaxes toward the unique equilibrium state. We find that the system evolves first into the metastable state quickly and remains there for considerably long times until it finally relaxes into the stable state. For not too large magnetic fields, this transition passes through

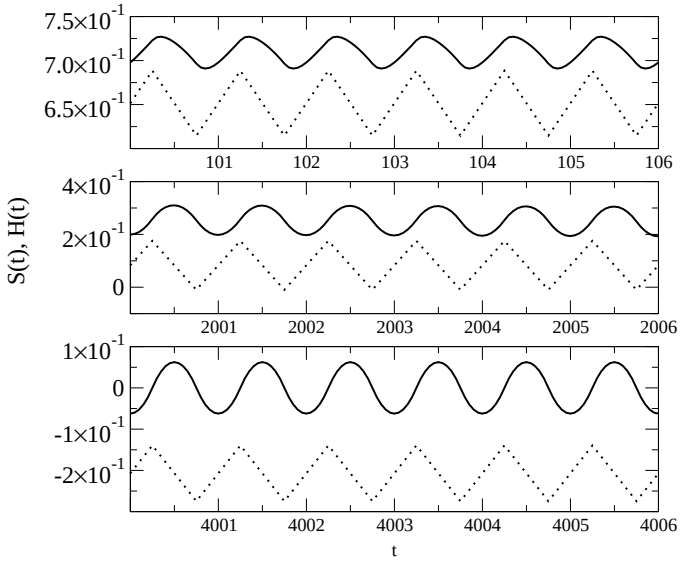

Figure 2.15: Time evolution of the mean magnetization $S(t)$ (full line) compared to the one of a triangular magnetic field $H(t)$ with amplitude $H_0 = 0.5$ (dotted line, scaled and shifted) for different time regimes; the other parameters are as in fig. 2.12.

transient states with long-ranged correlations of fluctuations, which means that during the magnetization-reversal transition whole domains rather than single uncorrelated spins turn over.

The two-time autocorrelation function is mainly determined by the magnetization so that connected correlation functions, which are more sensible to fluctuations, reveal more information. Again we find that the transition involves long-ranged correlations. For times smaller than the transition time ϑ we find an effective equilibrium behavior although the system is merely in the metastable state. In many respects, notably the fluctuation-dissipation relations, we find a close analogy with the aging behavior encountered in the absence of an external field. But approaching the magnetization-reversal the autoresponse function and the fluctuation-dissipation ratio show unusual behavior, indicating that the process is rather complex. Therefore, although the non-vanishing magnetic field H sets a finite time scale for the relaxation toward the single equilibrium state, we have found a very rich transient behavior which in many respects is quite analogous to the true aging behavior found without an external field.

Second, the scaling of the linear response function was investigated. It was numerically verified that the scaling forms describe a crossover between

two power law regimes. For the integrated response functions, the zero–field cooled susceptibility χ_{ZFC} and the thermoremanent magnetization ρ_{TRM}, it is shown that the behavior of the former is not suitable to investigate aging while the one of the latter is. This is done by demonstrating that the field–cooled susceptibility is unrelated to aging and this behavior dominates the scaling of χ_{ZFC}. These results are crucial when numerical results are interpreted.

Third, we looked for a dynamic phase transition in a time-dependent external magnetic field $H(t)$. Surprisingly, we find evidence that a dynamic non-equilibrium phase transition, which is known to occur e.g. in the Ising model, apparently does not exist in the spherical model. For sufficiently low temperatures, we rather find that although the dynamic order parameter $Q(t)$ reaches a plateau value for small times, there is always a cross-over to a late-time regime where $Q(t)$ decays away to zero. On a technical level, this finding can be represented through the conjecture Eq. (2.68) which points to an unexpected similarity with the phase-ordering kinetics of the *zero-field* spherical model.

Given that several equilibrium properties of the isotropic O(3) Heisenberg model are closer to the ones of the spherical model than they are to the Ising model (see introduction), our results raise the question whether a dynamic phase transition for the *isotropic* O(3) Heisenberg model in an oscillating field exists.[4] Recently it has been argued [78] that in the Heisenberg model the existence of uniaxial unisotropy is essential for observing a DPT which affirms our results.

Lastly, our results raise the questions what are the effects of a magnetic field on the kinetics of a spin-glass and what becomes of the magnetization reversal transition and the dynamical phase transition. However, because of the well-known equivalence [36] between the spherical spin-glass and the spherical ferromagnet, studies in different systems with a true glassy behavior[5] are needed to shed light on this issue.

[4]Existing articles on the DPT in Heisenberg models are either mean–field studies [50] or consider the anisotropic case [76, 77] (which should be more Ising-like). One might anticipate the existence of a critical n_c such that in the O(n)-model in an oscillating field, there is a DPT for $n < n_c$ analogously to the Ising model and none for $n > n_c$.

[5]The equilibrium behavior of the Ising spin glass in a magnetic field has been studied in detail, see Ref. [79] and references therein. For the spherical spin glass in an oscillating magnetic field short-time numerical calculations give evidence in favor of a dynamic phase transition *at* $T = 0$ [66].

2.7 Appendix: Numerical method

The numerical solution of the nonlinear Volterra equation (2.20) is discussed briefly, adapting standard methods [80] to the case at hand.

Eq. (2.20) is cast into the following form, using the equations (2.22) and (2.23)

$$\begin{aligned} g(t) &= (1-S_0^2)f(t) + S_0^2 + 2T\int_0^t \mathrm{d}t'\, f(t-t')g(t') + 2S_0\int_0^t \mathrm{d}t'\, H(t')\sqrt{g(t')} \\ &\quad + \left(\int_0^t \mathrm{d}t'\, H(t')\sqrt{g(t')}\right)^2 . \end{aligned} \tag{2.69}$$

As a first step we will discretize the time by dividing the time interval in $N-1$ segments of length k

$$t_i = k\,i \;\;;\;\; i = 0, 1, \ldots, N-1. \tag{2.70}$$

The continuous functions $f(t)$ are replaced by the N–dimensional vectors

$$\boldsymbol{f} = (f_0, f_1, \ldots, f_N - 1)^T \;\;,\;\; f_i = f(t_i) \tag{2.71}$$

and the integrals are replaced by a sum by means of the extended trapezoidal rule [80]

$$\int_{x_0}^{x_{N-1}} \mathrm{d}x f(x) \approx k\left[\frac{1}{2}f_0 + f_1 + f_2 + \ldots + f_{N-2} + \frac{1}{2}f_{N-1}\right]. \tag{2.72}$$

Therefore, we have the set of equations

$$\begin{aligned} F_0\left((g_0, \sqrt{g_0}\right), \boldsymbol{f}, \boldsymbol{H}, k) &= 0 \\ F_1\left((g_0, \sqrt{g_0}\right), (g_1, \sqrt{g_1}), \boldsymbol{f}, \boldsymbol{H}, k) &= 0 \\ &\ldots \\ F_{N-1}\left((g_0, \sqrt{g_0}\right), (g_1, \sqrt{g_1}), \ldots, (g_{N-1}, \sqrt{g_{N-1}}), \boldsymbol{f}, \boldsymbol{H}, k) &= 0, \end{aligned} \tag{2.73}$$

depending on the known vectors $\boldsymbol{f}$ and $\boldsymbol{H}$ and the step size k. We have

$F_0 = g_0 - 1$ and

$$F_i\left(\left(g_0, \sqrt{g_0}\right), \ldots, \left(g_i, \sqrt{g_i}\right), \boldsymbol{f}, \boldsymbol{H}, k\right) = g_i \left[Tkf_0 + \frac{1}{4}k^2 H_i^2 - 1\right]$$
$$+\sqrt{g_i}\left[S_0 k H_i + k^2\left(\frac{1}{2}H_0\sqrt{g_0} + \sum_{j=1}^{i-1} H_j\sqrt{g_j}\right) H_i\right]$$
$$+\left(1 - S_0^2\right) f_i + S_0^2 + 2Tk\left(\frac{1}{2}f_i g_0 + \sum_{j=1}^{i-1} f_{i-j} g_j\right)$$
$$+2S_0 k\left(\frac{1}{2}H_0\sqrt{g_0} + \sum_{j=1}^{i-1} H_j\sqrt{g_j}\right) + k^2\left(\frac{1}{2}H_0\sqrt{g_0} + \sum_{j=1}^{i-1} H_j\sqrt{g_j}\right)^2 . \quad (2.74)$$

This set of equations can be solved iteratively: F_0 determines g_0, F_1 then leads to g_1 and so on. However, since the F_i are functions of g_i and $\sqrt{g_i}$ at each step of iteration two *a priori* distinct solutions for the g_i are found. They may be obtained by replacing $G_i = \sqrt{g_i}$ and solving the resulting quadratic equation in G_i. So the question arises which of these solutions has to be used.

We calculated the two solutions for $\boldsymbol{g}$ when only using either the solution according to the positive root ('+'–curve) or the negative one ('–'–curve) — the exact solution should evolve somewhere between these two limiting curves. We found that decreasing the step size k results in an approach of the '–'–curve to the '+'–curve where the latter one only slightly changes. Finally choosing a sufficient small k the two curves collapse, so that the exact solution is found. For larger values of k the '+'–curve shows only small deviations to the limiting curve, so that in all calculations this solution was used.

For all calculations a step size of $k = 10^{-2}$ was sufficient, except for the data shown in Fig. 2.2 where $k = 10^{-4}$ was used because there the time scale is much smaller.

The evaluation of the one– or two–time observables proceeds by a straightforward implementation of their defining integrals by the extended trapezoidal rule.

Chapter 3

Bosonic pair contact process with diffusion

3.1 Introduction

In this chapter the variance of the local density of the pair contact process with diffusion (PCPD) is investigated in a bosonic description. The results are partly published in Ref. [4].

A prototypical example for critical phenomena in non–equilibrium statistical physics are the absorbing phase transitions. These are transitions from an active fluctuating phase with a finite particle density to an absorbing state where any dynamics is suppressed. One has found rather robust universality classes, e.g. the class of directed percolation (DP) and the parity conserving universality class (PC). For a review see Ref. [81]. A member of the DP–class is the pair contact process where two neighboring particles may create an offspring on a third lattice site or may annihilate each other.

This model extended by particle diffusion – the pair contact process with diffusion (PCPD) – has attracted much interest because it is not known to which universality class it belongs. Several possibilities have been discussed: It was found that some exponents are very close to those of the PC class [82], more recent investigations however give hints for a DP behavior [83]. It was also suggested that the critical behavior of the PCPD defines a new universality class [84, 85], or may depend on the diffusion constant [86]. Analytical results are rare in this field and one has to revert to numerical methods like the density matrix renormalization group (DMRG) or Monte Carlo simulations. For a comprehensive review of the current state of the art we refer to [87].

In most cases models with exclusion interaction, which constraints the number of particles at a site to at most one, are considered. However, analytical treatment becomes easier for the bosonic description of the model where the exclusion interaction is dropped. In this case a field theoretic approach due to Howard and Täuber [88] is available. A drawback of this approach is that it is not suitable for deciding the universality class of the model with particle number restriction. In this chapter we show by an exact treatment of the model that the diffusion constant and the lattice dimension have considerable impact on the phase transition and correlations of the bosonic PCPD. To this end the first, second and third moment of the particle distribution function are solved. Although the particle exclusion interaction is crucial for the behavior of the system this investigation gives some insight on the role of diffusion in the PCPD.

In the theory of absorbing phase transitions the calculation of critical exponents plays a central role in order to determine the respective universality class. One possibility to determine critical exponents is to consider the scaling of stationary quantities with respect to the distance from the critical

point $\Delta = p - p_c$ where p is the control parameter and p_c the critical point. One defines the exponents $\beta, \beta', \nu_\perp, \nu_\parallel$ by

$$\begin{aligned} \rho^{\text{stat}} &\propto \Delta^{\beta}, \\ P_\infty &\propto \Delta^{\beta'}, \\ \chi_\perp &\propto |\Delta|^{\nu_\perp}, \\ \chi_\parallel &\propto |\Delta|^{\nu_\parallel}, \end{aligned} \tag{3.1}$$

where ρ^{stat} is the stationary particle density, P_∞ is the ultimate survival probability, i.e. the probability that a randomly chosen site belongs to an infinite cluster, and $\chi_\perp, \chi_\parallel$ are the spatial and temporal correlation lengths.

Another possibility is given by dynamical scaling where the time dependence of the quantities when started from an initial seed is used to define the exponents. At the critical point, $\Delta = 0$, one defines:

$$\begin{aligned} P(t) &\propto t^{-\delta}, \\ \rho(t) &\propto t^{-\alpha}, \\ \langle N(t) \rangle &\propto t^{\theta}, \end{aligned} \tag{3.2}$$

where $P(t)$ is the probability that a system survives at time t, i.e. that there are still active particles left, $\rho(t)$ is the particle density *inside* an active cluster and $\langle N(t) \rangle$ is the particle number averaged over *all*, i.e., active and inactive, systems. This set of exponents is not independent of the previous set, one can deduce generally [81]

$$\delta = \beta'/\nu_\parallel, \qquad \alpha = \beta/\nu_\parallel. \tag{3.3}$$

Furthermore the following argument gives another relation between the exponents: The particle density inside an active cluster is given by the particle number in a specific *active* system, $N(t)$ divided by the spreading region $R(t)$

$$\rho(t) = \left\langle \frac{N(t)}{R(t)} \right\rangle_{\text{active}}, \tag{3.4}$$

here $\langle \cdot \rangle_{\text{active}}$ indicates that the average is taken only over active systems. For large times one expects that

$$\left\langle \frac{N(t)}{R(t)} \right\rangle_{\text{active}} \propto \frac{\langle N(t) \rangle / P(t)}{\langle R(t) \rangle} \propto t^{\theta+\delta-d/z}, \tag{3.5}$$

as the spreading region scales like $t^{d/z}$ where d is the dimension and $z = \nu_\parallel/\nu_\perp$ is the dynamical exponent. Thus we get the hyperscaling relation

$$\theta - d/z = -(\alpha + \delta). \tag{3.6}$$

A more rigorous derivation of the hyperscaling relation for continuous transitions can be found in Ref. [81] which is not applicable here.

An outstanding property of the bosonic PCPD is the fact that some of the critical exponents are known exactly. We use this information to test the commonly considered hyperscaling relation for the critical exponents. As still some quantities are not accessible analytically Monte Carlo simulations are used to get the complete set of exponents. It turns out that in some cases simulations of the bosonic PCPD are misleading in general.

In section 3.2 the definition of the model given in Ref. [88] is recalled in a general form and the formalism used to derive the differential equations is explained. In section 3.3 a special case, the bosonic contact process with diffusion, is investigated. In section 3.4 a more interesting case, the PCPD is considered and the solution of the autocorrelation function is derived; in section 3.5 the spatial dependence of the correlations is calculated. Section 3.6 deals with the 3^{rd} moment of the PCPD. While all the previous sections consider spatially homogeneous initial conditions, in section 3.7 the case of an initial seed consisting of only two particles is investigated. This situation is usually called spreading.

3.2 Model

We define the following process: On a infinite d–dimensional cubic lattice particles ('A') are diffusing with rate D, in each spatial direction. Additionally they branch and annihilate: $k \geq 1$ particles A are created with rate μ out of any set of $m \geq 1$ particles (m fixed), and $l \geq 1$ particles are annihilated with rate λ out of any set of $p \geq l$ particles (l fixed):

$$\begin{aligned} mA &\xrightarrow{\mu} (m+k)A \\ pA &\xrightarrow{\lambda} (p-l)A \\ A\cdot &\xleftrightarrow{D} \cdot A. \end{aligned} \tag{3.7}$$

The number of particles on each lattice site is not restricted – the creation and annihilation processes take place on one lattice site. Thus the bosonic representation of the process is used. We try to keep the description as general as possible, but as we will see, analytical results are available only for few cases. In this chapter we investigate the two cases where $p = m = 1$ or $p = m = 2$ and arbitrary k and $l \leq p$. One special case is the PCPD, where $m = p = l = 2$ and $k = 1$.

Following the notation and formalism introduced in Refs. [89, 90] we define the site occupation numbers as $\boldsymbol{n} = \{n(\mathbf{x})\}$. Then the time dependent

probability vector describing the system can be expressed as

$$|F(t)\rangle = \sum_{n(\mathbf{x})} P(\boldsymbol{n}, t)\, |\boldsymbol{n}\rangle \tag{3.8}$$

where the $|\boldsymbol{n}\rangle$ are the basis vectors spanning the state space and $P(\boldsymbol{n}, t)$ is the probability distribution of the site occupation numbers. The master equation describing the time evolution of the probability distribution can then be written as

$$\frac{\partial}{\partial t} |F(t)\rangle = -\mathcal{H} |F(t)\rangle , \tag{3.9}$$

$\mathcal{H}$ is the stochastic generator of the system, often called as "Hamiltonian" due to the analogy of the master equation to the Schrödinger equation (in imaginary time) [91]. Let $a(\mathbf{x})$ and $a(\mathbf{x})^\dagger$ be the space dependent annihilation and creation operators and $n(\mathbf{x}) = a^\dagger(\mathbf{x})a(\mathbf{x})$ the particle number operator, then the Hamiltonian is given by

$$\begin{aligned} \mathcal{H} \;=\; & -D \sum_{k=1}^{d} \sum_{\mathbf{x}} \left[a(\mathbf{x})a^\dagger(\mathbf{x}+\mathbf{k}) + a^\dagger(\mathbf{x})a(\mathbf{x}+\mathbf{k}) - 2n(\mathbf{x}) \right] \\ & -\lambda \sum_{\mathbf{x}} \left[\left(a^\dagger(\mathbf{x})\right)^{(p-l)} \left(a(\mathbf{x})\right)^p - \prod_{i=1}^{p} \left(n(\mathbf{x}) - i + 1\right) \right] \\ & -\mu \sum_{\mathbf{x}} \left[\left(a^\dagger(\mathbf{x})\right)^{(m+k)} \left(a(\mathbf{x})\right)^m - \prod_{i=1}^{m} \left(n(\mathbf{x}) - i + 1\right) \right], \end{aligned} \tag{3.10}$$

where $\mathbf{k} \equiv \mathbf{k}(k) = (\ldots, 0, 1, 0, \ldots)^T$ is the k-th unit space vector. The time evolution of an operator $b(\mathbf{y})$ is calculated by

$$\frac{\partial}{\partial t} b(\mathbf{y}) = [\mathcal{H}, b(\mathbf{y})]. \tag{3.11}$$

Using the commutator rule $\left[a(\mathbf{x}), a^\dagger(\mathbf{y})\right] = \delta_{\mathbf{x},\mathbf{y}}$ we get after straightforward

calculations

$$\begin{aligned}
\frac{\partial}{\partial t}\langle a(\mathbf{x})\rangle &= D\sum_{k=1}^{d}\{\langle a(\mathbf{x}-\mathbf{k})\rangle + \langle a(\mathbf{x}+\mathbf{k})\rangle - 2\langle a(\mathbf{x})\rangle\} \qquad (3.12)\\
&\quad -\lambda l\langle a(\mathbf{x})^p\rangle + \mu k\langle a(\mathbf{x})^{\mathbf{m}}\rangle\\
\frac{\partial}{\partial t}\langle a(\mathbf{x})a(\mathbf{y})\rangle &\underset{\mathbf{x}\neq\mathbf{y}}{=} D\sum_{k=1}^{d}\{\langle a(\mathbf{x})a(\mathbf{y}-\mathbf{k})\rangle + \langle a(\mathbf{x})a(\mathbf{y}+\mathbf{k})\rangle + \qquad (3.13)\\
&\quad \langle a(\mathbf{x}-\mathbf{k})a(\mathbf{y})\rangle + \langle a(\mathbf{x}+\mathbf{k})a(\mathbf{y})\rangle - 4\langle a(\mathbf{x})a(\mathbf{y})\rangle\}\\
&\quad -\lambda l\{\langle a(\mathbf{x})a(\mathbf{y})^p\rangle + \langle a(\mathbf{x})^p a(\mathbf{y})\rangle\}\\
&\quad +\mu k\{\langle a(\mathbf{x})a(\mathbf{y})^m\rangle + \langle a(\mathbf{x})^m a(\mathbf{y})\rangle\}\\
\frac{\partial}{\partial t}\left\langle (a(\mathbf{x}))^2\right\rangle &= 2D\sum_{k=1}^{d}\left\{\langle a(\mathbf{x})a(\mathbf{x}-\mathbf{k})\rangle + \langle a(\mathbf{x})a(\mathbf{x}+\mathbf{k})\rangle - 2\left\langle a(\mathbf{x})^2\right\rangle\right\}\\
&\quad +\lambda l\{\ (1+l-2p)\ \langle a(\mathbf{x})^p\rangle - 2\left\langle a(\mathbf{x})^{p+1}\right\rangle\} \qquad (3.14)\\
&\quad -\mu k\{\ (1-k-2m)\langle a(\mathbf{x})^m\rangle - 2\left\langle a(\mathbf{x})^{m+1}\right\rangle\}.
\end{aligned}$$

Using $\langle n(\mathbf{x})\rangle = \langle a(\mathbf{x})\rangle$ and $\langle n(\mathbf{x})^2\rangle = \langle a(\mathbf{x})^2\rangle + \langle a(\mathbf{x})\rangle$ this set of coupled difference–differential equation allows for the analytical calculation of the time–dependent expectation value of the particle density and its autocorrelation in some special cases.

We restrict to the case $p = m$ where the creation and annihilation processes are balanced and an absorbing phase transition can be found. For $\lambda l > \mu k$ the particles die out exponentially ($p = m = 1$) or according to a power law ($p = m > 1$), while for $\lambda l < \mu k$ the particle density diverges. Here a crucial difference between the description with and without particle number restriction can be seen: While in the models with exclusion interaction the absorbing phase transition is of second order, the bosonic model exhibits a first order transition.

In analogy to the exclusion model we call the rate which divides the two different behaviors the "critical" rate, which from Eq. (3.12) can be read off as

$$\lambda_c = \mu k/l \qquad (3.15)$$

for given μ. For this rate the particle density is constant for all times $\langle a(\mathbf{x},t)\rangle = \rho_0$ (for homogeneous initial conditions), as can be seen from Eq. (3.12) which reduces to a diffusion equation. Thus the interesting quantity is the variance $\sigma^2 = \langle n(\mathbf{x})^2\rangle - \langle n(\mathbf{x})\rangle^2$ which we shall investigate in what follows.

Eliminating p and λ in Eqs. (3.12)-(3.14) one gets

$$\begin{aligned}
\frac{\partial}{\partial t}\langle a(\mathbf{x})\rangle =& D\sum_{k=1}^{d}\{\langle a(\mathbf{x}-\mathbf{k})\rangle + \langle a(\mathbf{x}+\mathbf{k})\rangle - 2\langle a(\mathbf{x})\rangle\} \\
\frac{\partial}{\partial t}\langle a(\mathbf{x})a(\mathbf{y})\rangle \underset{\mathbf{x}\neq\mathbf{y}}{=} & D\sum_{k=1}^{d}\{\ \langle a(\mathbf{x})a(\mathbf{y}-\mathbf{k})\rangle + \langle a(\mathbf{x})a(\mathbf{y}+\mathbf{k})\rangle + \\
& \langle a(\mathbf{x}-\mathbf{k})a(\mathbf{y})\rangle + \langle a(\mathbf{x}+\mathbf{k})a(\mathbf{y})\rangle - 4\langle a(\mathbf{x})a(\mathbf{y})\rangle\ \} \\
\frac{\partial}{\partial t}\left\langle (a(\mathbf{x}))^2\right\rangle =& 2D\sum_{k=1}^{d}\left\{\langle a(\mathbf{x})a(\mathbf{x}-\mathbf{k})\rangle + \langle a(\mathbf{x})a(\mathbf{x}+\mathbf{k})\rangle - 2\left\langle a(\mathbf{x})^2\right\rangle\right\} \\
& + \mu k(k+l)\langle a(\mathbf{x})^m\rangle\,.
\end{aligned} \tag{3.16}$$

We see that this set of equations is only closed for the cases $m = 1$ or $m = 2$.

In the case of a vanishing diffusion constant, $D = 0$, the lattice sites are independent of each other. Thus the description of the process reduces to the zero–dimensional case $d = 0$,

$$\begin{aligned}
\frac{\partial}{\partial t}\langle a(\mathbf{x})\rangle =& 0 \\
\frac{\partial}{\partial t}\left\langle (a(\mathbf{x}))^2\right\rangle =& \mu k(k+l)\langle a(\mathbf{x})^m\rangle\,,
\end{aligned} \tag{3.17}$$

and has to be treated separately.

3.3 Contact process with diffusion, $m = 1$

Here, only $l = 1$ is possible. Additionally by rescaling μ we may fix $k = 1$. This case has already been considered in Ref. [92] as a model for clustering of biological organisms [93]. For convenience we summarize the main results here.

For $D = 0$ or $d = 0$ Eq. (3.17) directly yields $\langle a(\mathbf{x})^2\rangle = c_0 + c_1\, t$ and thus the variance diverges. For $D \neq 0$ the fluctuations of the particle density diverges for dimensions $d \leq 2$ while they remain finite for $d > 2$,

$$\left\langle (a(\mathbf{x}))^2\right\rangle = \begin{cases} c_1\, t^{-d/2+1} & d < 2 \\ c_2\, \ln t & d = 2 \\ c_3 + c_4\, t^{-d/2+1} & d > 2 \end{cases} \tag{3.18}$$

where $t \gg 1$ and $c_0, \ldots, c_4$ are positive constants.

3.4 Pair contact process with diffusion, $m = 2$

We now analytically derive the late time behavior of the solution for $m = 2$.

For $D = 0$ or $d = 0$ Eq. (3.17) yields

$$\begin{aligned} \left\langle (a(\mathbf{x}))^2 \right\rangle &= \rho_0^2 \exp(t/\tau), \\ \tau &= \frac{1}{\mu k(k+l)}. \end{aligned} \tag{3.19}$$

The variance diverges exponentially in time as opposed to $m = 1$ where the divergence is linear. Only for times small compared to τ the variance Eq. (3.19) grows linearly.

For $D \neq 0$ we get the solution by applying Fourier– and Laplace–transformations. We also present the crossover from short to late time behavior, which has to be calculated numerically.

First we rescale time by

$$t \to \frac{t}{2D}, \tag{3.20}$$

and define

$$\begin{aligned} F_{\mathbf{x}}(\mathbf{r}, t) &= \langle a(\mathbf{x}) a(\mathbf{x}+\mathbf{r}) \rangle = \langle n(\mathbf{x}) n(\mathbf{x}+\mathbf{r}) \rangle - \delta_{\mathbf{r},\mathbf{0}} \langle n(\mathbf{x}) \rangle \\ \alpha &= \frac{\mu k(k+l)}{2D}. \end{aligned} \tag{3.21}$$

The parameter α is a measure for the weighting of reaction rates to diffusion, small α corresponds to dominant diffusion, while large α corresponds to dominating reaction rates. In what follows we consider only translational invariant initial conditions, in which case $F_{\mathbf{x}}(\mathbf{r}, t)$ is independent of $\mathbf{x}$. Using Eq. (3.16) we get the following difference–differential equation for F:

$$\begin{aligned} \frac{\partial}{\partial t} F(\mathbf{r}, t) &= \sum_{k=1}^{d} \{F(\mathbf{r}-\mathbf{k}, t) + F(\mathbf{r}+\mathbf{k}, t) - 2F(\mathbf{r}, t)\} + \delta_{\mathbf{r},\mathbf{0}} \alpha F(\mathbf{0}, t) \\ &= \sum_{k=1}^{d} \Delta_k F(\mathbf{r}, t) + \delta_{\mathbf{r},\mathbf{0}} \alpha F(\mathbf{0}, t) \end{aligned} \tag{3.22}$$

where Δ_k is the discrete Laplacian concerning the k–th component. The variance σ^2 is related to F as follows

$$\sigma(t)^2 = F(\mathbf{0}, t) + \rho_0 - \rho_0^2. \tag{3.23}$$

Here, we see that there is no qualitative difference between parity conserving models (k and l even) and non–parity conserving models — models with different k and l differ only by different creation and annihilation rates.

This kind of equation can be solved using the Fourier–transformation:

$$f(\mathbf{q},t)=\sum_{\mathbf{r}}\mathrm{e}^{-i\mathbf{q}\mathbf{r}}F(\mathbf{r},t),\qquad F(\mathbf{r},t)=\int\frac{\mathrm{d}^d\mathbf{q}}{(2\pi)^d}\mathrm{e}^{i\mathbf{q}\mathbf{r}}f(\mathbf{q},t). \tag{3.24}$$

We get

$$\frac{\partial}{\partial t}f(\mathbf{q},t)=-w(\mathbf{q})f(\mathbf{q},t)+\alpha F(\mathbf{0},t), \tag{3.25}$$

with the dispersion relation $w(\mathbf{q})=-2\sum_{k=1}^{d}(\cos(q_k)-1)$. Integration yields

$$f(\mathbf{q},t)=\mathrm{e}^{-w(\mathbf{q})t}\left\{f(\mathbf{q},0)+\alpha\int_0^t\mathrm{d}\tau F(\mathbf{0},\tau)\mathrm{e}^{w(\mathbf{q})\tau}\right\}. \tag{3.26}$$

As initial condition we choose a Poisson–distribution $F(\mathbf{r},0)=\rho_0^2$ so that $f(\mathbf{q},0)=\delta_{\mathbf{q},\mathbf{0}}\rho_0^2$. Thus we get

$$F(\mathbf{r},t)=\rho_0^2+\alpha\int_0^t\mathrm{d}\tau F(\mathbf{0},\tau)b(\mathbf{r},t-\tau) \tag{3.27}$$

with

$$\begin{aligned}b(\mathbf{r},t)=&\int\frac{\mathrm{d}^d\mathbf{q}}{(2\pi)^d}\mathrm{e}^{-w(\mathbf{q})t+i\mathbf{q}\mathbf{r}}\\ =&\mathrm{e}^{-2dt}I_{r_1}(2t)\cdot\ldots\cdot I_{r_d}(2t)\end{aligned} \tag{3.28}$$

where $I_r(t)$ is the modified Bessel function of order r. The dimension d is now just a parameter which can formally take real values. Although this is not physical it allows for the investigation of the dependence on the dimension.

For $\mathbf{r}=\mathbf{0}$ the long–time behavior of the solution of the Volterra integral–equation Eq. (3.27) with the function $b(t)$ given by Eq. (3.28) is known from the mean spherical model [1]. In this context α plays the role of the temperature. This analogy enables us to use known results from the spherical model. Eq. (3.27) can be solved using temporal Laplace transformation [37],

$$\tilde{F}(p)=\int_0^\infty\mathrm{d}t\,\mathrm{e}^{-pt}F(\mathbf{0},t). \tag{3.29}$$

We get

$$\begin{aligned}\tilde{F}(p)&=\frac{\rho_0^2}{p}+\alpha\tilde{F}(p)\tilde{b}(p)\\ \Leftrightarrow\tilde{F}(p)&=\frac{\rho_0^2}{p(1-\alpha\tilde{b}(p))}.\end{aligned} \tag{3.30}$$

[1] In the mean spherical model the spherical constraint is parametrized mathematically by a Lagrangian multiplier, see chapter 2. This multiplier is determined by the Volterra integral–equation Eq. (3.27) where ρ_0^2 is replaced by $b(\mathbf{0},t)$ which does not change the long time–time behavior.

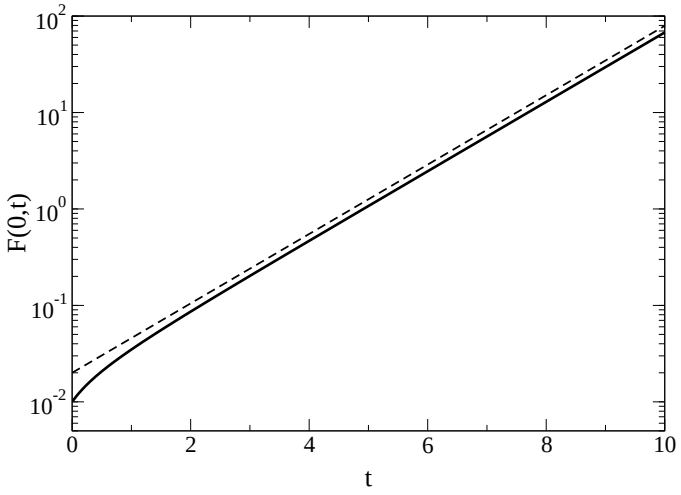

Figure 3.1: Numerical calculation of $F(\mathbf{0}, t)$ for $d = 1, \alpha = 2, \rho_0 = 0.1$. The dashed line shows the theoretical predicted slope $\tau \approx 1.2071$.

For late times $F(\mathbf{0}, t)$ is given by the behavior of $\tilde{b}(p)$ for small p, which crucially depends on the dimension d (see for example [37], notice: the function $f(p)$ used there is $f(p) = \tilde{b}(p/2)/2$):

$$\tilde{b}(p) = \begin{cases} (4\pi)^{-d/2}\Gamma(1-d/2)p^{-(1-d/2)} & d < 2 \\ 2A_1 - (4\pi)^{-d/2}|\Gamma(1-d/2)|p^{d/2-1} & 2 < d < 4 \\ 2A_1 - 4A_2 p & d > 4 \end{cases} \tag{3.31}$$
$$A_k = \int \frac{\mathrm{d}^d\mathbf{q}}{(2\pi)^d} \frac{1}{(2w(\mathbf{q}))^k}$$

This results in different behavior of $F(\mathbf{0}, t)$ as we shall see in the next sections. For all even integral dimensions $d = 2, 4, \ldots$ logarithmic corrections arise whose investigation goes beyond the scope of this work.

$\mathbf{d < 2}$

As for $d < 2$ the quantity $\tilde{b}(p)$ diverges for $p \to 0$ the denominator of Eq. (3.30) has always a zero for $p \neq 0$, so that $\tilde{F}(p)$ has a pole at a positive value $p = 1/\tau$. A pole of the Laplace transform corresponds to exponential behavior of the original function and we get

$$F(\mathbf{0}, t) \underset{t\to\infty}{\propto} \mathrm{e}^{t/\tau}. \tag{3.32}$$

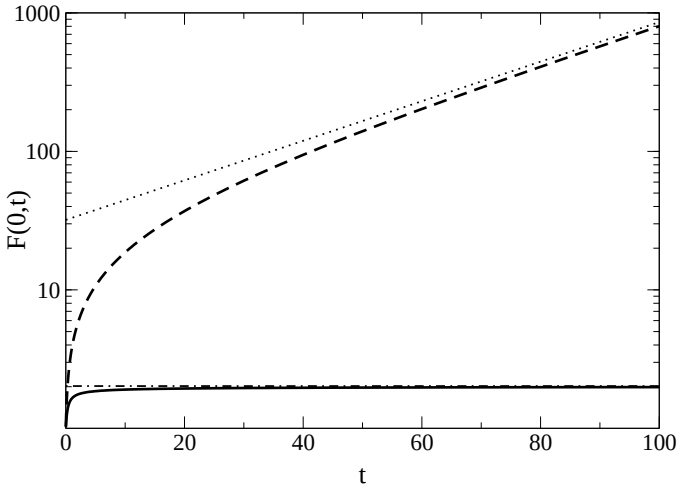

Figure 3.2: Numerical calculation of $F(\mathbf{0}, t)$ for $d = 3, \rho_0 = 1$, $\alpha = 2 < \alpha_c$ (solid line) and $\alpha = 4.2 > \alpha_c$ (dashed line). The dotted line shows the theoretical predicted slope $\tau \approx 30.4$, the dashed–dotted line the theoretical predicted asymptotic value $F(\mathbf{0}, t = \infty) \approx 2.02$.

For $d = 1$ the exact expression of $\tilde{b}$ is known [37]:

$$\tilde{b}(p) = \frac{1}{\sqrt{p(p+4)}} \tag{3.33}$$

which yields

$$\tau_{d=1} = \frac{1}{\sqrt{4+\alpha^2} - 2}. \tag{3.34}$$

For any finite value of α the time scale τ is finite but diverges if $\alpha \searrow 0$. This is in analogy to the spherical model, where in one dimension the critical temperature is zero.

In order to investigate how the predicted asymptotic behavior for large times is approached we have performed a numerical integration of $F(\mathbf{0}, t)$, shown in Fig. 3.1. For details of the numerical calculation see chapter 2 – the numerical method explained in section 2.7 can be applied to equation 3.27 in a straight forward way. We see that the asymptotic behavior is approached quickly and the solution Eq. (3.32) is a good approximation for times $t > 1$.

$2 < d < 4$

For $d > 2$ the quantity $\tilde{b}(p)$ shows qualitatively different behavior: It approaches the finite value $2A_1$ for $p \to 0$. Therefore the $\tilde{F}(p)$ has a pole for

positive p only for α larger than a critical value given by

$$\alpha_c = \frac{1}{2A_1}, \tag{3.35}$$

which is identical to the critical temperature in the spherical model. Thus we find a phase transition in the behavior of the autocorrelation $F(\mathbf{0}, t)$: For $\alpha > \alpha_c$ (low diffusion constant) we recover the exponential divergence

$$F(\mathbf{0}, t) \underset{t\to\infty}{\propto} \mathrm{e}^{t/\tau} \tag{3.36}$$

with a time scale

$$\tau = \left(\frac{\alpha'}{c_2 \alpha}\right)^{-\frac{1}{d/2-1}} \tag{3.37}$$

where the reduced control parameter

$$\alpha' = \frac{\alpha - \alpha_c}{\alpha_c} \tag{3.38}$$

is introduced. And $c_2 = (4\pi)^{-d/2}|\Gamma(1 - d/2)|$. This time scale diverges if we approach $\alpha \searrow \alpha_c$.

For $\alpha < \alpha_c$ (high diffusion constant) the pole of $\tilde{F}(p)$ vanishes and $F(\mathbf{0}, t)$ asymptotically approaches a finite value

$$F_\infty = \lim_{t\to\infty} F(\mathbf{0}, t) = \frac{\rho_0^2}{1 - \alpha/\alpha_c} > \rho_0^2 \tag{3.39}$$

which diverges if we approach $\alpha \nearrow \alpha_c$.

Therefore a suitable order parameter for this phase transition is F_∞^{-1} which decreases linearly to zero for $\alpha \nearrow \alpha_c$ and is equal to zero for $\alpha > \alpha_c$.

For $\alpha = \alpha_c$ we get

$$\tilde{F}(p) = \frac{(4\pi)^{d/2}\rho_0^2}{|\Gamma(1 - d/2)|\,\alpha_c} \frac{1}{p^{d/2}} \tag{3.40}$$

which results in a power law

$$F(\mathbf{0}, t) \propto t^{d/2-1} \tag{3.41}$$

and hence in a power law divergence of the variance.

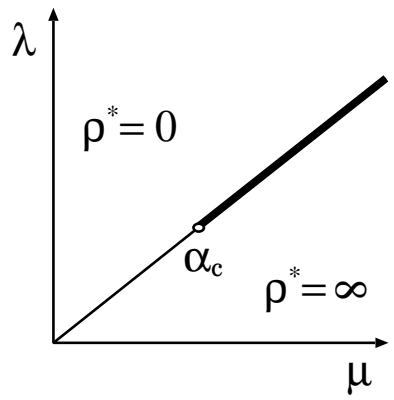

Figure 3.3: The phase diagram of the system for fixed diffusion constant D: In the limit of $t \to \infty$ for $\lambda > \mu k/l$ the stationary density ρ^* is zero while it diverges for $\lambda < \mu k/l$. For $\lambda = \mu k/l$ the density is constant, $\rho^* = \rho_0$, and the variance function is bounded for $\alpha < \alpha_c$, while it diverges exponentially for $\alpha > \alpha_c$ and algebraically for $\alpha = \alpha_c$, where $\alpha = \mu k(k+l)/(2D)$.

$d > 4$

For $d > 4$ we find qualitatively the same behavior as for $2 < d < 4$. Like in the previous case, $\tilde{F}(p)$ has a pole at a positive p only for values $\alpha > \alpha_c = 1/(2A_1)$. For $\alpha > \alpha_c$ the time scale of the exponential increase is given by

$$\tau = \left(\frac{\alpha'}{4A_2\alpha} \right)^{-1}. \tag{3.42}$$

The difference to the case $2 < d < 4$ is, that this time scale is now independent of the dimension d, indicating that we are in the mean–field region.

For $\alpha < \alpha_c$, $F(\mathbf{0}, t)$ approaches the asymptotic value given by Eq. (3.39).

For $\alpha = \alpha_c$ we get

$$\tilde{F}(p) = \frac{\rho_0^2}{4A_2\alpha_c p^2} \tag{3.43}$$

which results in a power law

$$F(\mathbf{0}, t) \propto t. \tag{3.44}$$

These results are summed up in the phase diagram Fig. 3.3.

3.5 Spatial correlations

In the mean–field regime ($d > 4$) the behavior of the correlation function $F(\mathbf{r}, t)$ can be calculated analytically in the limit of large $\mathbf{r}$ and t. As derived

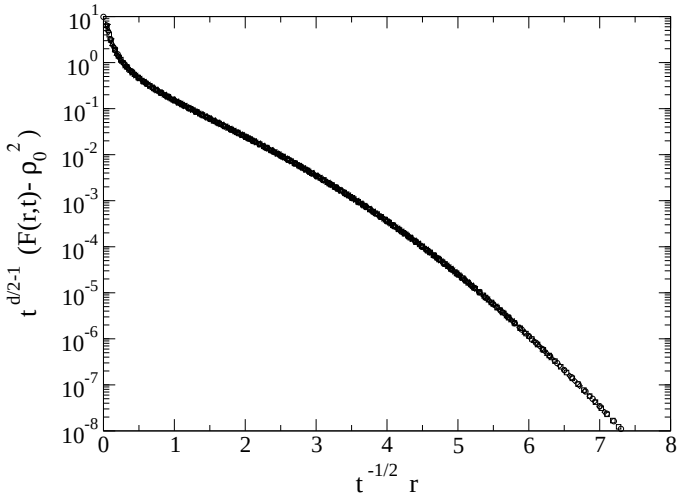

Figure 3.4: Numerical calculation of $F(\mathbf{r}=(r,0,...),t)$ for $d=3, \alpha=2<\alpha_c, \rho_0=1$ and times $t=50,100,150,\ldots,400$.

in the appendix, section 3.9 we get:

$$F(\mathbf{r},t)-\rho_0^2=\begin{cases}\frac{\rho_0^2\alpha}{4\pi^{d/2}|\alpha'|}\ r^{2-d}\,\Gamma\left(\frac{d}{2}-1,\frac{r^2}{4t}\right) & \alpha'<0\\ \frac{\rho_0^2}{64A_2\pi^{d/2}}\ r^{4-d}\ \Psi\left(d,\frac{r^2}{4t}\right) & \alpha'=0\\ \frac{\rho_0^2}{(8\pi)^{(d-1)/2}A_2^{(d-2)/2}}\left(\frac{\alpha'}{\alpha}\right)^{(d-4)/2}\ \left(\frac{r}{\xi}\right)^{(1-d)/2}\exp\left(t/\tau-r/\xi\right) & 1\gg\alpha'>0\end{cases} \tag{3.45}$$

where $\alpha'=(\alpha-\alpha_c)/\alpha_c$ is the reduced control parameter, Γ is the incomplete Gamma function and Ψ is a scaling function defined by

$$\Psi(d,u)=\int_u^\infty \mathrm{d}y\frac{\Gamma\left(\frac{d}{2}-1,y\right)}{y^2}. \tag{3.46}$$

Above the critical point the correlations diverge; the time scale τ is given by Eq. (3.42) and the correlation length by

$$\xi=\sqrt{\tau}=\sqrt{\frac{4A_2\alpha}{\alpha'}}. \tag{3.47}$$

Interestingly, as for $\alpha_c>0$ the correlations increase with time, what in usual dynamical critical phenomena would be called the correlation time is

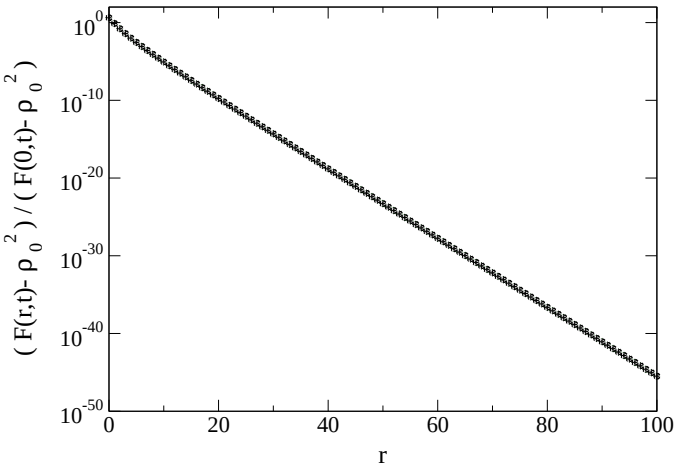

Figure 3.5: Numerical calculation of $F(\mathbf{r} = (r, 0, ...), t)$ for $d = 3, \alpha = 6 > \alpha_c, \rho_0 = 1$ and times $t = 50, 100, 150, \ldots, 400$.

negative while the correlation length is positive. For $\alpha' \leq 0$ the dependence on r^2/t directly shows that the dynamical exponent is $z = 2$. For $\alpha' > 0$ the time scale τ is the square of the length scale ξ, therefore also in this case the dynamical exponent is $z = 2$.

No analytical solution is available in the case $2 < d < 4$, thus we evaluate the integral (3.27) numerically. Fig. 3.4 shows the spatial dependence of the correlation function along the axis $\mathbf{r} = (r, 0, ...)$, for $\alpha < \alpha_c$; Fig. 3.5 shows the case $\alpha > \alpha_c$. A collapse of the calculated data points is achieved if we assume the following functional dependence:

$$F(r,t) - \rho_0^2 \propto \begin{cases} r^{2-d} f_1(r^2/t) & \alpha' < 0 \\ \\ F(0,t) f_2(d,r) & \alpha' > 0, \end{cases} \tag{3.48}$$

where f_1 is a scaling function and $f_2(d, r)$ is a function that only depends on d and r. This result is in qualitative agreement with the previously derived formula for $d > 4$.

3.6 Phase transitions of the 3^{rd} moment

In this section we investigate the time evolution of the 3^{rd} moment for spatial homogeneous initial conditions and $l = 2$. According to the formalism presented in section 3.2 we get the following differential equation for the 3^{rd}

moment at the critical point $\lambda = \mu k/2$:

$$\begin{aligned}\frac{\partial}{\partial t}\langle a(\mathbf{x})a(\mathbf{y})a(\mathbf{z})\rangle =& D\sum_{k=1}^{d}\{\langle a(\mathbf{x})a(\mathbf{y})\left(\Delta_k a(\mathbf{z})\right)\rangle + \langle a(\mathbf{x})\left(\Delta_k a(\mathbf{y})\right)a(\mathbf{z})\rangle \\ &+ \langle\left(\Delta_k a(\mathbf{x})\right)a(\mathbf{y})a(\mathbf{z})\rangle\} \\ &+ \mu(k+2)k\{(\delta_{\mathbf{x},\mathbf{y}}+\delta_{\mathbf{x},\mathbf{z}}+\delta_{\mathbf{y},\mathbf{z}})\langle a(\mathbf{x})a(\mathbf{y})a(\mathbf{z})\rangle \\ &+(k+1)\delta_{\mathbf{x},\mathbf{y}}\delta_{\mathbf{y},\mathbf{z}}\left\langle\left(a(\mathbf{x})\right)^2\right\rangle\}.\end{aligned} \tag{3.49}$$

This equation is solved numerically. To this end we define

$$G(\mathbf{r},\mathbf{s},t) \equiv G_{\mathbf{x}}(\mathbf{r},\mathbf{s},t) = \langle a(\mathbf{x})a(\mathbf{x}+\mathbf{r})a(\mathbf{x}+\mathbf{s})\rangle - \rho_0^3 \tag{3.50}$$

which is independent of $\mathbf{x}$ for spatially homogeneous initial conditions. We choose as initial condition a Poisson distribution for each lattice site, such that

$$\begin{aligned}\langle n(\mathbf{x})\rangle = \left\langle\left(\delta n(\mathbf{x})\right)^2\right\rangle = \left\langle\left(\delta n(\mathbf{x})\right)^3\right\rangle = \rho_0 \\ \Rightarrow \left\langle\left(a(\mathbf{x})\right)^3\right\rangle = \left\langle\left(n(\mathbf{x})-\langle n(\mathbf{x})\rangle\right)^3\right\rangle - \langle n(\mathbf{x})\rangle + \left\langle n(\mathbf{x})^3\right\rangle = \left\langle n(\mathbf{x})^3\right\rangle \\ \Rightarrow G(\mathbf{r},\mathbf{s},t=0) = 0.\end{aligned} \tag{3.51}$$

With the definition of $G(\mathbf{r},\mathbf{s})$ and rescaling time by $t \to t/(2D)$ equation (3.49) takes the form

$$\begin{aligned}\frac{\partial}{\partial t}G(\mathbf{r},\mathbf{s},t) =& \sum_{k=1}^{d}\{\, G(\mathbf{r}+\mathbf{k},\mathbf{s}) + G(\mathbf{r}-\mathbf{k},\mathbf{s}) \\ &+ G(\mathbf{r},\mathbf{s}+\mathbf{k}) + G(\mathbf{r},\mathbf{s}-\mathbf{k}) \\ &+ G(\mathbf{r}+\mathbf{k},\mathbf{s}+\mathbf{k}) + G(\mathbf{r}-\mathbf{k},\mathbf{s}-\mathbf{k}) - 6G(\mathbf{r},\mathbf{s})\,\} \\ &+ 2\alpha\left\{(\delta_{\mathbf{r},\mathbf{0}}+\delta_{\mathbf{s},\mathbf{0}}+\delta_{\mathbf{r},\mathbf{s}})\left(G(\mathbf{r},\mathbf{s},t)+\rho_0^3\right)\right) \\ &+(k+1)\delta_{\mathbf{r},\mathbf{0}}\delta_{\mathbf{s},\mathbf{0}}\left\langle a(\mathbf{x})^2\right\rangle\}\end{aligned} \tag{3.52}$$

Here, $\alpha = \mu k(k+2)/(2D)$. The calculation of $G(\mathbf{r},\mathbf{s},t)$ has the advantage that it is a rapidly decreasing function of $\mathbf{r}$ and $\mathbf{s}$ and therefore already small lattices lead to accurate results. Equation (3.52) is integrated iteratively using the numerical solution of $\langle(a(\mathbf{x}))^2\rangle$ as obtained in section 3.4.

Fig. 3.6 shows the calculation for $d = 3$ and a time step of $\Delta t = 0.01$. The fact that the memory requirement grows with the 6^{th} power of the edge length L, only small L can be calculated. We compared the results for

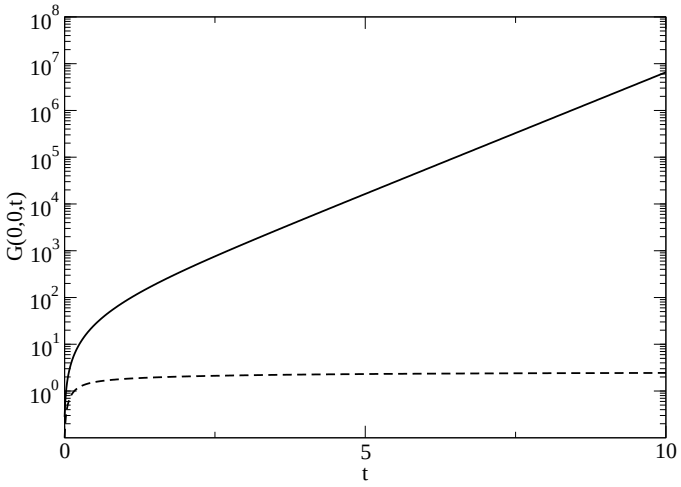

Figure 3.6: The function $G(\mathbf{0},\mathbf{0},t)$ for $d = 3$, a system size of 10^3 and a time step of $\Delta t = 0.01$. The straight line corresponds to $\alpha = 2.8$, it follows an exponential law for large t. The dashed line corresponds to $\alpha = 1$ and approaches asymptotically a constant.

$L = \{5, 10, 15\}$ and found no strong dependence on L such that $L = 10$ provides data with satisfying accuracy. Like in the case of the second moment a phase transition can be found: For $\alpha < \alpha_c$ the 3^{rd} moment approaches asymptotically a constant value while it diverges exponentially for $\alpha > \alpha_c^{(3)}$:

$$G(\mathbf{0},\mathbf{0},t) = \begin{cases} c_0 & \alpha < \alpha_c^{(3)} \\ c_1 e^{t/\tau} & \alpha > \alpha_c^{(3)} \end{cases} \tag{3.53}$$

where c_0 and c_1 are some constants . The measurement of τ for several values of α in the supercritical regime is shown in Fig. 3.7. The correlation time diverges according to a power law if $\alpha_c^{(3)} = 2.42$ is approached as shown by the fit. The constant c_0 diverges if $\alpha_c^{(3)}$ is approached from below but the cross–over times are too large to determine the critical point by these data.

The critical point $\alpha_c^{(3)} = 2.42$ of the 3^{rd} moment in $d = 3$ dimensions is clearly smaller than the critical point of the 2^{nd} moment $\alpha_c^{(2)} = 3.96$. It would be interesting to investigate whether this trend continues for higher moments.

3.7 Activity spreading

The calculations in the previous sections are based on spatially homogeneous initial conditions. In the theory of absorbing phase transitions often a differ-

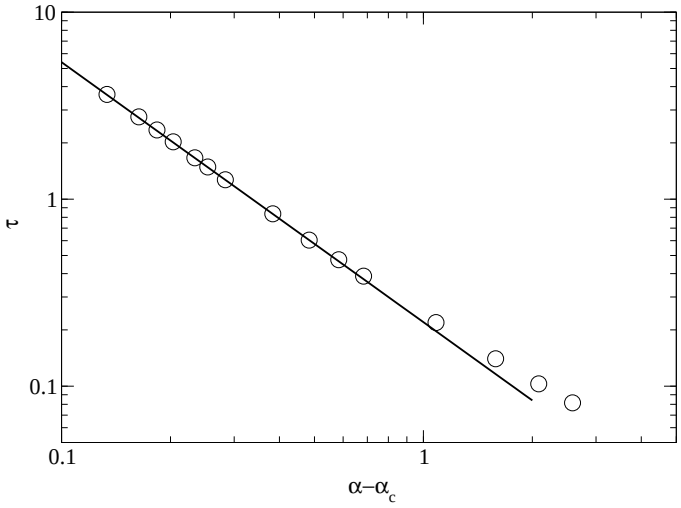

Figure 3.7: The correlation time τ in dependence of $\alpha - \alpha_c = \alpha - 2.42$. The line shows the fit $\tau = 0.22(\alpha - 2.42)^{-1.39}$.

ent scenario is used: Initially the lattice is empty except for the origin where just as many particle are located as needed for the dynamics to start. It is then investigated how this activity spreads into the system. In this section the question is addressed what can be learned from this initial condition in the bosonic PCPD.

After presenting analytically solvable cases we test the hyperscaling relation of the critical exponents. To this end additional information is needed which can only be obtained from Monte Carlo simulations.

3.7.1 Analytical calculation

As initial condition of the system we choose two particles at the origin

$$\rho(\mathbf{x}, t = 0) = 2\delta_{\mathbf{x},\mathbf{0}}. \tag{3.54}$$

For the average particle number $\langle \sum_{\mathbf{x}} a(\mathbf{x}) \rangle$ we recover the same result as for the density in the case of spatially homogeneous initial conditions: for $\lambda l < \mu k$ the particle number diverges ("active phase") while all particles die out for $\lambda l > \mu k$ ("inactive phase"). In the active phase a spreading cone forms, i.e. a growing region with non–zero density. If $\lambda = \mu k/l$ is chosen the time evolution of the density is simply a lattice diffusion equation and the solution is given by

$$\rho(\mathbf{x}, t) = 2\mathrm{e}^{-2dt} I_{x_1}(2t) \cdot \ldots \cdot I_{x_d}(2t). \tag{3.55}$$

For large arguments $\mathbf{x}$ and t this function asymptotically approaches a Gaussian distribution, thus the dynamical exponent is $z = 2$ and the average particle number is constant, $\theta = 0$.

By defining

$$F_{\mathbf{x}}(\mathbf{r}, t) = \langle a(\mathbf{x}) a(\mathbf{x} + \mathbf{r}) \rangle \tag{3.56}$$

and rescaling time by

$$t \to \frac{t}{2D} \tag{3.57}$$

the time evolution of the second moment can be rewritten as

$$\begin{aligned} F_{\mathbf{x}}(\mathbf{r}, t) =& \frac{1}{2} \sum_{k=1}^{d} \{ F_{\mathbf{x}}(\mathbf{r} - \mathbf{k}, t) + F_{\mathbf{x}}(\mathbf{r} + \mathbf{k}, t) \\ & + F_{\mathbf{x}-\mathbf{k}}(\mathbf{r} + \mathbf{k}, t) + F_{\mathbf{x}+\mathbf{k}}(\mathbf{r} - \mathbf{k}, t) - 4 F_{\mathbf{x}}(\mathbf{r} - \mathbf{k}, t) \} \\ & + \delta_{\mathbf{r},\mathbf{0}} F_{\mathbf{x}}(\mathbf{0}, t), \end{aligned} \tag{3.58}$$

where

$$\alpha = \frac{\mu k (k + l)}{2D}. \tag{3.59}$$

We rescaled time by the factor $1/(2D)$ instead of $1/D$ in order to keep the notation consistent with the previous sections.

Equation (3.58) can be solved using a two–component Fourier–transformation

$$\begin{aligned} f(\mathbf{s}, \mathbf{q}, t) &= \sum_{\mathbf{x}} \sum_{\mathbf{r}} \mathrm{e}^{-i\mathbf{s}\mathbf{x}} \mathrm{e}^{-i\mathbf{q}\mathbf{r}} F_{\mathbf{x}}(\mathbf{r}, t), \\ F_{\mathbf{x}}(\mathbf{r}, t) &= \int \frac{\mathrm{d}^d \mathbf{s}\, \mathrm{d}^d \mathbf{q}}{(2\pi)^{2d}} \mathrm{e}^{i\mathbf{s}\mathbf{x}} \mathrm{e}^{i\mathbf{q}\mathbf{r}} f(\mathbf{s}, \mathbf{q}, t). \end{aligned} \tag{3.60}$$

The differential equation for the Fourier–transform f can be cast into the form

$$\frac{\partial}{\partial t} f(\mathbf{s}, \mathbf{q}, t) = -\frac{1}{2} v(\mathbf{s}, \mathbf{q}) f(\mathbf{s}, \mathbf{q}, t) + \alpha \hat{F}(\mathbf{s}, t), \tag{3.61}$$

with the dispersion relation $v(\mathbf{s}, \mathbf{q}) = -\sum_{k=1}^{d} (\cos(q_k) + \cos(q_k - s_k) - 2)$ and

$$\hat{F}(\mathbf{s}, t) = \sum_{\mathbf{x}} \mathrm{e}^{-i\mathbf{s}\mathbf{x}} F_{\mathbf{x}}(\mathbf{0}, t) = \int \frac{\mathrm{d}^d \mathbf{q}}{(2\pi)^d} f(\mathbf{s}, \mathbf{q}, t). \tag{3.62}$$

Integration yields

$$f(\mathbf{s}, \mathbf{q}, t) = \mathrm{e}^{-v(\mathbf{s},\mathbf{q})t} \left\{ f(\mathbf{s}, \mathbf{q}, 0) + \alpha \int_0^t \mathrm{d}\tau \hat{F}(\mathbf{s}, \tau) \mathrm{e}^{v(\mathbf{s},\mathbf{q})\tau} \right\}. \tag{3.63}$$

The initial condition equation (3.54) reads in Fourier space $f(\mathbf{s},\mathbf{q},0)=2$. Thus we get for the correlation function

$$F_{\mathbf{x}}(\mathbf{r},t)=2A(\mathbf{x},\mathbf{r},t)+\alpha\sum_{x'}\int_0^t \mathrm{d}\tau F_{x'}(\mathbf{0},\tau)A(\mathbf{x}-\mathbf{x}',\mathbf{r},t-\tau), \tag{3.64}$$

where

$$A(\mathbf{x},\mathbf{r},t)=\int \frac{\mathrm{d}^d\mathbf{s}\,\mathrm{d}^d\mathbf{q}}{(2\pi)^{2d}}\exp\left(-v(\mathbf{s},\mathbf{q})t+i\mathbf{s}\mathbf{x}+i\mathbf{q}\mathbf{r}\right). \tag{3.65}$$

An analytical solution of this integral equation could not be found. But for the sum of the autocorrelations,

$$\hat{F}(\mathbf{0},t)=\sum_{\mathbf{x}}F_{\mathbf{x}}(\mathbf{0},t), \tag{3.66}$$

the situation simplifies because of the following identity

$$b(t):=\sum_{\mathbf{x}}A(\mathbf{x}-\mathbf{x}',\mathbf{0},t)=\sum_{\mathbf{x}}A(\mathbf{x},\mathbf{0},t)=\int\frac{\mathrm{d}^d\mathbf{s}}{(2\pi)^d}\mathrm{e}^{-v(\mathbf{0},\mathbf{q})t}=\left(e^{-2t}I(2t)\right)^d \tag{3.67}$$

where I is a modified Bessel function. We thus get

$$\hat{F}(0,t)=2b(t)+\alpha\int_0^t \mathrm{d}\tau\hat{F}(0,\tau)b(t-\tau). \tag{3.68}$$

This equation is exactly the one for the Lagrangian multiplier in the mean spherical model and we can use the already known results here [37]. Using a Laplace transformation,

$$\tilde{F}(p)=\int_0^\infty \mathrm{d}t\,\mathrm{e}^{-pt}\hat{F}(\mathbf{0},t), \tag{3.69}$$

we get

$$\tilde{F}(p)=\frac{2\tilde{b}(p)}{1-\alpha\tilde{b}(p)}. \tag{3.70}$$

An analysis of the behavior for small p gives the late time behavior of $\hat{F}(\mathbf{0},t)$. Depending on the dimension we find a phase transition with respect to α. The critical point is given by the same α_c as found before for spatially homogeneous initial conditions, section 3.4. Above the critical point, $\alpha>\alpha_c$, the sum of the autocorrelations diverges as before. At the critical point $\alpha=\alpha_c$ the sum of the autocorrelations follows a power law $t^{-(2-d/2)}$ for $2<d<4$ and approaches a constant for $d>4$. Below the critical point $\alpha<\alpha_c$ the

sum of the autocorrelations follows a power law $t^{-d/2}$. Note that for $d = 1$ the critical point is zero, $\alpha_c = 0$.

The behavior below the critical point can be understood using the interpretation from spatial homogeneous initial conditions that in this regime the diffusion is dominant. A diffusive system without reactions shows the same late time behavior of the autocorrelator:

$$\begin{aligned}
\left\langle (n(\mathbf{x},t))^2 \right\rangle &= \sum_n n^2 p_n(\mathbf{x},t) \\
&= \sum_n n^2 \left(P(\mathbf{x},t|\mathbf{0},0)\right)^n \\
\Rightarrow \sum_{\mathbf{x}} \left\langle (n(\mathbf{x},t))^2 \right\rangle - \langle n(\mathbf{x},t)\rangle &= \\
&= \sum_{\mathbf{x}} \sum_{n=2} n^2 \left(\mathrm{e}^{-2dt} I_{x_1}(2t) \cdot \ldots \cdot I_{x_d}(2t)\right)^n \\
&= \sum_x 4 \int \frac{\mathrm{d}^d\mathbf{q}\,\mathrm{d}^d\mathbf{q}'}{(2\pi)^{2d}} \exp\left(i(\mathbf{q}+\mathbf{q}')\mathbf{x} - (w(\mathbf{q})+w(\mathbf{q}'))\,t\right) + \ldots \\
&= 4 \int \frac{\mathrm{d}^d\mathbf{q}}{(2\pi)^d} \exp\left(-2w(\mathbf{q})t\right) + \ldots \\
&\underset{t\to\infty}{=} 4\,(8\pi t)^{-d/2}\,,
\end{aligned} \tag{3.71}$$

where $p_n(\mathbf{x},t)$ is the probability to find n particles at site $\mathbf{x}$ at time t which for independent particles starting from the origin can be expressed as products of the propagator $P(\mathbf{x},t|\mathbf{0},0)$.

Above the critical point the reaction processes are dominant. As on average the particle number in each system is 2 in most of the systems the particles have to vanish in order that in few systems a divergence of the second moment is possible. This has crucial influence on the possibility to simulate the process as discussed in the next section.

3.7.2 Hyperscaling relation

Analytical predictions

The hyperscaling relation Eq. (3.6) shall now be verified in the bosonic PCPD where we know after all some of the exponents exactly. The arguments given for the hyperscaling relation should hold irrespectively of the type of density/number which is measured. While in the description of the process with exclusion interaction there are only two possibilities – the number of

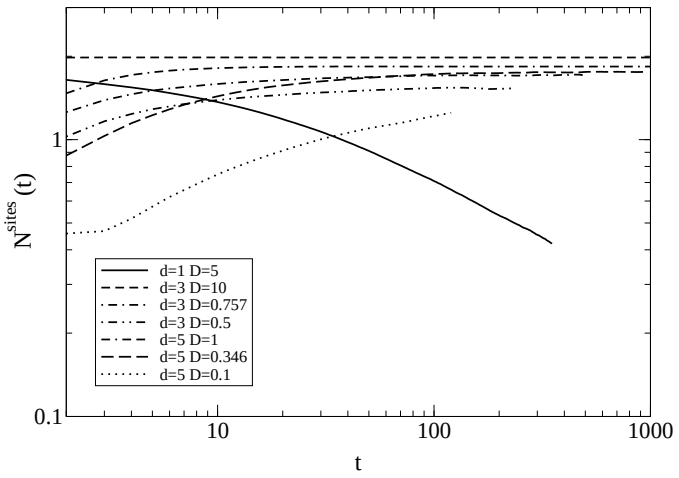

Figure 3.8: Time evolution of the average number of active sites for different parameters, the reaction rates are fixed to $\mu = 2$ and $\lambda = 1$. For $d = 1$ always $\alpha > \alpha_c$, for $d = 3$ and $d = 5$ the diffusion constant D is chosen such that $\alpha < \alpha_c$, $\alpha = \alpha_c$ and $\alpha > \alpha_c$ (with decreasing D). One observes that only in one dimension the number of active sites does not approach a constant, a fit yields $\theta_{d=1}^{\text{sites}} \approx -0.450$.

particles and pairs, i.e. two particles on neighboring sites – in the bosonic description there are three possibilities. The number of active sites, these are sites with at least one particle, have to be distinguished from the number of particles. So one may consider the number of active sites, of particles or of particle pairs. The number of particles is constant at the critical point, thus we have $\theta^{\text{part}} = 0$. The number of pairs is given by $\sum_{\mathbf{x}} \left\langle (a^\dagger(\mathbf{x}))^2 (a(\mathbf{x}))^2 \right\rangle = \sum_{\mathbf{x}} \langle a^2(\mathbf{x}) \rangle$ whose behavior is calculated in subsection 3.7.1:

$$\theta^{\text{pairs}} = \begin{cases} -d/2 & \alpha < \alpha_c \\ -(2 - d/2) & \alpha = \alpha_c \text{ and } 2 < d < 4 \\ 0 & \alpha = \alpha_c \text{ and } d > 4. \end{cases} \tag{3.72}$$

For $\alpha > \alpha_c$ the number of pairs diverges exponentially and thus no exponent can be defined.

In $d > 2$ it is expected that $\delta = 0$: After some initial time there is a fraction of systems consisting only of two particles at different sites. They are diffusing freely on the lattice and hence their distance vector describes as well a random walk in d dimensions. As a random walk is transient for $d > 2$ the probability that the two particles ever meet again is zero and consequently those active systems survive for ever and one concludes $\delta = 0$.

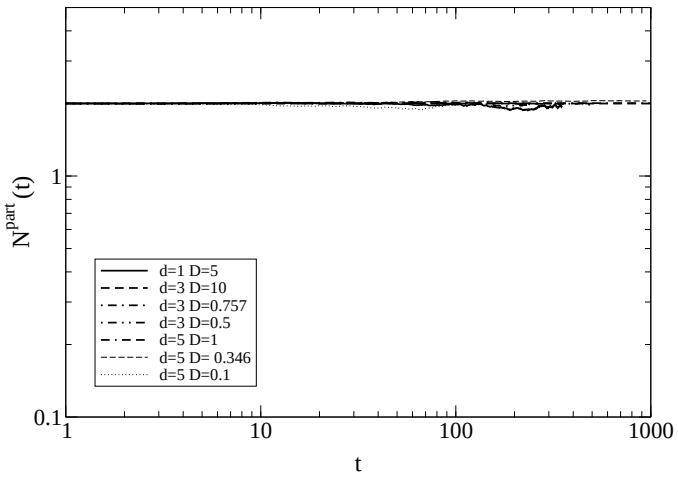

Figure 3.9: Time evolution of the average number of particles, parameters as before. As expected from the analytical calculations the number of particles is constant for any set of parameters.

Additionally we have shown exactly that $z = 2$. The remaining exponents, $\theta^{\text{sites}}, \alpha^{\text{sites}}, \alpha^{\text{part}}, \alpha^{\text{pairs}}$ and $\delta_{d=1}$ have to be determined numerically in a Monte–Carlo simulation. To sum up, the theoretical considerations predict (see Eq. (3.6) and Tab. 3.1):

$$\begin{aligned}
\alpha^{\text{sites}} &= \begin{cases} -\theta^{\text{sites}} - \delta_{d=1} + \frac{1}{2} & d = 1 \\ -\theta^{\text{sites}} + \frac{d}{2} & d > 2 \end{cases} \\
\alpha^{\text{part}} &= \begin{cases} \frac{1}{2} - \delta_{d=1} & d = 1 \\ \frac{d}{2} & d > 2 \end{cases} \\
\alpha^{\text{pairs}} &= \begin{cases} d & \alpha < \alpha_c (d > 2) \\ 2 & \alpha = \alpha_c \text{ and } 2 < d < 4 \\ \frac{d}{2} & \alpha = \alpha_c \text{ and } d > 4 \end{cases}
\end{aligned} \tag{3.73}$$

It should be mentioned that above the upper critical dimension the hyperscaling relation is generally not expected to hold [81]. The upper critical dimension of the bosonic PCPD is $d_c = 2$ [88] such that $d = 1$ should be the only relevant case here. Nevertheless it will be shown that surprisingly the hyperscaling relation holds aswell in $d = 3$ and $d = 5$.

Simulations

For the Monte–Carlo (MC) simulation of the bosonic PCPD a list of active sites i is used. In contrast to the model with exclusion interaction the number

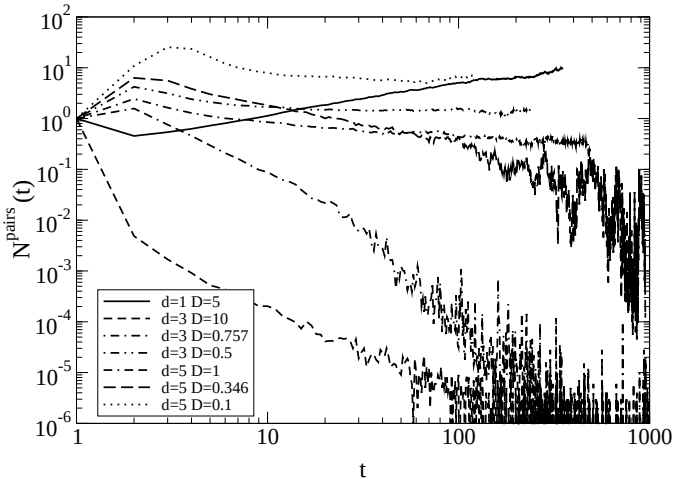

Figure 3.10: Time evolution of the average number of pairs, parameters as before. In contrast to the analytical result one can not observe the divergence for $\alpha > \alpha_c$ as explained in the text. For $\alpha = \alpha_c$ and $\alpha < \alpha_c$ the fluctuations are still very large and the agreement of the slopes with the analytically predicted values is not very high. Fitting yields $\theta_{d=3}^{\text{pairs}} = -0.23$ to be compared to -0.5, $\theta_{d=5}^{\text{pairs}} = -0.76$ (analytically: 0) for $\alpha = \alpha_c$ and $\theta_{d=3}^{\text{pairs}} = -1.7$ (analytically: -1.5), $\theta_{d=5}^{\text{pairs}} \approx -2.5(\pm 0.5)$ (analytically -2.5) for $\alpha < \alpha_c$.

of particles n_i on the sites has to be tracked. The number of pairs on each site is then given by $n_i(n_i - 1)/2$. For each system in one MC time step $D\sum_i n_i$ diffusion processes, $\mu\sum_i n_i(n_i-1)/2$ creation and $\lambda\sum_i n_i(n_i-1)/2$ annihilation processes take place on average. One of these possibilities is chosen randomly according to its statistical weight and the time is updated by $t \to t + [D\sum_i n_i + (\mu+\lambda)\sum_i n_i(n_i-1)/2]^{-1}$. A difficulty is that the number of possible processes varies extremely from system to system as the number of pairs fluctuates enormously. Consequently it is not convenient to determine a target time and simulate each system up to this time one after each other because for a badly estimated target time the program might get stuck in only one of the systems with a large number of pairs. We rather determined target times in small steps up to which the systems were simulated step by step. Although the systems have to be kept simultaneously in memory one gains the advantage that the results can be tracked during the simulations and one does not have to estimate the maximal simulation time in advance.

Still the simulation of the process takes much effort. Therefore compared to the simulations of the model with exclusion interaction only small times

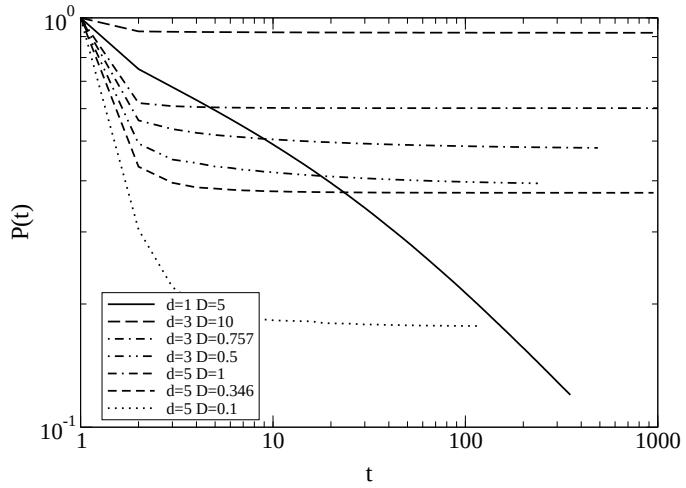

Figure 3.11: Time evolution of the survival probability, parameters as before. As predicted, only for $d = 1$ the curve does not approach a constant, a fit yields in this case $\delta_{d=1} = 0.471$.

could be simulated. Especially in the case of diverging autocorrelations reliable results are computationally demanding. Standard simulation methods simply fail in this case as the number of needed systems in the ensemble is far too large. This number of systems M can be estimated as follows: The average number of pairs diverges as $\left\langle N^{\text{pairs}} \right\rangle \approx N_0^{\text{pairs}} \exp(t/\tau)$ while the average number of particles N_0 is constant. To determine a lower bound for M one may assume that all the particles available in the simulation MN_0 pile up at one site of a single system. Then the number of pairs is well approximated by $(MN_0)^2/2$. This has to be equal to $MN_0^{\text{pairs}} \exp(t/\tau)$ as this is the only contribution to the ensemble average of the number of pairs. Thus we conclude that

$$M > 2\frac{N_0^{\text{pairs}}}{N_0^2} \exp(t/\tau) \tag{3.74}$$

systems are needed in order to allow for the divergence of autocorrelations.

In our simulations we have typically $\tau \approx 1$, for example for the $3d$–case with $D = 0.5, \mu = 2, \lambda = 1$ one gets $\tau = 0.86$. Already for the simulation time $t = 100$ one would need an ensemble consisting of roughly 10^{40} systems to observe the divergence numerically. Consequently it is not expected that for $\alpha > \alpha_c$ (which is especially true in $d = 1$) the simulation produces correct results.

Simulations with several parameters were performed: As dimensions $d = 1$, $d = 3$ and $d = 5$ are chosen in order to simulate systems below the lower

		z	δ	θ^{part}	θ^{pairs}
$d = 1$	$\alpha > \alpha_c$	2	?	0	-
$2 < d < 4$	$\alpha < \alpha_c$	2	0	0	-d/2
$2 < d < 4$	$\alpha = \alpha_c$	2	0	0	-(2-d/2)
$2 < d < 4$	$\alpha > \alpha_c$	2	0	0	-
$d > 4$	$\alpha < \alpha_c$	2	0	0	-d/2
$d > 4$	$\alpha = \alpha_c$	2	0	0	0
$d > 4$	$\alpha > \alpha_c$	2	0	0	-

Table 3.1: The exactly calculated exponents. Not defined exponents are represented by '-' and the exponents to be determined in the simulations with '?'. The exponents θ^{sites}, α^{sites}, α^{part} and α^{pairs} have to be determined numerically.

d	D	δ	θ^{sites}	α^{sites}	$\alpha^{\text{sites}}_{\text{calc}}$	α^{part}	$\alpha^{\text{part}}_{\text{calc}}$	α^{pairs}	$\alpha^{\text{pairs}}_{\text{calc}}$
1	5	0.47	-0.45±0.05	0.57	0.48	0.52	0.029	–	–
3	0.5	0.009	0.01	1.48	1.49	1.49	1.5	–	–
3	0.76	0.006	0.004	1.49	1.49	1.49	1.5	1.9±0.1	2
3	10	0.0002	$2{\cdot}10^{-5}$	1.50	1.5	1.50	1.5	3.58±1	3
5	0.1	0.004	0.15	2.3	2.35	2.3	2.5	–	–
5	0.35	$5{\cdot}10^{-5}$	0.0048	2.49	2.5	2.49	2.5	3.76±1	2.5
5	1	$<10^{-10}$	$3{\cdot}10^{-5}$	2.51	2.5	2.51	2.5	≈ 6	5

Table 3.2: The numerically determined values of the exponents compared to the values expected form the hyperscaling relation (3.6). For $\alpha > \alpha_c$ the exponent α^{pairs} is not defined. It can be seen that for the number of sites and the number of particles the hyperscaling relation is satisfied in good agreement while for the number of pairs larger deviations appear. Due to the fact that huge data sets are used the statistical errors provided by the fitting routine are in most cases too small to affect the last digits given above, otherwise they are given explicitly. Systematical errors are dominant arising from too small simulation times in which crossover effects are still present.

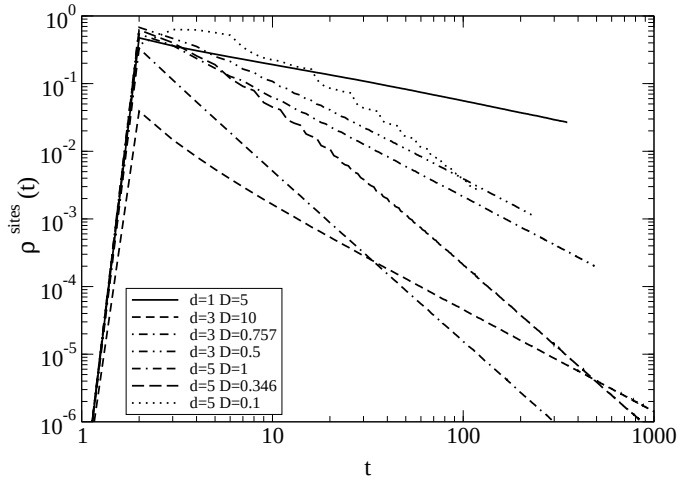

Figure 3.12: Time evolution of the density of active sites, parameters as before. By fitting these curves we observe that the exponents are given by $\alpha^{\text{sites}} = d/2$ in good agreement, for exact values see table 3.2.

critical dimension, above the lower but below the upper critical dimension and in the mean–field regime of the phase transition of the second moment. The reaction rates are fixed to $\mu = 2$ and $\lambda = \lambda_c = 1$ such that the average number of particles remains constant in time. For $d = 3$ and $d = 5$ the diffusion constant D is chosen such that $\alpha < \alpha_c$ ($D = 10$ for $d = 3$ and $D = 1$ for d=5), $\alpha = \alpha_c$ ($D = 0.757$ for $d = 3$ and $D = 0.346$ for $d = 5$) and $\alpha > \alpha_c$ ($D = 0.5$ for $d = 3$ and $D = 0.1$ for $d = 5$). In the ensemble $M = 10^6$ systems are simulated in parallel.

Fig. 3.8 shows the time evolution of the average number of active sites. For $d = 1$ the number of active sites decreases according to a power law with an exponent $\theta^{\text{sites}}_{d=1} = -0.45$. For $d = 3$ and $d = 5$ for all parameters the curves approach a constant. As explained above this is expected as a certain fraction of the systems will consist of at least two particles performing a random walk without meeting again.

In Fig. 3.9 the time evolution of the average number of particles is shown. In agreement with the analytical calculations the particle number is constant in time and thus $\theta^{\text{part}} = 0$ for all parameters.

The time evolution of the average number of pairs is shown in Fig. 3.10. Among the three quantities considered this is clearly the most fluctuating one. The simulation indeed fails in reproducing the exponential divergence of the number of pairs for $\alpha > \alpha_c$ as discussed above. While for $d = 1$ the number of pairs is increasing according to a power law, for the higher

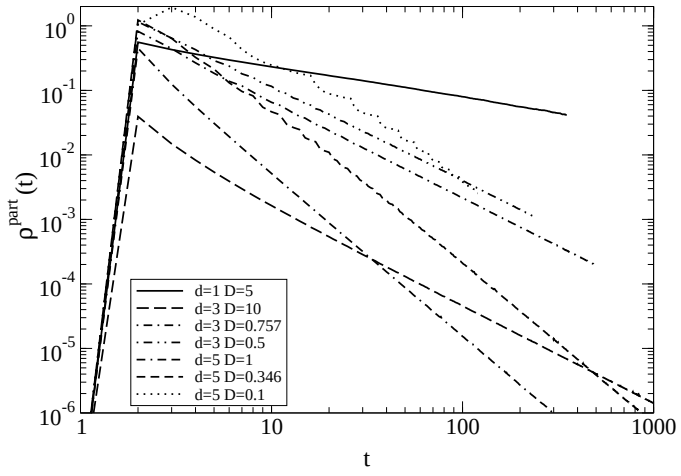

Figure 3.13: Time evolution of the density of particles, parameters as before. By fitting we again observe that the exponents are given by $\alpha^{\text{part}} = d/2$ in good agreement, for exact values see table 3.2.

dimensions it approaches a constant. Interpreting the results for $\alpha > \alpha_c$ has thus to be done carefully.

The survival probability $P(t)$ is shown in Fig. 3.11. It is verified for $d = 3$ and $d = 5$ that $P(t)$ approaches a constant while for $d = 1$ it decays according to a power law. The fitted values for δ can be found in table 3.2. For $d = 3$ and $d = 5$ the values are very close to zero and $\delta_{d=1} \approx 1/2$.

The directly measured densities are shown in Fig. 3.12 (active sites), Fig. 3.13 (particles) and Fig. 3.14 (pairs). For the densities of active sites and particles the fitted values for α are in most cases in good agreement with the values obtained by the hyperscaling relation, only for $d = 1$ and $d = 5, \alpha > \alpha_c$ larger deviations appear. As most of the exponents take simple values, we conjecture in these cases that $\alpha^{\text{sites}}_{d=1} = 1/2$ and $\alpha^{\text{sites}}_{d=5} = 5/2$ and that the measured deviations result from the numerical problems. An obvious disagreement between measured values and the hyperscaling relation is found for $\alpha^{\text{part}}_{d=1}$, where the directly measured value is approximately $1/2$ while the hyperscaling relation predicts it to be approximately zero. The question arises whether the hyperscaling relation is violated or which of the values is wrong. As the hyperscaling relation turns out to hold in the other cases we believe it to hold in this case as well – the inacuracy in the MC results stems from the fact for $d = 1$ the numerical problem is always present because $\alpha_c = 0$. We conjecture that $\delta = 1/2$ and $\alpha^{\text{part}}_{d=1} = 0$. This can be imagined as follows: In the surviving systems the active regions spreads diffusively and inside the active region the reaction kinetics generates a constant density.

Consequently the particle number increases in these systems proportional to $t^{0.5}$, but as more and more systems die out according to $t^{-0.5}$ the particle number averaged over all systems remains constant. In $d = 3$ and $d = 5$ the situation is different, the particle density inside the active region decays and the number of active systems remains constant.

The values for α^{pairs} for $\alpha \leq \alpha_c$ could not be determined with high accuracy due to the high fluctuations. It would be surprising if the hyperscaling relation did not hold for this quantity but the accuracy of our data allows neither for proving nor for disproving the relation in this case.

3.8 Conclusions

In summary, we have shown that for $d > 2$ the bosonic PCPD exhibits a phase transition for $\langle a(\mathbf{x})^2 \rangle$ and thus for the autocorrelation function $\sigma(t)^2 = \langle n(\mathbf{x})^2 \rangle - \langle n(\mathbf{x}) \rangle^2 = \langle a(\mathbf{x})^2 \rangle + \langle n(\mathbf{x}) \rangle - \langle n(\mathbf{x}) \rangle^2$. The order parameter F_∞^{-1} decreases linearly to zero for $\alpha \nearrow \alpha_c$ and is equal zero for $\alpha > \alpha_c$, where α is proportional to the ratio of the reaction rates and the diffusion constant. Thus diffusion has a considerable influence on this process, it must be high enough in order to avoid a divergence of the autocorrelation.

Apart from the spherical model the phase transition of the second moment of the PCPD is related to a much simpler model: On a d–dimensional cubic lattice non interacting particles are diffusing with rate D and additionally at site $\mathbf{x} = \mathbf{0}$ particles may branch $A \to 2A$ with rate $\alpha' = \alpha D$. The equation for the time evolution of the particle density $\langle n(\mathbf{x}, t) \rangle$ is just given by Eq. (3.22). We can adopt the solutions for $F(\mathbf{r}, t)$ by substituting the initial condition by $\rho_0^2 \to \rho_0$. In particular we recover a phase transition for the particle density at the origin. While in the original process it is rather complicated to understand the physical meaning of the behavior of the second moment, in this model we understand the behavior of the first moment: For $d = 1$ diffusion does not suffice to spread the particles on the lattice fast enough and the particle density at $\mathbf{x} = \mathbf{0}$ diverges for any given parameters. For higher dimensions additional spatial directions are accessible to spread particles and as a consequence the particle density at $\mathbf{x} = \mathbf{0}$ remains finite for high enough diffusion constant D.

The fact that the autocorrelation function is diverging while the particle density remains constant allows some conclusions concerning the distribution function for the particles $p(n)$ for late times. On the one hand, if $\langle n \rangle = \sum_n n\, p(n)$ is finite then for large n the distribution function $p(n) < c_1\, n^{-\beta}$ with $\beta > 2$. On the other hand, if $\langle n^2 \rangle = \sum_n n^2\, p(n)$ is infinite then for large n the distribution function $p(n) > c_2\, n^{-\beta}$ with $\beta < 3$ with some positive

constants c_1, c_2. Thus the distribution function follows for large n a power law $p(n) \propto n^{-\beta}$ with $2 < \beta < 3$.

The investigation of the 3^{rd} moment reveals that here a phase transition between a bounded and an unbounded correlator is present as well. The critical point of this transition is found numerically and is clearly different from the one of the second moment. It might be speculated how this behavior continues for higher moments – the calculation of this is still an open problem.

The evolution of the system out of an initial seed (activity spreading) is investigated and it is shown that the second moment exhibits a phase transition with the same critical point as for spatially homogeneous initial conditions. Above the critical point the sum of autocorrelations diverges and below the critical point it decreases according to a power law. This power law behavior can be related to purely diffusive dynamics. This shows that below the critical point it can be neglected that the particles react because most of the time the particles are diffusing freely. The time during which two particles occupy the same lattice site is too short to react because below the critical point diffusion dominates above reactions.

We tested a hyperscaling relation for the dynamical critical exponents. To this end exponents have to be determined which are not accessible analytically and are thus calculated numerically in a Monte–Carlo simulation. It is shown that for the case of a diverging second moment it is impossible to produce accurate data as the necessary size of the ensemble diverges exponentially in the desired simulation time. At or below the critical point of the divergence of the second moment the hyperscaling relation can be approved. It turns out that good accuracy can be achieved for the number and density of active sites and the number and density of particles while measuring these quantities for the number of pairs is difficult due to large fluctuations.

We have also shown that the critical properties of this process are related to the mean spherical model. As the spherical model is a model for magnetism this analogy is rather intriguing and the question arises whether it is just accidental.

3.9 Appendix: Calculation of the spatial dependence

For the mean–field case $d > 4$ the solution of $F(\mathbf{r}, t)$ in the limit of large $\mathbf{r}$ and t can derived analytically, as presented in what follows.

With the definition

$$G(\mathbf{r}, t) = F(\mathbf{r}, t) - \rho_0^2 \tag{3.75}$$

the integral equation can be transformed to

$$G(\mathbf{r},t) = \alpha \int_0^t \mathrm{d}\tau G(\mathbf{0},\tau) b(\mathbf{r},t-\tau) + \alpha\rho_0^2 \int_0^t \mathrm{d}\tau b(\mathbf{r},t). \tag{3.76}$$

Using a Laplace transformation we get

$$\tilde{G}(\mathbf{r},p) = \alpha\tilde{G}(\mathbf{0},p)\tilde{b}(\mathbf{r},p) + \alpha\rho_0^2 \frac{\tilde{b}(\mathbf{r},p)}{p}, \tag{3.77}$$

setting $\mathbf{r} = \mathbf{0}$ determines $\tilde{G}(\mathbf{0},p)$ which yields

$$\tilde{G}(\mathbf{r},p) = \alpha\rho_0^2 \frac{\tilde{b}(\mathbf{r},p)}{p\left(1-\alpha\tilde{b}(\mathbf{0},p)\right)}. \tag{3.78}$$

The Fourier transform of this equation is

$$\tilde{g}(\mathbf{q},p) = \rho_0^2\alpha \frac{1}{p\left(1-\alpha\tilde{b}(\mathbf{0},p)\right)} \frac{1}{p+w(\mathbf{q})}. \tag{3.79}$$

For the mean–field case, $d > 4$, $\tilde{b}(\mathbf{0},p)$ takes the simple form

$$\tilde{b}(\mathbf{0},p) = 1/\alpha_c - p\gamma/\alpha, \tag{3.80}$$

and we get

$$\tilde{g}(\mathbf{q},p) = \frac{\rho_0^2\alpha}{\gamma} \frac{1}{p\,(p-\alpha'/\gamma)} \frac{1}{p+w(\mathbf{q})}. \tag{3.81}$$

Here we defined the reduced control parameter $\alpha' = (\alpha-\alpha_c)/\alpha_c$ and $\gamma = 4A_2\alpha$. Although the function $\tilde{b}$ does not depend on dimension for $d > 4$, generally a dependence of the solution $G(\mathbf{r},t)$ on dimension is still possible as the inverse Fourier transform depends on d, which does not affect the critical exponents. Using an expansion into partial fractions we get

$$\begin{aligned}\tilde{g}(\mathbf{q},p) =& \rho_0^2\alpha \left(-\frac{1}{\alpha' w(\mathbf{q})} \frac{1}{p} + \frac{1}{\alpha'\left(w(\mathbf{q})+\alpha'/\gamma\right)} \frac{1}{p-\alpha'/\gamma} \right. \\ &\left. + \frac{1}{\gamma w(\mathbf{q})\left(w(\mathbf{q})+\alpha'/\gamma\right)} \frac{1}{p+w(\mathbf{q})} \right).\end{aligned} \tag{3.82}$$

The inverse Laplace transform of this expression reads

$$\begin{aligned}g(\mathbf{q},t) =& \rho_0^2\alpha \left(-\frac{1}{\alpha' w(\mathbf{q})} + \frac{1}{\alpha'\left(w(\mathbf{q})+\alpha'/\gamma\right)} \exp\left(\frac{\alpha'}{\gamma}t\right) \right. \\ &\left. + \frac{1}{\gamma w(\mathbf{q})\left(w(\mathbf{q})+\alpha'/\gamma\right)} \exp\left(-w(\mathbf{q})t\right) \right).\end{aligned} \tag{3.83}$$

Although the second term is not Laplace transformable for $\alpha' > 0$ this result is correct and can be derived by transforming the function $H(\mathbf{r},t) = \exp\left(-(\frac{\alpha'}{\gamma}+\epsilon)t\right) G(\mathbf{r},t)$ with $\epsilon > 0$.

The inverse Fourier transform of the first term of (3.83) is

$$\begin{aligned}
\int \frac{\mathrm{d}^d\mathbf{q}}{(2\pi)^d}\,\mathrm{e}^{i\mathbf{q}\mathbf{r}}\frac{1}{w(\mathbf{q})} &= \int_0^\infty \mathrm{d}x \int \frac{\mathrm{d}^d\mathbf{q}}{(2\pi)^d}\,\exp\left(-w(\mathbf{q})x\right)\mathrm{e}^{i\mathbf{q}\mathbf{r}} \\
&= \int_0^\infty \mathrm{d}x\,\mathrm{e}^{-2dx} I_{r_1}(2x)\cdot\ldots\cdot I_{r_d}(2x) \\
&\underset{|\mathbf{r}|\gg 1}{\approx} \int_0^\infty \mathrm{d}x\,(4\pi x)^{-d/2}\exp\left(-\frac{r^2}{4x}\right) \\
&= \frac{\Gamma\left(\frac{d}{2}-1\right)}{4\pi^{d/2}} r^{2-d}
\end{aligned} \tag{3.84}$$

For the long time limit the second term contributes significantly only for $\alpha' > 0$. Defining $b^2 = \alpha'/\gamma$ we get for this case:

$$\begin{aligned}
&\int \frac{\mathrm{d}^d\mathbf{q}}{(2\pi)^d}\frac{\mathrm{e}^{i\mathbf{q}\mathbf{r}}}{w(\mathbf{q})+b^2} = \\
&= \int_0^\infty \mathrm{d}x \int \frac{\mathrm{d}^d\mathbf{q}}{(2\pi)^d}\exp\left(-\left(w(\mathbf{q})+b^2\right)x\right)\mathrm{e}^{i\mathbf{q}\mathbf{r}} \\
&= \int_0^\infty \mathrm{d}x \exp(-b^2x)\mathrm{e}^{-2dx} I_{r_1}(2x)\cdot\ldots\cdot I_{r_d}(2x) \\
&\underset{b^2\ll 1,|\mathbf{r}|\gg 1}{\approx} (4\pi)^{-d/2}\int_0^\infty \mathrm{d}x\,x^{-d/2}\exp\left(-\frac{r^2}{4x}-b^2x\right) \\
&= (4\pi)^{-d/2}\left(\frac{r^2}{4}\right)^{1-d/2}\int_0^\infty \mathrm{d}z\,z^{d/2-2}\exp\left(-z-\frac{b^2r^2}{4z}\right) \\
&= (4\pi)^{-d/2}\left(\frac{r^2}{4}\right)^{1-d/2} 2^{2-d/2}\,(br)^{d/2-1}\,K_{d/2-1}\,(br) \\
&\underset{r\gg 1}{\approx} (4\pi)^{-d/2}\left(\frac{r^2}{4}\right)^{1-d/2} 2^{2-d/2}\,(br)^{d/2-1}\sqrt{\frac{\pi}{2}}\frac{\exp(-br)}{\sqrt{br}} \\
&= \frac{1}{2^{(d+1)/2}\pi^{(d-1)/2}} b^{(d-3)/2} r^{(1-d)/2}\exp(-br) \\
&= \frac{1}{2^{(d+1)/2}\pi^{(d-1)/2}}\left(\frac{\alpha'}{\gamma}\right)^{(d-3)/4} r^{(1-d)/2}\exp\left(-\sqrt{\frac{\alpha'}{\gamma}}r\right),
\end{aligned} \tag{3.85}$$

where $K_{d/2-1}$ is the modified Bessel function of second kind.

For $\alpha' > 0$ the third term is transformed to:

$$
\begin{aligned}
&\int \frac{\mathrm{d}^d\mathbf{q}}{(2\pi)^d} \frac{\mathrm{e}^{i\mathbf{qr}} \exp\left(-w(\mathbf{q})t\right)}{w(\mathbf{q})\left(w(\mathbf{q})+b^2\right)} \\
&= \int_0^\infty \mathrm{d}x \int \frac{\mathrm{d}^d\mathbf{q}}{(2\pi)^d} \exp\left(-(w(\mathbf{q})+b^2)x\right) \frac{\mathrm{e}^{i\mathbf{qr}} \exp\left(-w(\mathbf{q})t\right)}{w(\mathbf{q})} \\
&= \int_0^\infty \mathrm{d}x \exp(-b^2x) \int_{t+x}^\infty \mathrm{d}y \int \frac{\mathrm{d}^d\mathbf{q}}{(2\pi)^d} \exp\left(-w(\mathbf{q})y\right) \mathrm{e}^{i\mathbf{qr}} \\
&= \int_0^\infty \mathrm{d}x \exp(-b^2x) \int_{t+x}^\infty \mathrm{d}y\, \mathrm{e}^{-2dy} I_{r_1}(2y) \cdot \ldots \cdot I_{r_d}(2y) \\
&\underset{|\mathbf{r}|\gg 1}{\approx} (4\pi)^{-d/2} \int_0^\infty \mathrm{d}x \exp(-b^2x) \int_{t+x}^\infty \mathrm{d}y\, y^{-d/2} \exp\left(-\frac{r^2}{4y}\right) \\
&= (4\pi)^{-d/2} t^{1-d/2} \left(\frac{r^2}{4t}\right)^{1-d/2} \int_0^\infty \mathrm{d}x \exp(-b^2x) \int_0^{\frac{r^2}{4t(1+x/t)}} \mathrm{d}z\, z^{d/2-1} \exp(-z) \\
&\underset{t\gg 1}{\approx} \frac{r^{2-d}}{4\pi^{d/2}} \int_0^\infty \mathrm{d}x \exp(-b^2x) \times \\
&\qquad \times \left(\int_0^{\frac{r^2}{4t}} \mathrm{d}z\, z^{d/2-1} \exp(-z) - \left(\frac{r^2}{4t}\right)^{d/2-1} \exp(-\frac{r^2}{4t})\frac{x}{t} \right) \\
&= \frac{r^{2-d}}{4\pi^{d/2}} \int_0^\infty \mathrm{d}x \exp(-b^2x) \times \\
&\qquad \times \left(\Gamma\left(\frac{d}{2}-1\right) - \Gamma\left(\frac{d}{2}-1, \frac{r^2}{4t}\right) - \left(\frac{r^2}{4t}\right)^{d/2-1} \exp(-\frac{r^2}{4t})\frac{x}{t} \right) \\
&= \frac{r^{2-d}}{4\pi^{d/2}} b^{-2} \left(\Gamma\left(\frac{d}{2}-1\right) - \Gamma\left(\frac{d}{2}-1, \frac{r^2}{4t}\right) - \frac{b^{-2}}{t} \left(\frac{r^2}{4t}\right)^{d/2-1} \exp(-\frac{r^2}{4t}) \right),
\end{aligned}
\tag{3.86}
$$

with the incomplete Gamma-function $\Gamma(a,x) = \int_x^\infty \mathrm{d}t\, t^{a-1}\mathrm{e}^{-t}$.

For $\alpha' < 0$ the same result can be derived by substituting $x \to -x$.

At the critical rate $\alpha' = 0$ equation (3.81) reduces to

$$
\tilde{g}(\mathbf{q},p) = \frac{\rho_0^2\alpha}{\gamma} \frac{1}{p^2} \frac{1}{p+w(\mathbf{q})}. \tag{3.87}
$$

The inverse Laplace transform of this expression is given by

$$
\begin{aligned}
\mathcal{L}^{-1}\left(\frac{1}{p^2\left(p+w(\mathbf{q})\right)}, t\right) &= \int_0^t \mathrm{d}\tau \int_0^\tau \mathrm{d}\tau' \mathcal{L}^{-1}\left(\frac{1}{p+w(\mathbf{q})}, \tau'\right) \\
&= \int_0^t \mathrm{d}\tau \int_0^\tau \mathrm{d}\tau' \exp(-w(\mathbf{q})\tau').
\end{aligned}
\tag{3.88}
$$

The necessary conditions for this equality are fulfilled [94]:

$$\begin{aligned} \lim_{t\to\infty}\left(\mathrm{e}^{-pt}\int_0^t \mathrm{d}\tau \exp(-w(\mathbf{q})\tau)\right) &= 0 \\ \lim_{t\to\infty}\left(\mathrm{e}^{-pt}\int_0^t \mathrm{d}\tau \int_0^\tau \mathrm{d}\tau' \exp(-w(\mathbf{q})\tau')\right) &= 0. \end{aligned} \tag{3.89}$$

This yields

$$\begin{aligned} G(\mathbf{r},t) &= \frac{\rho_0^2\alpha}{\gamma}\int_0^t \mathrm{d}\tau \int_0^\tau \mathrm{d}\tau' \int \frac{\mathrm{d}^d\mathbf{q}}{(2\pi)^d}\exp(-w(\mathbf{q})\tau') \\ &= \frac{\rho_0^2\alpha}{\gamma}\int_0^t \mathrm{d}\tau \int_0^\tau \mathrm{d}\tau' \,\mathrm{e}^{-2dx} I_{r_1}(2x)\cdot\ldots\cdot I_{r_d}(2x) \\ &\underset{|\mathbf{r}|\gg 1}{\approx} \frac{\rho_0^2\alpha}{\gamma}\int_0^t \mathrm{d}\tau \int_0^\tau \mathrm{d}\tau' \,(4\pi\tau')^{-d/2}\exp\left(-\frac{r^2}{4\tau'}\right) \\ &= \frac{\rho_0^2\alpha}{\gamma(4\pi)^{d/2}}\left(\frac{r^2}{4}\right)^{-d/2+1}\int_0^t \mathrm{d}\tau \int_{\frac{r^2}{4\tau}}^\infty \mathrm{d}z z^{d/2-2}\exp(-z) \\ &= \frac{\rho_0^2\alpha}{4\gamma\pi^{d/2}} r^{2-d}\int_0^t \mathrm{d}\tau \Gamma\left(\frac{d}{2}-1,\frac{r^2}{4\tau}\right) \\ &= \frac{\rho_0^2\alpha}{16\gamma\pi^{d/2}}\; r^{4-d}\int_{\frac{r^2}{4t}}^\infty \mathrm{d}z \frac{\Gamma\left(\frac{d}{2}-1,z\right)}{z^2} \end{aligned} \tag{3.90}$$

Thus we get the expressions Eq. (3.45) in the limit of large $\mathbf{r}$ and t.

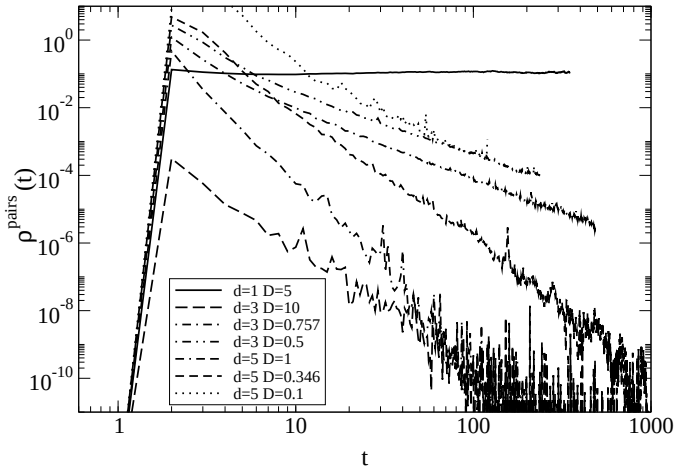

Figure 3.14: Time evolution of the density of pairs, parameters as before. Due to the fluctuations the accuracy of the exponent α^{pairs} is not very high. A fit yields the values $\alpha^{\mathrm{pairs}}_{d=3} = 1.92$ to be compared to the theoretical value 2, $\alpha^{\mathrm{pairs}}_{d=5} = 3.76$ to be compared to 2.5 for the case $\alpha = \alpha_c$ and $\alpha^{\mathrm{pairs}}_{d=3} = 3.58$ (analytically: 3), $\alpha^{\mathrm{pairs}}_{d=5} \approx 6$ (analytically: 5) for the case $\alpha < \alpha_c$.

Chapter 4

Hysteresis in driven diffusive systems

4.1 Introduction

In this chapter a simple non–equilibrium model for a driven diffusive system with non–conservative reaction kinetics in one dimension is presented, whose steady state exhibits a phase with broken ergodicity and hysteresis. This work was done in collaboration with A. Rákos. The results are published in Ref. [5].

The closely related questions of phase coexistence, ergodicity breaking and hysteresis in noisy one–dimensional systems with short range interactions and finite local state space (such as in spin systems or vertex models) are intriguing and have received wide attention in the context of driven diffusive systems [91, 95, 96, 97, 98, 99, 100, 101].

In thermal equilibrium there is no one–dimensional noisy system with short ranged interactions and finite local state space showing ergodicity breaking and hysteresis. Far from equilibrium one has found the closely related phenomena of phase separation and spontaneous symmetry breaking only if the local dynamics are constrained by either bulk conservation laws or vanishing local transition rates. A few examples will be given here.

In Ref. [95] a one–dimensional stochastic driven diffusive system – which is usually called the 'bridge model' – with open boundaries is introduced which shows spontaneous symmetry breaking. In this system the underlying mechanism is based on a bulk conservation law: There are two species of particles ('+','−') and vacancies ('∅') in the system. One type of particles ('+') enters the system on the left, hops to the right and may leave on the right boundary. The other type of particles ('−') moves according to the space reflected dynamics. In the bulk the two species may interchange places:

$$+\varnothing \xrightarrow{1} \varnothing +;\ \varnothing - \xrightarrow{1} -\varnothing;\ +- \xrightarrow{q} -+\,. \tag{4.1}$$

Depending on the creation and annihilation rates on the boundaries and q the system shows phases in which the densities of the two types of particles are asymmetric even though the dynamics is completely symmetric.

Phase separation is demonstrated in Ref. [96] for a three species ('A', 'B', 'C') system on a ring. The particle number is conserved for each species: Particles may interchange places with a cyclical bias, i.e.

$$AB \underset{1}{\overset{q}{\rightleftharpoons}} BA;\ BC \underset{1}{\overset{q}{\rightleftharpoons}} CB;\ CA \underset{1}{\overset{q}{\rightleftharpoons}} CA, \tag{4.2}$$

which favors a phase separated state $A\cdots AB\cdots BC\cdots C$. The boundaries of the phases are fluctuating, i.e. particles of the neighboring phases are penetrating the domain for a finite distance. A model where fluctuations within the phase separated domains occur is presented in Ref. [102].

A general criterion for phase separation in one–dimensional driven systems can be found in Ref. [100]. In Ref. [97] phase separation is claimed for a stochastic model on a ring based on numerical calculations. It could be shown that the conclusion drawn from simulations are in this case misleading as they are just the result of the enormous correlation length of the system [103, 104].

For a overview about critical phenomena in one–dimensional driven diffusive systems with two species of particles we refer to Ref. [105].

The only known model which shows ergodicity breaking without a bulk conservation law is the error–correcting model by Gacs which rather complicated and still not widely understood. The model presented in this chapter is based on a quite simple definition and the mechanism leading to ergodicity breaking is apparent.

4.1.1 Driven diffusive systems

The models used in this chapter are one–dimensional lattice gases, i.e. particles which are diffusing on a discrete chain. In the steady state there exists a non vanishing particle current, consequently detailed balance is violated and the systems are out of equilibrium. This type of non–equilibrium behavior is different to the one considered in chapter 2, where despite the existence of an equilibrium steady state the choice of initial conditions prevented the system from reaching equilibrium.

Most of the phenomena of physical reality are described in three dimensions (plus time), but more mechanisms can be reduced effectively to one dimension than might be expected on first glance. In those phenomena the dynamics are constrained in two directions by the topology of the system. Additionally the description by a discrete lattice is not only often a good idealization, but as well a feature inherent in the nature of the process.

A good example which inspired one of the most important lattice gas models, the asymmetric simple exclusion process (ASEP) (s. below), is the kinetics of protein synthesis: Ribosomes are moving along the codons of the messenger RNA [106]. This system does not only lead to a one–dimensional dynamics, but additionally gives rise to a *discrete* movement of the molecules. Hence the system is best modeled by a lattice structure of space. The ASEP displays how traffic jams of the ribosomes emerge.

Related to this the phenomenon of vehicular traffic jams can be understood as well. While here the discrete structure of space is not justified (cars do not hop in order to progress) a continuous space variable is not essential for understanding the main mechanism behind the emergence of jams.

But there also exist more complex systems, where the origin of the effective reducibility to one dimension and the lattice structure is not that obvious. In Refs. [107, 108] it is demonstrated how the viscosity of polymer melts can be calculated using an (equilibrium) one–dimensional lattice gas. Here, the network structure build up by the polymers is used to divide space into cells, which gives rise to the lattice structure. A particular molecule occupies a certain number of cells and it can enter or leave cells only at the ends. This gives rise to an effective discrete and one–dimensional description.

ASEP

An important driven lattice gas model is the ASEP. It is important because it is simple and can be solved exactly, but nevertheless shows a non trivial phase diagram. In this chapter the ASEP is used as the underlying model in order to demonstrate hysteresis in driven diffusive systems,

The ASEP is a model of diffusing particles on a one–dimensional lattice with a hopping bias. Each site from 1 to L is either empty ('$\varnothing$') or occupied by at most one particle ('A'). In the bulk particles hop stochastically from site i to $i+1$ ($i-1$) with rate p (q), provided that the target site is empty. If $q = 0$, i.e. the particles only hop into one direction, the process is called totally asymmetric simple exclusion process (TASEP).

For closed boundary conditions the particles accumulate on one end and the current vanishes. If periodic boundary conditions are applied, the steady state is a product measure with density $\rho = N/L$ where N is the total particle number which is conserved. Open boundaries are often chosen in a way that they act as particle reservoirs with densities ρ_- on the left resp. ρ_+ on the right: On site 1 particles are created with rate $p\rho_-$, provided the site is empty, which corresponds to a particle hopping from the left reservoir onto the first site. Particles are annihilated with rate $q(1-\rho_-)$ corresponding to a particle hopping into the reservoir. Particles on site L are created with rate $q\rho_+$ and annihilated with rate $p(1-\rho_+)$, corresponding to a hopping from the right reservoir into the lattice respectively from the lattice into the right reservoir.

The ASEP with open boundaries shows the most interesting behavior and can be solved exactly [91]. Depending on the boundary densities ρ_- and ρ_+ three different phases are found as shown in figure 4.1. They are characterized by the steady state which in the bulk is a product measure: 1. A low density phase (LD), where the bulk density is $\rho = \rho_-$, 2. a high density phase (HD), where $\rho = \rho_+$ and 3. a maximal current phase, where the bulk density is $\rho = 1/2$ independent of the boundary densities.

Crossing the lines separating the maximal current phase from LD respec-

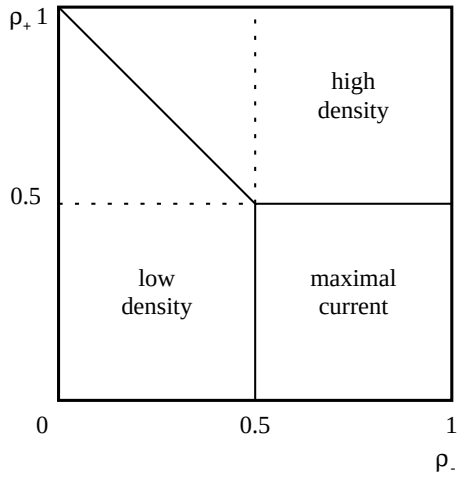

Figure 4.1: The phase diagram of the ASEP, ρ_- and ρ_+ are the densities of the reservoir.

tively HD results in a non–equilibrium second order phase transition. The line separating LD and HD is of special interest. Crossing this line results in a first order transition and exactly on the line phase coexistence occurs: A domain of ρ_- to the left is connected to a domain of ρ_+ to the right. This domain wall is diffusing freely without a bias. The motion of domain walls will be investigated more detailed in section 4.2 and chapter 5.

The fact that the steady states of the respective phases are product measures in the bulk simplifies the determination of the current–density relation for the TASEP. The rate of successful hopping events to the right on a specific site is given by the probability that this site is occupied ρ times the rate of hopping p and the probability that the destination site is empty $(\rho - 1)$. The rate of successful hopping to the left is calculated accordingly and the net current is given by the difference:

$$j(\rho) = (p - q)\rho\,(1 - \rho). \tag{4.3}$$

4.1.2 Coupling to a bulk reservoir

It has been demonstrated that phase coexistence occurs in a one–dimensional driven diffusive system even if the bulk conservation law is violated. To this end the TASEP with open boundaries is coupled to a bulk reservoir, i.e. particles are created and annihilated on each lattice site,

$$\varnothing \underset{\omega_d}{\overset{\omega_a}{\rightleftharpoons}} A, \tag{4.4}$$

which is called "Langmuir kinetics" [109]. This mechanism is inspired by the process of motor proteins moving along actin filaments. Earlier this model was introduced as a toy model reproducing stylized facts in limit order markets [110, 111].

The phase diagram of this system exhibits a phase where a domain of low particle density coexists with a domain of high density. The domain wall, i.e. a particle shock, is localized in the bulk and has been studied in Refs. [112, 113], see next section.

However, the two different domains do not represent two possible *global* steady states. The process is ergodic even in the thermodynamic limit and no hysteresis is possible.

4.2 Method

Our investigations are based on techniques presented in Refs. [111, 112] whose main results will be presented in the subsequent paragraphs. The formation of localized shocks in one–dimensional lattice-gas models is studied. To this end one–dimensional driven diffusive systems with particle number conservation in the bulk, like the totally asymmetric exclusion process (TASEP) or the Katz–Lebowitz–Spohn (KLS) model, are investigated. At the boundaries the particle injection and extraction rates are chosen to be the consequence of particle reservoirs with densities ρ_- at the left and ρ_+ at the right boundary. These systems are coupled to creation and annihilation dynamics acting equally on all sites, "Langmuir kinetics" (LK), where particles are attached to an empty site with rate ω_a and particles detached with rate ω_d. The systems are investigated in the *hydrodynamic* limit, i.e., taking the limit of infinite system size $L \to \infty$ while rescaling the lattice spacing a and time t both by a factor of $1/L$ (Eularian scaling). By this the discrete lattice variable $1 \leq i \leq L$ is transformed into a continuous variable $0 \leq x \leq 1$.

If the order of the rates ω_a and ω_d is larger than $1/L$ the steady state of the system is governed by the LK solely in the hydrodynamic limit. If the order of these rates is smaller than $1/L$ the system will behave like the original driven diffusive system. For the choice

$$\omega_a = \Omega_a/L, \qquad \omega_d = \Omega_d/L, \tag{4.5}$$

where $\Omega_{a,d}$ are of order one such that $\omega_{a,d}$ scale like $1/L$, the effects of the diffusion dynamics and the LK are balanced and qualitatively new behavior can be expected.

It is argued that the hydrodynamic equation describing the time evolution

of the density $\rho(x,t)$ is given by

$$\frac{\partial}{\partial t}\rho + \frac{\partial}{\partial x}j(\rho) = S(\rho), \tag{4.6}$$

which is a modification of the differential equation originally describing the conservative system in the hydrodynamic limit. For the TASEP this is the Burgers' equation with an additional source term.

Here, $j(\rho)$ is the exact current in the driven diffusive system with homogeneous density ρ without coupled non–conservative dynamics and

$$S(\rho) = \Omega_a(1-\rho) - \Omega_d\rho \tag{4.7}$$

is the source term resulting from the non–conservative dynamics. This equation allows for the calculation of the steady state density profile $\rho(x)$. As boundary conditions the two reservoirs fix the densities at $x = 0$ and $x = 1$ but as the differential equation (4.6) is only of first order the solution will fit in general only one of these conditions. This inconsistency is resolved by the appearance of a shock and/or boundary layers. In this context a shock is a jump in the density connecting a density profile fitting the left boundary to a profile fitting the right boundary.

Due to the special choice of rates Eq. (4.5) the shock velocity in the coupled system of conservative and non–conservative dynamics is the same as in the conservative system itself [91, 114]:

$$v_s(x) = \frac{j(\rho^R(x)) - j(\rho^L(x))}{\rho^R(x) - \rho^L(x)} \tag{4.8}$$

where $\rho^L(x)$ ($\rho^R(x)$) is the solution fitting the left (right) boundary. This results from the fact that the timescale in which the shock moves by one lattice site is of order $\mathcal{O}(1)$ while the rate of non–conservative events in the vicinity of the shock is of order $\mathcal{O}(1/L)$, such that in the limit $L \to \infty$ the shock movement might be considered as being independent from the coupled non–conservative dynamics [112]. But as an effect of the non–conservative dynamics the density profiles are space dependent and by this the shock velocity itself becomes space dependent.

A jump in the density profile can only be considered as a "shock" if its form is preserved in time. This is insured by the condition [91]

$$v_c(\rho^L) > v_s(\rho^L, \rho^R) > v_c(\rho^R), \tag{4.9}$$

where $v_c = \frac{\partial}{\partial\rho}j(\rho)$ is the collective velocity which describes how a perturbation spreads into the system.

4.3 Criterion for ergodicity breaking

In general, ergodicity breaking is the separation of the phase space into unconnected parts. According to the initial condition the system will remain in the part in which it was started. An example is the Ising model below the critical temperature where two stationary states are possible. Although in finite systems transitions from one stationary state to the other are possible, they are improbable for large systems and the transitions times diverge exponentially with system size. Consequently, in the thermodynamic limit the state space is clearly separated into two parts, one with a positive and one with a negative net magnetization.

We can now use the investigation above to find a noisy one–dimensional system which shows ergodicity breaking: If it is possible to construct an unstable shock position in the bulk the phase space shows two (meta–)stable states: The high– and low–density solution do not coexist any more – either the one or the other is present. As the shock–positions are fluctuating in finite systems transitions between the states are possible, but we will show that the transition times diverge exponentially in system size, thus ergodicity is broken.

A necessary condition for a stationary (both stable and unstable) shock position in the bulk is

$$v_s(x_0) = 0 \Rightarrow j(\rho^R(x_0)) = j(\rho^L(x_0)) \tag{4.10}$$

for a $x_0 \in (0,1)$.

The stationary shock position might be stable, i.e., small elongations out of this position result in a drift back toward the stationary position, $\frac{\partial}{\partial x} v_s(x)\big|_{x=x_0} < 0$. For the case

$$\left.\frac{\partial}{\partial x} v_s(x)\right|_{x=x_0} = \frac{\frac{\partial}{\partial x}\left[j(\rho^R(x)) - j(\rho^L(x))\right]\big|_{x=x_0}}{\rho^R(x_0) - \rho^L(x_0)} > 0. \tag{4.11}$$

the shock position x_0 is *unstable* – the shock will always have a drift away from this position (Fig. 4.2) once it has left the stationary point due to fluctuations. Eq. (4.10) together with Eq. (4.11) provide a sufficient condition for the existence of an unstable shock position. The spatial derivative of the currents j^L and j^R in Eq. (4.11) are directly given by Eq. (4.6) which in the stationary case takes the form

$$\frac{\partial}{\partial x} j\left(\rho^{L,R}(x)\right) = S\left(\rho^{L,R}(x)\right). \tag{4.12}$$

For further investigations the special form of the current density relation of the driven diffusive system needs to be known. As a specific system we

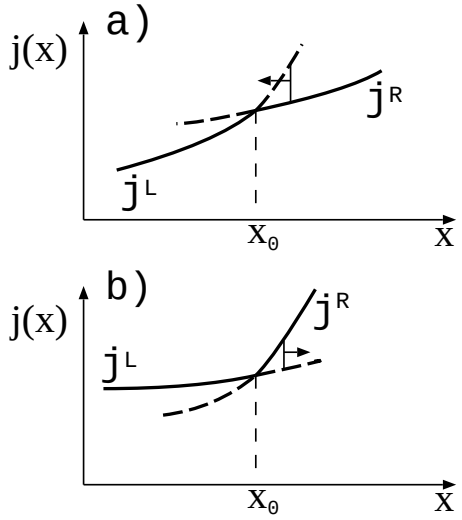

Figure 4.2: The spatial derivative of the current j decides whether a shock position is stable or unstable. a) $\partial_x j^R < \partial_x j^L$, a small perturbation to the right (left) results in a larger (smaller) current into the shock than out of it and thus the shock moves back to the left (right). b) $\partial_x j^R > \partial_x j^L$, now a perturbation to the right (left) results in a smaller (larger) current into the shock than out of it and thus the shock moves further away from its stationary position. Here it is assumed that $\rho^R(x_0) > \rho^L(x_0)$, in the other case the conditions have to be considered with the opposite sign.

choose the TASEP whose current density relation is quite simple. This choice is only one example – the formalism can be applied to many other models.

In this case the necessary condition Eq. (4.10) simplifies

$$\rho^R(x_0) = 1 - \rho^L(x_0); \tag{4.13}$$

hence, in the TASEP only *symmetric* jumps are allowed.

Eq. (4.9) forces that $\rho^L < \rho^R$ – only upward shocks are preserving the form. The stationary shock position is thus unstable, if

$$\begin{aligned} \frac{\partial}{\partial x} j(\rho^R(x)) &> \frac{\partial}{\partial x} j(\rho^L(x)) \\ \Leftrightarrow S\left(\rho^R(x)\right) &> S\left(\rho^L(x)\right) \\ \Leftrightarrow S\left(1-\rho^L(x)\right) &> S\left(\rho^L(x)\right). \end{aligned} \tag{4.14}$$

For the LK Eq. (4.14) and (4.7) imply that $\rho^L > 1/2$ which is impossible for symmetric upward shocks. Hence one–point interactions are inappropriate for constructing unstable shock positions. This result does not depend on

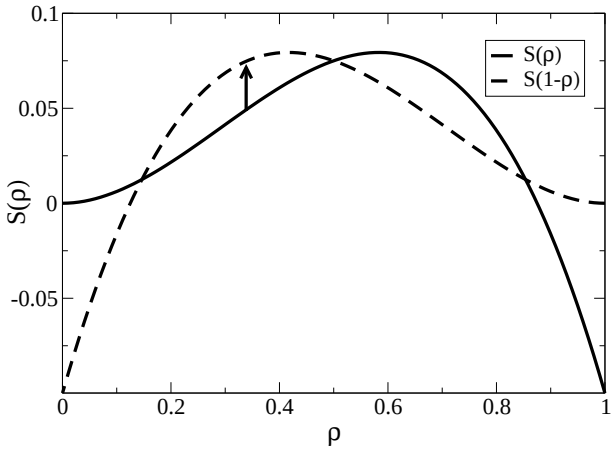

Figure 4.3: The source term $S_3(\rho)$ compared to $S_3(1-\rho)$ for $\Omega_a = 0.7$ and $\Omega_d = 0.2$: It exists a $\rho^L < 1/2$ such that $S_3(\rho^L) < S_3(1-\rho^L)$.

the choice of the TASEP but holds for any driven diffusive system. This is because for one–point interactions the source term $S(\rho)$ is always a linearly decreasing function of ρ and therefore equation (4.11) together with equation (4.12) state that all shock positions must be stable.

Now we consider the general source term resulting from two–point interactions (e.g. $A\varnothing \leftrightharpoons AA$),

$$S_2(\rho) = \Omega_{1,a}(1-\rho)^2 + (\Omega_{2,a} - \Omega_{1,d})\rho(1-\rho) - \Omega_{2,d}\rho^2 \qquad (4.15)$$

where $\Omega_{1,a}$ and $\Omega_{2,a}$ are the attachment rates resulting from the processes $\varnothing\varnothing \to \cdot\cdot$ respectively $A\varnothing/\varnothing A \to \cdot\cdot$ and $\Omega_{1,d}$ and $\Omega_{2,d}$ are the detachment rates resulting from $A\varnothing/\varnothing A \to \cdot\cdot$ respectively $AA \to \cdot\cdot$. Again Eq. (4.14) implies that $\rho^L > 1/2$ so we conclude that neither one–point nor two–point interaction models lead to unstable shock position when coupled to the TASEP.

For other models with more complicated current–density relations the situation is different. For example in the 2-hop TASEP [115] the jumps need not to be symmetric and as a consequence it is sufficient to consider non–conservative two–point interactions in order to allow for unstable shock positions.

4.4 Model

As argued above at least three–point interaction models have to be coupled to the ASEP such that unstable shock positions can be found. In this section

it is shown that indeed three–point interactions suffice by giving an example. Again we stress that the presented model is only one special choice – there are many more possibilities for the conservative dynamics as well as for the non–conservative dynamics.

Consider the following process,

$$A\varnothing A \underset{\omega_a}{\overset{\omega_d}{\rightleftharpoons}} AAA, \tag{4.16}$$

which may be interpreted as activated Langmuir kinetics because for the attachment and detachment processes two neighbors are required. It yields a source term

$$S_3(\rho) = \Omega_a \rho^2 (1-\rho) - \Omega_d \rho^3. \tag{4.17}$$

As illustrated in Fig. (4.3) for a specific choice of rates this source term fulfills the conditions for the existence of unstable shock positions.

The stationary state of the kinetics $A\varnothing A \leftrightharpoons AAA$ (not coupled to diffusion) is a product measure, i.e. the probability to find a particle on a specific lattice site is independent of the remaining sites and equal to the stationary density. The stationary density is given by $K = \frac{\omega_a}{\omega_a+\omega_d} = \frac{\Omega_a}{\Omega_a+\Omega_d}$ or zero. This can be seen using the quantum Hamiltonian formalism as described in Ref. [91]:

$$\begin{aligned} H &= -\sum_{k=1}^{L-2} h_k \\ h_k &= \omega_a \left(n_k s^-_{k+1} n_{k+2} - n_k v_{k+1} n_{k+2} \right) + \omega_d \left(n_k s^+_{k+1} n_{k+2} - n_k n_{k+1} n_{k+2} \right) \end{aligned} \tag{4.18}$$

where n is particle number operator, $v = 1-n$ and s^- and s^+ are the creation and annihilation operators. For a product measure

$$|\rho\rangle = \begin{pmatrix} \rho \\ 1-\rho \end{pmatrix} \otimes \cdots \otimes \begin{pmatrix} \rho \\ 1-\rho \end{pmatrix} \tag{4.19}$$

one gets the condition

$$H|\rho\rangle = 0 \Rightarrow \frac{1-\rho}{\rho}\omega_a = \omega_d \text{ or } \rho = 0. \tag{4.20}$$

In this model the emergence of shocks is possible – the step from zero density to K is stable and the shock position does not fluctuate.

In order to calculate the stationary density profiles for the reaction kinetics coupled to the TASEP we rewrite the (stationary) hydrodynamic equation

Eq. (4.6) as

$$\begin{aligned} \underbrace{\frac{\partial j(\rho)}{\partial \rho}}_{v_c(\rho)} \frac{\partial \rho(x)}{\partial x} &= S_3(\rho) \\ \Rightarrow \frac{\partial \rho(x)}{\partial x} &= \frac{S_3(\rho)}{v_c(\rho)}. \end{aligned} \tag{4.21}$$

Integration directly yields the implicit formula for the flow–field $\rho(x)$:

$$x(\rho) = -\frac{1}{\Omega_a \rho} + \frac{\Omega_a - \Omega_d}{\Omega_a^2} \ln \left| \frac{1}{K} - \frac{1}{\rho} \right| + c \tag{4.22}$$

where $K = (\Omega_a + \Omega_d)/\Omega_a$ is the stationary density of the undisturbed reaction kinetics (4.16) and c is an integration constant. The flow–field $\rho(x)$ is shown in Fig. 4.3. The direct calculation of the inverse function is unfavorable although possible (the Lambert–W–functions are then used). A better way is to iterate the differential equation numerically with standard algorithms (we used a 4th order Runge–Kutta method) in order to get $\rho(x)$.

The flowfield provides information about the course of the stationary solution in space – we can read off the solutions ρ^L and ρ^R by choosing those two lines of the flowfield which match the left respectively the right boundary condition. As the collective velocity $v_c(\rho)$ is zero at $\rho = 1/2$ the differential equation becomes singular when the flowfield reaches this value. To the right of this point the solution ρ^L does not exist and the density is given by ρ^R.

If the collective velocity of the given boundary value ρ_- (ρ_+) tends to the left (right) boundary, the according line of the flowfield does not provide the solution in the bulk. One has rather to determine a density ρ' given by a extremal principle of the current as discussed in Refs. [112, 116]. The bulk solution then follows the line of the flowfield starting from ρ' and is connected to ρ_- (ρ_+) by a boundary layer whose width scales down with increasing L. Consequently in the hydrodynamic limit this boundary layer vanishes and there is a jump at the boundary.

For the current density relation of the TASEP with a maximum at $\rho = 1/2$ it follows that for all left boundary values $\rho_- > 1/2$ the starting point of the flowfield is given by $\rho' = 1/2$ and for all right boundary values $\rho_+ < 1/2$ by $\rho' = 1/2$.

4.5 Phase diagram

These results for the two bulk solution $\rho^L(x)$ and $\rho^R(x)$ for the right and left boundary values enables us to determine the stationary phase diagram of the

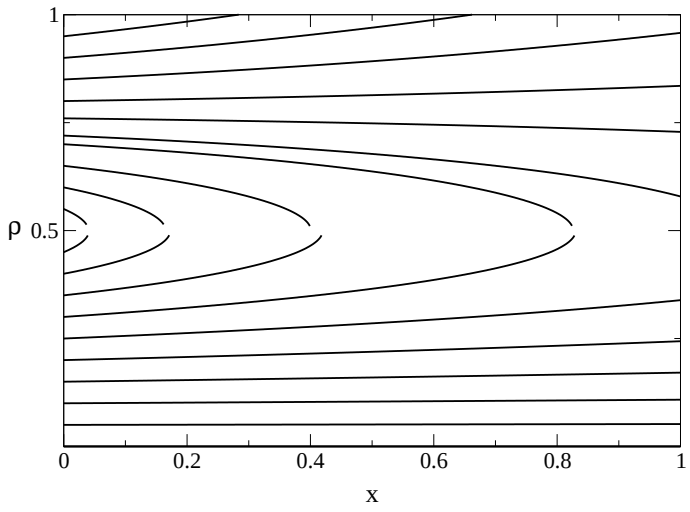

Figure 4.4: The flowfield $\rho(x)$ of the differential equation obtained by an iterative solution, here $\Omega_a = 0.7$ and $\Omega_d = 0.2$.

system, shown in figure 4.5.

As explained before the two solutions are connected by a shock. Due to the boundary layers $\rho^R(x) > \rho^L(x)$ and equation (4.9) is always satisfied such that the form of the shock is stable.

In order to understand quantitatively the selection of the stationary shock position – which determines the phase diagram – and also to explain the phenomenon of hysteresis from a microscopic viewpoint, we describe the dominant dynamical mode of the particle system in terms of the random motion of the shock. To this end we generalize the approach of Ref. [117] and introduce space–dependent hopping rates

$$\begin{aligned} w_{x\to x+a} &= \frac{j_R(x)}{\rho^R(x) - \rho^L(x)}, \\ w_{x+a\to x} &= \frac{j_L(x)}{\rho^R(x) - \rho^L(x)}, \end{aligned} \tag{4.23}$$

for jumps of the shock over a lattice constant a. Similar hopping rates are used in Ref. [113]. The space–dependent hopping rates furnish us with the picture of a random walker in an effective energy landscape $E(x)$ inside a box. The energy landscape is generated by the interplay of the particle current with the reaction kinetics. In this way we relate the original non–equilibrium many–particle system to an equilibrium single particle model.

Let $p(x)$ be the equilibrium probability of the shock being at position x.

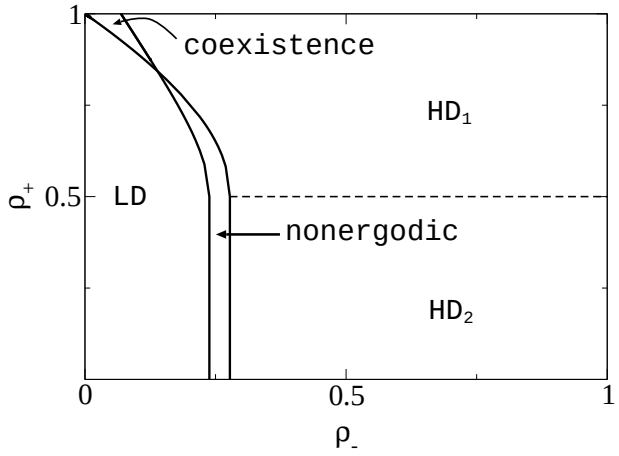

Figure 4.5: Phase diagram for $\Omega_a = 0.7$ and $\Omega_d = 0.1$ with two high density phases (HD1, HD2), a low density phase (LD), a coexistence phase and the nonergodic phase.

Then due to detailed balance

$$\frac{w_{x\to x+a}}{w_{x+a\to x}} = \frac{p(x+a)}{p(x)} = \exp(-E(x+a) + E(x)). \tag{4.24}$$

which defines the energy landscape.

In figure 4.6 four qualitatively different energy profiles which are present in the given model are shown. They are calculated by inserting the analytical solutions of $\rho(x)$ into equation (4.24). The energy profiles determine the phases shown in figure 4.5: There is a region in parameter space where the potential $E(x)$ is monotonically decreasing and thus the stationary shock position is at the right boundary. Consequently the bulk solution is given by $\rho^L(x)$ – this is the low density phase (LD). In another region the potential $E(x)$ is monotonically increasing and thus the stationary shock position is at the left boundary. The bulk solution is then given by $\rho^R(x)$ and this is the high density phase (HD1 and HD2). Due to the boundary layers the bulk density profile is independent of both boundaries in HD2 while it depends on ρ_+ in HD1.

Yet, these phases are comparable to those of the usual TASEP with open boundaries, where as well a high–density phases with $\rho(x) > 1/2$ and a low density phase (LD) $\rho(x) < 1/2$ are found. In the maximal current phase of the TASEP the density profile is independent of both boundaries as in the HD2 phase.

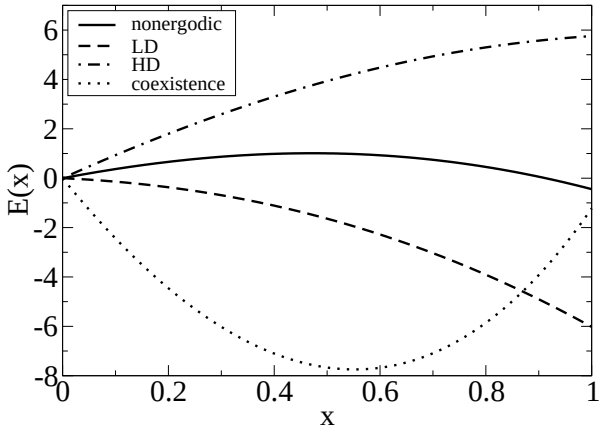

Figure 4.6: Examples for the energy landscape in the four phases. Note that in the HD and LD phases $E(x)$ can be either convex or concave.

Two additional phases exist: A coexistence phase which is characterized by a stable shock position in the bulk of the system corresponding to a minimum of the potential. Notice that in the usual TASEP there is a coexistence line in the phase diagram with a *nonlocalized* shock. In a different parameter regime we indeed find a novel phase with an unstable shock position in the bulk according to a local maximum of the potential in the bulk. The two minima at the left and right boundaries correspond to the two (meta–)stable stationary states.

With the picture of the moving shock in mind it is also possible to derive exactly the two lines in the phase diagram shown in figure 4.5. The quantity of interest is the sign of the slope of the energy profile which gives the stability of the shock position. It can be analyzed by considering the average shock velocity v_s (4.8). A shock position at the boundary is stable when it is driven toward the boundary; i.e., $v_s(0) < 0$ at the left boundary, and $v_s(1) > 0$ at the right boundary. Thus the lines separating the phases are calculated by comparing the values of $\rho^L(x)$ and $\rho^R(x)$ at the positions $x = 0$ and $x = 1$. The line separating the LD and the coexistence phase, respectively the nonergodic and the HD phases are defined by $v_s(0) = 0$. In the LD phase $v_s(0) > 0$ while in the region right of the line $v_s(0) < 0$. The other line, separating the coexistence and the HD phases, respectively the LD and the nonergodic phase are defined by $v_s(1) = 0$. In the HD phase $v_s(1) < 0$ while in the region left of this line $v_s(1) > 0$. Thus in the coexistence region the shocks drifts always into the bulk while in the nonergodic region it always

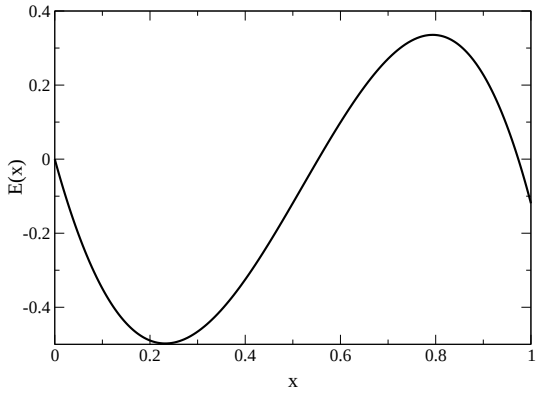

Figure 4.7: The energy profile in the analytically predicted additional phase near the intersection point of the two lines in the phase diagram.

drifts to the boundaries.

The analytical treatment predicts a phase near the intersection point of the two lines in the phase diagram with an energy profile having a minimum and also a maximum in the bulk as illustrated in figure 4.7. However, the region in the (ρ_-, ρ_+) space is rather narrow and the energy landscape is too flat to observe this in simulations.

4.6 First passage times

As discussed above the existence of two metastable states is not a sufficient condition for ergodicity breaking. Here we prove that the transitions from one state to the other are impossible in the thermodynamic limit. This is done by showing that the mean first passage times of the shock from one boundary to the other grow exponentially in system size.

The height of the energy barrier $E(x_{\max})$ which the random walker has to cross in order to reach the other local minimum is proportional to L as can be understood by the following consideration: The energy profile is calculated by

$$E(i/L) = \sum_{k=0}^{i} \Delta E(k/L), \tag{4.25}$$

where

$$\Delta E(x = k/L) = \log \frac{w_{k+1\to k}}{w_{k\to k+1}} = \log \frac{j_L(x)}{j_R(x)} \tag{4.26}$$

is the energy difference between site k and $k+1$. For large L the finite–size effects like the boundary layers are only of minor influence, thus $\Delta E(x)$ is

independent of L. By this $E(i/L)/L$ is the lower sum of the area under the curve $f(x) = \log \frac{j_L(x)}{j_R(x)}$ from 0 to i/L and thus converges to a constant value. Consequently $E(i/L)$ and $E(x_{\max})$ in particular are proportional to L.

The mean first passage time, $\bar{\tau}_{0,L}$, of a random walker in an energy landscape from site 0 to L can be calculated using a formula derived by Murthy and Kehr,

$$\bar{\tau}_{0,L} = \sum_{k=0}^{L-1} \frac{1}{p_k} + \sum_{k=0}^{N-2} \frac{1}{p_k} \sum_{i=k+1}^{N-1} \prod_{j=k+1}^{i} \frac{q_j}{p_j} \tag{4.27}$$

where p_j is the rate of the random walker for jumping from site j to $j+1$ and q_j for jumping from site j to $j-1$ [118]. This formula reduces only in some special cases to a closed form and one has to revert to numerical evaluations in general. We tested the scaling with respect to L for several shapes (parabolic, rectangular and Gaussian) of the wells whose maxima are chosen to be proportional to L. Independent of the precise shape of the well $\bar{\tau}$ diverges exponentially in L.

Thus the transition times of the shock front from one boundary to the other diverge exponentially in system size and hence ergodicity is broken in the thermodynamic limit.

Of course the transition times can be checked directly using the energy profiles which result from the density profiles. Energy profiles for different system sizes are shown in figure 4.8. They are determined using the density profiles obtained from the integration of the differential equation (4.6), the currents resulting from the current density relation are plugged into Eq. (4.25). The height of the barrier increases linearly with system size and this results in an exponential increase of the mean first passage times $\bar{\tau}_{0,L}$.

4.7 Simulations

The previously discussed behavior of the system can be illustrated and verified by Monte Carlo (MC) simulations. For tracing the position of the shock we use the second–class particle technique [119], which allows for tracking the flow of local fluctuations required to determine the shock position on the lattice scale. In conservative systems the dynamics of a second class particle ('B') is such that it hops like the original particles in an environment of holes but behaves as a hole with respect to the particles. Thus for the TASEP the dynamics is given by

$$A\varnothing \to \varnothing A; \qquad B\varnothing \to \varnothing B; \qquad AB \to BA. \tag{4.28}$$

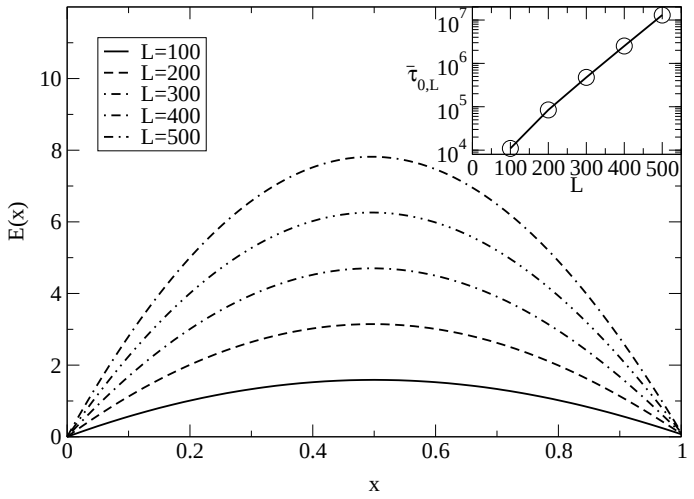

Figure 4.8: Energy profiles for $\rho_- = 0.26$, $\rho_+ = 0.53$, $\Omega_a = 0.7$, $\Omega_d = 0.1$ and different system sizes. The inset shows mean the first passage times $\bar{\tau}_{0,L}$ in dependence of the system size.

When coupling the system to a reservoir the bulk conservation law is broken and one is faced with the problem how the second class particle behaves under creation and annihilation events. We resolve this problem by introducing a sublattice on which the second–class particle moves. The hopping rates of the second–class particle depend on the configuration of the primary lattice. In the bulk the complete dynamics is given by

$$\begin{array}{cccc} A & \varnothing & \to & \varnothing & A \\ \varnothing & \varnothing & & \varnothing & \varnothing \end{array}$$

$$\begin{array}{cccc} \varnothing & \varnothing & \to & \varnothing & \varnothing \\ B & \varnothing & & \varnothing & B \end{array} \qquad \begin{array}{cccc} A & \varnothing & \to & \varnothing & A \\ B & \varnothing & & B & \varnothing \end{array} \tag{4.29}$$

$$\begin{array}{cccc} A & \varnothing & \to & \varnothing & A \\ \varnothing & B & & B & \varnothing \end{array} \qquad \begin{array}{cccc} A & A & \to & A & A \\ \varnothing & B & & B & \varnothing \end{array} .$$

The first line corresponds to the normal dynamics of the TASEP. In the second line the analogy to the move $B\varnothing \to \varnothing B$ and in the third line the move $AB \to BA$ are shown. In this dynamics the second class particle may correspond either to a particle or a hole on the primary lattice. The non–conservative reaction kinetics $A\varnothing A \leftrightharpoons AAA$ acts only on the primary lattice without influencing the second–class particle.

At the boundaries it is possible that the second–class particle leaves the system. The dynamics is chosen such that the second–class particle rests on

the "first" site of the reservoir. This is realized by introducing two additional sites, 0 and $L+1$ on the secondary lattice:

$$\begin{array}{cccc} & \varnothing & \overset{\rho_-}{\longrightarrow} & A \\ \varnothing & \varnothing & & \varnothing \quad \varnothing \end{array}$$

$$\begin{array}{cccc} & \varnothing & \overset{\rho_-}{\longrightarrow} & A \\ \varnothing & B & & B \quad \varnothing \end{array} \qquad \begin{array}{cccc} & A & \overset{\rho_-}{\longrightarrow} & A \\ \varnothing & B & & B \quad \varnothing \end{array} \tag{4.30}$$

$$\begin{array}{cccc} & \varnothing & \overset{\rho_-}{\longrightarrow} & A \\ B & \varnothing & & \varnothing \quad B \end{array} \qquad \begin{array}{cccc} & \varnothing & \overset{1-\rho_-}{\longrightarrow} & \varnothing \\ B & \varnothing & & \varnothing \quad B \end{array}$$

for the left boundary and correspondingly for the right boundary:

$$\begin{array}{cccc} A & & \overset{1-\rho_+}{\longrightarrow} & \varnothing \\ \varnothing & \varnothing & & \varnothing \quad \varnothing \end{array}$$

$$\begin{array}{cccc} \varnothing & & \overset{1-\rho_+}{\longrightarrow} & \varnothing \\ B & \varnothing & & \varnothing \quad B \end{array} \qquad \begin{array}{cccc} A & & \overset{1-\rho_+}{\longrightarrow} & \varnothing \\ B & \varnothing & & \varnothing \quad B \end{array} \tag{4.31}$$

$$\begin{array}{cccc} A & & \overset{\rho_+}{\longrightarrow} & A \\ \varnothing & B & & B \quad \varnothing \end{array} \qquad \begin{array}{cccc} A & & \overset{1-\rho_+}{\longrightarrow} & \varnothing \\ \varnothing & B & & B \quad \varnothing \end{array}$$

This dynamics represents the straightforward extension to the original rules for only one lattice as presented in Ref. [120].

In order to achieve reasonable statistics, a multispin code was used [121]. In this programming technique a state of a lattice site is stored by an integer number like usual but in contrast to conventional methods one uses all the bits in order to store systems in parallel. The lattice update is performed by binary bit operators such that with one instruction up to 64 systems may be updated synchronously which speeds up the calculations considerably. As in the present case each lattice site has four possible states two bits have to be used for each system and consequently only 32 systems are simulated in parallel. However, the simulation is still quite efficient.

4.7.1 Hysteresis

As a first simulation result we demonstrate that indeed the broken ergodicity leads to the phenomenon of hysteresis. To this end the right density is fixed to $\rho_+ = 0.45$ and the rates of the reaction kinetics are chosen as $\Omega_a = 0.7$ and $\Omega_d = 0.1$. The left density is varied such that the system starts in LD ($\rho_- = 0.22$), crosses the ergodic phase and ends in the HD2 ($\rho_- = 0.30$) phase. A relevant parameter in hysteresis phenomena is the speed of sweeping: in our simulations ρ_- was changed by 10^{-4} in every k MC time steps. Then the process of changing ρ_- is reversed. As an order parameter of the hysteresis

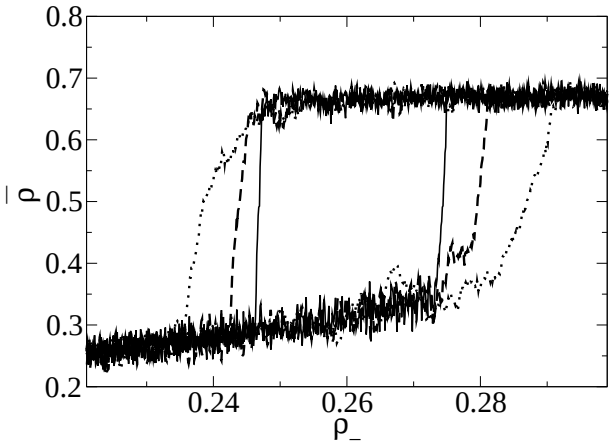

Figure 4.9: Hysteresis plot for $L = 2000, \Omega_a = 0.7, \Omega_d = 0.1, \rho_+ = 0.45$. ρ_- was changed by 10^{-4} in every 5000 (solid line), 1500 (dashed line) and 500 (dotted line) MC steps. The hysteresis loops gets wider as the speed of changing ρ_- is increased.

the space–averaged density $\bar{\rho}$ which is considerably different in the low– and high–density state is measured every k–th step. In figure 4.9 the resulting hysteresis loops are shown. We find that the hysteresis loop inflates with increasing speed which is reminiscent of hysteresis in usual magnetic systems. When starting in the LD (HD) phase the shock position is stable at the right (left) boundary. Entering the nonergodic phase the other boundary gets locally but not globally stable. At a certain point the two minima change roles – the originally metastable state gets globally stable and vice versa. But it takes a certain time for the system to trespass the barrier. If the tuning speed is slow enough the system is able to relax, but for higher speeds the parameters are changed while the systems remains in the metastable state.

4.7.2 Random transitions

Next, the one–particle picture shall be confirmed. For judiciously chosen parameters it is possible to perform simulation to times much larger than $\bar{\tau}$. A typical realization of the position of the second–class particle and thus of the position of the shock is shown figure 4.10. The waiting time τ which is the time the system spends in one of the stationary states before switching to the others are measured as follows. As the position of the second–class particle is fluctuating at the boundaries between the transitions it is conve-

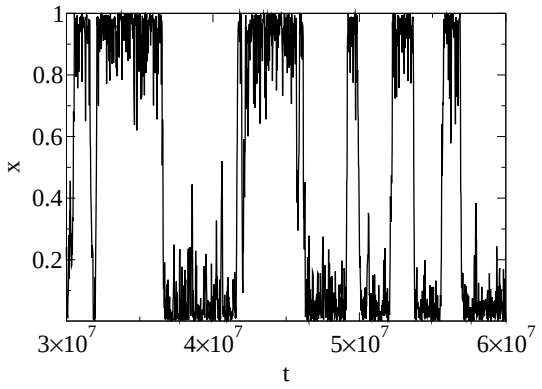

Figure 4.10: Snapshot of the time evolution of the scaled position of the second–class particle for $L = 1000, \rho_- = 0.2705, \rho_+ = 0.63, \Omega_a = 0.5, \Omega_d = 0.1$. A position of the second–class particle near the left boundary ($x \approx 0$) corresponds to the high–density state, while a position near the right boundary ($x \approx 1$) corresponds to the low–density state.

nient to determine the time the second–class particle does *not* spend at the opposite boundary. Thus in the vicinity of each boundary certain thresholds are defined and the particle is considered to be at a boundary from the point of time it first passes the threshold of this boundary until it hits the other threshold for the first time. As the transition itself is rather quick compared to the waiting time the value of τ does not crucially depend on the exact position of the thresholds, thus they may just as well be set to the boundaries themself.

If the picture of the random walker in an energy landscape is correct the transition from one boundary to the other is a random event and the waiting times should follow an exponential distribution,

$$P(\tau) = \bar{\tau} \exp(\tau/\bar{\tau}). \tag{4.32}$$

This can be directly checked in our simulations. The mean first passage times are not equal for the forth and back transitions as the potential is not symmetric in general. One thus has to perform separate statistics for each. In order to avoid binning it is convenient to consider the cumulative distribution rather than the probability density. For the exponential distribution the cumulative distribution is given by

$$\Phi(\tau) = 1 - \exp(-\tau/\bar{\tau}). \tag{4.33}$$

As shown in figure 4.11 the numerically determined statistics follows in very good agreement an exponential distribution which affirms the picture of the random walker.

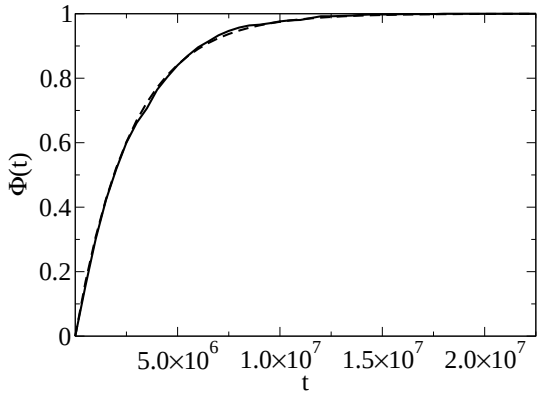

Figure 4.11: Numerically determined cumulative distribution of the transition times from the upper state to the lower (solid line) compared to the exponential distribution (dashed line) with parameters as in Fig. 4.10.

4.8 Conclusions

In this chapter it is generally discussed under which conditions a driven diffusive system coupled to a non–conservative reaction kinetics may show ergodicity breaking in the thermodynamic limit. For this purpose a hydrodynamic description is used leading to a modified Burgers' equation. While the Burgers' equation generally describes conservative systems in this case due to the special rates of the non–conservative reactions the non–conservative dynamics can be included by a source term.

For the TASEP the reaction kinetics must include at least three lattice sites in order to lead to ergodicity breaking. For a special choice of non–conservative dynamics we calculate the exact phase diagram of the system exhibiting five distinct phases. While some of the phases have analogs in the ASEP two additional phases are found not existing in the ASEP, the coexistence and the nonergodic phase. In the coexistence phase a localized shock separates in the bulk a low–density domain from a high–density domain. The nonergodic phase is characterized by an unstable shock position in the bulk, such that the shock position is locally stable at both boundaries. It is shown that the transition times between the metastable states diverge exponentially in system size and hence ergodicity is broken in the thermodynamic limit.

It is shown that the behavior of this non–equilibrium many body problem can be described in terms of an equilibrium process, a random walker in a space dependent potential. The random walker represents the shock position and its hopping rates are calculated by considering the particle currents in the vicinity of the shock.

Monte Carlo simulations confirm this picture. By introducing a second–class particle the position of the shock can be tracked. The usual dynamics of a second–class particle has to be adopted for the present case as it is usually only defined for conservative dynamics. In the nonergodic phase the predicted random transitions can be observed. The waiting times of the transitions follow an exponential distribution as for a random process resulting from a random walker in a potential.

By tuning the system parameters such that the nonergodic phase is traversed the phenomenon of hysteresis can be demonstrated in the Monte Carlo simulations. A suitable order parameter is the space averaged density which is clearly distinct in the low– and high–density state. It is observed that the hysteresis loop inflates with increasing tuning speed of parameters which results from the fact that the system does not relax immediately from the metastable state into the stable one.

Chapter 5

Reactions fronts in models with three–point interactions

5.1 Introduction

In this chapter the movement of reaction fronts in reacting and diffusing particle systems is investigated.

The emergence of patterns and fronts is a challenging problem in biology, chemistry and physics, for a review see Ref. [122]. In biology for example bacteria aggregate building up regions with a high density in coexistence with regions with a low density of organisms [123]. A typical example in chemistry is the movement of reaction fronts. In physics the movement of domain walls is directly related to the problem of coarsening, see chapter 2. In chapter 4 the phenomenon of hysteresis in a driven diffusive system is explained by the movement of shocks, i.e., a jump in the density profile. Various other phenomena in many particle systems can be attributed to the emergence of shocks, for example the first order transition in the phase diagram of the asymmetric exclusion process (ASEP) (see section 4.1.1 and Ref. [91]) or phase coexistence in a driven diffusive system coupled to reaction kinetics [109, 112]. Recently, shocks in quantum systems have been also discussed [124, 125].

On a macroscopic level shock fronts are described by partial differential equations. The most prominent equations are the Fisher and the Burgers' equations. The Fisher equation [126]

$$\frac{\partial}{\partial t}\rho(x,t) = D\frac{\partial^2}{\partial x^2}\rho(x,t) + a\rho(x,t) - b\rho^2(x,t) \tag{5.1}$$

was originally proposed as a model for the propagation of a mutant gene. It shows traveling wave solutions and may be used for modeling systems without conservation of the order parameter.

The inviscid Burgers' equation [127]

$$\frac{\partial}{\partial t}\rho(x,t) = -a\frac{\partial}{\partial x}\left[\rho(x,t)\left(1-\rho(x,t)\right)\right] \tag{5.2}$$

was proposed as a model for turbulent fluid motion. It as well shows shock solutions, but it may be used for modeling systems with particle conservation.

In this chapter it is demonstrated for some models how these macroscopic shocks originate from the microscopic dynamics. It is known that some driven diffusive systems can be described by the Fisher or Burgers' equation in the hydrodynamic limit. This limit is achieved by scaling the lattice constant to zero while keeping the overall length of the system constant, the time has to be rescaled appropriately. One of these models is the ASEP which is in the hydrodynamic limit described by the Burgers' equation. Another model is the branching and coalescing random walk, which is in the hydrodynamic limit

described by the Fisher equation [128]. In these two models the microscopic dynamics can be described by exact shock measures. An exact shock measure is a state where two product measures with different densities are connected. The time evolution of this state is given by a diffusion equation with respect to the position of the density step [129, 130, 131]. In particular this implies that the microscopic structure of the system is known at all times.

The physical properties of large classes of one–species reaction–diffusion models with *nearest neighbor* interactions have been widely studied [91, 132, 133, 134]. There are only four known models wich show shocks without correlations [131, 135, 136]: the ASEP, the branching and coalescing random walk (BCRW), the asymmetric Kawasaki–Glauber process (AKGP) and the brick layer model. While the former three models are exclusion models where the number of particles on each lattice site is restricted to at most one, the particle number is not restricted in the latter one. Here, the investigation shall be extended to three–site interaction exclusion models [137, 138] and it will be shown that three–site interactions give rise to models with exact shock measures which show aspects not seen in nearest neighbor models, viz. double shocks and additional symmetries even though no free fermion condition is met.

At this point we remark that the question of phase separation is directly linked to the movement of domain walls because coarsening is generic for this phenomenon. But although some of the models presented in this chapter show growing domains we will argue that this mechanism cannot be used for constructing nonequilibrium models with two species (one type of particles and vacancies) showing phase separation in one dimension [139, 140, 141].

We present a survey of one–species models with three–site interactions and open boudaries whose time evolution is described by an exact diffusive shock measure, to be defined below. For the cases of shocks between two nonfluctuating phases (densities 0 to 1) and two fluctuating phases (both densities are different from 0 and 1) the list is complete. For the case of a shock from a nonfluctuating phase (density 0 or 1) to a fluctuating phase (density between 0 and 1) the variety of models is too large to give a complete survey – the number of free parameters rises from 12 to 56 when the interaction range is increased from two to three. But we present a classification of models with respect to their symmetries, where we considered models where at least two of the symmetries charge (C), parity (P) and time (T) are valid independently.

We also address the question to what extent the description of the dynamics of the model by the movement of shock fronts is sufficient. To this end the interactions of the domain walls are determined and possible parallels to free fermion systems are discussed.

5.2 Formalism

On each lattice site k ($k = 1, \ldots, L$) of a one–dimensional lattice there may be at most one particle (A) or a vacancy ($\varnothing$). One can also consider these two–state systems as spin systems, a particle is represented by a down spin ($|\downarrow\rangle$) and a vacancy by an up spin ($|\uparrow\rangle$). The stochastic dynamics of the models are defined by a master equation [142] which is conveniently expressed in the quantum–Hamiltonian formalism for spin–1/2 chains as described in Ref. [91]. To each lattice configuration η we assign a basis vector $|\eta\rangle$ which is given by the tensor product of the single–site states. The probability vector describing the system can then be written as

$$|P(t)\rangle = \sum_{\eta} P(\eta, t)\, |\eta\rangle \tag{5.3}$$

where $P(\eta, t)$ is the probability at time t to find the system in the state η. The time evolution of the system is described by a master equation which can be written as

$$\frac{d}{dt}\, |P(t)\rangle = -H\, |P(t)\rangle \tag{5.4}$$

where H is the stochastic generator of the process. Due to the analogy of equation (5.4) to the Schrödinger equation (in imaginary time) H is often called the Hamiltonian of the system. Conservation of probability requires that the sum of the entries of each column is zero,

$$\langle s|\, H = 0, \tag{5.5}$$

where $\langle s| = (1, 1, ...)$ is the so-called summation vector.

For finite interaction range and spatially homogeneous kinetics it is convenient to write the generator as

$$H = -\sum_{k} h_k - b_1 - b_{L-1}, \tag{5.6}$$

where the local Hamiltonians h_k contain the rates of the elementary local transitions and b_1, b_{L-1} account for events at the left respectively right boundary. The operators h_m include only operators acting on the sites m, $m+1$ and $m+2$; the operators b_m include only operators acting on m and $m+1$. They are formulated using the particle number operator (n_k), vacancy number operator ($v_k = \mathbf{1} - n_k$), the particle creation (s_k^-) and annihilation (s_k^+) operators. The lower index represents the lattice site on which the respective operator acts. The diagonal entries of the Hamiltonian have to be chosen such

that conservation of probability is fulfilled which can be easily constructed by considering

$$\langle s|\, s_k^- = \langle s|\, v_k; \qquad \langle s|\, s_k^+ = \langle s|\, n_k. \tag{5.7}$$

For example diffusion to the right ($A\varnothing \to \varnothing A$) with rate D_r is written as $h_k = D_r \left(s_k^+ s_{k+1}^- - n_k v_{k+1}\right)$.

5.3 Product– and shock–measures

In what follows $|\cdot\rangle_1$ denotes a probability vector for a single site and an operator without index a single site operator. If no correlations are present the probability vectors are simply given by

$$|P(t)\rangle = |\rho\rangle \equiv |\rho\rangle_1 \otimes \cdots \otimes |\rho\rangle_1 \tag{5.8}$$

with

$$|\rho\rangle_1 = \rho\,|\downarrow\rangle_1 + (1-\rho)\,|\uparrow\rangle_1 = \begin{pmatrix} 1-\rho \\ \rho \end{pmatrix}. \tag{5.9}$$

In this case the calculation of the action of the stochastic generator H can be simplified by using the following identities:

$$s^-\,|\rho\rangle_1 = \frac{1-\rho}{\rho} n\,|\rho\rangle_1\,; \qquad s^+\,|\rho\rangle_1 = \frac{\rho}{1-\rho} v\,|\rho\rangle_1\,. \tag{5.10}$$

A product measure $|\rho\rangle$ is a stationary state of the system, if

$$H\,|\rho\rangle = 0. \tag{5.11}$$

As a shock measure $|\rho_1, \rho_2, k\rangle$ we define the state which is a product measure with density ρ_1 up to and including site k and beginning from site $k+1$ a product measure with density ρ_2:

$$|\rho_1, \rho_2, k\rangle = |\rho_1\rangle_1^{\otimes k} \otimes |\rho_2\rangle_1^{\otimes L-k}\,. \tag{5.12}$$

We are interested in those systems, for which the time evolution of the shock measure is given by a diffusion equation (see figure 5.1)

$$\begin{aligned} \frac{d}{dt}\,|\rho_1, \rho_2, k\rangle = -H\,|\rho_1, \rho_2, k\rangle = \quad & \delta_1\,|\rho_1, \rho_2, k-2\rangle + \delta_2\,|\rho_1, \rho_2, k-1\rangle \\ + \quad & \delta_3\,|\rho_1, \rho_2, k+1\rangle + \delta_4\,|\rho_1, \rho_2, k+2\rangle \\ - \quad & \delta_5\,|\rho_1, \rho_2, k\rangle\,. \end{aligned} \tag{5.13}$$

Starting from an initial density step the system will evolve into an exact diffusive shock measure defined by

$$|P(t)\rangle = \sum_l p_l(t)\,|\rho_1, \rho_2, l\rangle \tag{5.14}$$

which is a time dependent superposition of sharp shocks weighted with $p_l(t)$. This can be seen by solving Eq. (5.13) for an initial shock at position k:

$$\begin{aligned} |\rho_1, \rho_2, k, t\rangle &= \sum_l G(l,t|k,0)\,|\rho_1, \rho_2, l\rangle \\ G(l,t|k,0) &= \frac{1}{2\pi}\int_{-\pi}^{\pi} dp \exp(-\epsilon_p t + i(k-l)p) \\ \epsilon_p &= -(\delta_1 \exp(-2ip) + \delta_2 \exp(-ip) + \delta_3 \exp(ip) + \delta_4 \exp(2ip) - \delta_5). \end{aligned} \tag{5.15}$$

$G(l,t|k,0)$ is the Green's function for this problem, for large arguments $(k-l)$ and late times it approaches a Gaussian, as expected for a diffusion problem. From Eq. (5.15) we read off $p_l(t) = G(l,t|k,0)$.

If we choose a shock measure (5.12) as initial condition of a system which obeys Eq. (5.13) the form of the shock is preserved in time but due to the diffusion the state of the system will evolve into a superposition of shocks. Thus when performing an ensemble average the density profile is not a sharp step but smears out in time (see figure 5.2) as seen in Monte–Carlo (MC) simulations. Nevertheless a typical configuration of a single systems shows a sharp shock.

Eq. (5.13) directly gives the diffusion coefficient D_s and the shock velocity v_s:

$$\begin{aligned} D_s &= 2\delta_1 + \delta_2 + \delta_3 + 2\delta_4 \\ v_s &= \delta_3 + 2\delta_4 - 2\delta_1 - \delta_2. \end{aligned} \tag{5.16}$$

The product measures to the left and to the right of the shock position are only possible for a special choice of boundary dynamics b_1 and b_{L-1}. A possible choice is always those boundary dynamics which is the effect of reservoirs with densities ρ_1 respectively ρ_2 [143]: One imagines that the lattice is extended by two additional sites at each boundary and one calculates the action of h_{-1} and h_{-2} (h_{L-1} and h_L) assuming that the sites are occupied according to the product measures in the bulk and determines the effective rates for the boundary action. Thus, n_{-1} and s^+_{-1} are substituted by ρ_1, v_{-1} and s^-_{-1} by $(1-\rho)$ – the other sites are handled accordingly. In this chapter

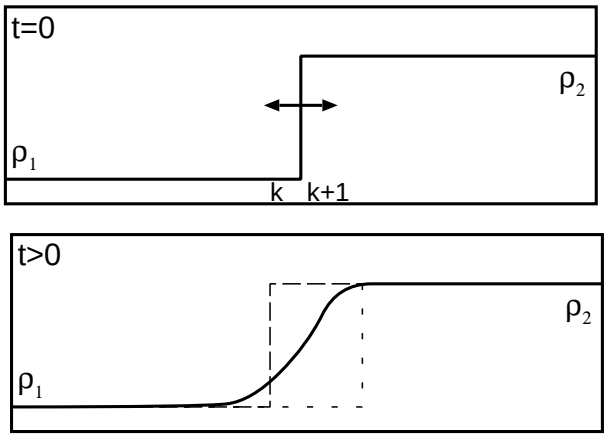

Figure 5.1: Ensemble average of a diffusive shock measure (schematically): Due to superposition the density profile smears out although the form of the shock is preserved in each realization.

we always consider the limit $L \to \infty$ such that the shock is assumed not to hit the boundaries.

Given specific microscopic processes we test for the existence of diffusive shock measures by the following procedure:

a) Check whether $|\rho_1\rangle$ is a product measure of the system with periodic boundaries.

b) Set up the boundary processes b_1 such that

$$\left(\sum_{m=1}^{k} h_m + b_1\right) |\rho_1, \rho_2, k\rangle = c_{k-1} |\rho_1, \rho_2, k\rangle \tag{5.17}$$

where c_{k-1} acts on sites $k-1$ to $k+2$.

c) Check whether $|\rho_2\rangle$ is a product measure of the system with periodic boundaries.

d) Set up the boundary processes b_{L-1} such that

$$\left(\sum_{m=k+1}^{L-2} h_m + b_{L-1}\right) |\rho_1, \rho_2, k\rangle = d_{k+1} |\rho_1, \rho_2, k\rangle \tag{5.18}$$

where d_{k+1} acts on sites $k+1$ to $k+2$.

e) Check whether

$$\begin{aligned}(c_{k-1}+d_{k+1})\,|\rho_1,\rho_2,k\rangle = \quad & \delta_1\,|\rho_1,\rho_2,k-2\rangle+\delta_2\,|\rho_1,\rho_2,k-1\rangle \\ + \quad & \delta_3\,|\rho_1,\rho_2,k+1\rangle+\delta_4\,|\rho_1,\rho_2,k+2\rangle \\ - \quad & \delta_5\,|\rho_1,\rho_2,k\rangle \end{aligned} \tag{5.19}$$

In detail we do the following: After having set up the local Hamiltonians h_k the action on a product measure is brought into a diagonal form as described above,

$$h_k\,|\rho\rangle = h_k^{\mathrm{diag}}\,|\rho\rangle \tag{5.20}$$

where h_k^{diag} contains only the operators n_m and $\mathbf{1}$ (v can be eliminated using $v=\mathbf{1}-n$) acting on sites $m=\{k,k+1,k+2\}$.

The requirement of a product measure (a) leads to the condition that the application of the Hamiltonian of the periodic system has to produce "telescope"–sums of diagonal operators which results in five equations of the rates for each density.

Condition e) can be checked using the identity

$$|\rho_1,\rho_2,k-1\rangle = \left(\frac{1-\rho_2}{1-\rho_1}v_k+\frac{\rho_2}{\rho_1}n_k\right)|\rho_1,\rho_2,k\rangle \tag{5.21}$$

and analogous identities for $|\rho_1,\rho_2,k-2\rangle$, $|\rho_1,\rho_2,k+1\rangle$ and $|\rho_1,\rho_2,k+2\rangle$. A comparison of coefficients of the (only diagonal) operators on the left and right hand site of Eq. (5.19) then leads to another seven equations of the rates, ρ_i ($i=1,2$) and δ_j ($j=1,\ldots,5$). Conservation of probability implies

$$\delta_5=\sum_{i=1}^{4}\delta_i, \tag{5.22}$$

which is not an additional equation but simplifies the calculation.

If one of the densities is either zero or one, the Hamiltonian cannot be brought to diagonal form using Eqs. (5.10) and (5.21). But in this case the action of the Hamiltonian simplifies and an analogous comparison of coefficients of creation and annihilation operators is possible.

5.4 Classification of models

In order to find the models with three–site interactions which exhibit shock diffusion one could in principle try to solve Eq. (5.13) for the general Hamiltonian. But as there are 56 microscopic processes (transitions from any of the $2^3=8$ states to any different state) this task is tedious, if not obnoxious.

We facilitate the procedure by writing a computer program which does all the symbolical calculation (transformation of the Hamiltonian into diagonal form, gathering of coefficients) and sets up the constituting set of equations. These equations are then solved by standard mathematical software. Still, the general solution of the problem is far too complex to extract useful informations. It is hence useful to investigate physically motivated sub–classes, as done in the following.

5.4.1 Shocks from $\rho_1 = 0$ to $\rho_2 = 1$

The completely empty lattice, $\rho = 0$, and the fully occupied one, $\rho = 1$, are nonfluctuating states. They are the two ground states of the zero–temperature Ising model. In this case only few processes play a role. All processes starting from $\varnothing\varnothing\varnothing$ or AAA are forbidden because otherwise product measures with densities 0 and 1 would not be stationary solutions of the system. The processes which act on the configurations $\varnothing A\varnothing$, $A\varnothing\varnothing$, $A\varnothing A$ and $AA\varnothing$ are ineffectual because none of these configurations is possible, if the system is initialized with a shock measure. The remaining processes are

$$\begin{array}{lll} \varnothing\varnothing A \stackrel{K_0}{\to} AAA; & \varnothing\varnothing A \stackrel{K_1}{\to} \varnothing AA; & \varnothing\varnothing A \stackrel{K_2}{\to} \varnothing\varnothing\varnothing; \\ \varnothing AA \stackrel{K_3}{\to} AAA; & \varnothing AA \stackrel{K_4}{\to} \varnothing\varnothing A; & \varnothing AA \stackrel{K_5}{\to} \varnothing\varnothing\varnothing. \end{array} \tag{5.23}$$

The diffusion constants are then given by

$$\delta_1 = K_0; \qquad \delta_2 = K_1 + K_3; \qquad \delta_3 = K_2 + K_4; \qquad \delta_4 = K_5. \tag{5.24}$$

The solution for a shock between $\rho_1 = 1$ and $\rho_2 = 0$ is obtained by exchanging the roles of particles and holes ($A \leftrightarrow \varnothing$).

This dynamics is a generalized zero temperature Ising model where the domain wall between spin up and spin down regions diffuses freely. As the space symmetric processes have no influence on the upward shock they can be included giving rise to a model allowing for both, upward and downward shocks. All ten rates are independent such that the drift of the domain walls can be chosen freely.

5.4.2 Shocks from $\rho_1 \in (0;1)$ to $\rho_2 \in (0;1)$

For each Hamiltonian with three–site interactions there is either none, exactly one product measure with a density in the open interval $\rho \in (0;1)$, or infinitely many. The latter is only possible for particle–conserving Hamiltonians. The proof of this assertion is possible for the case of three–site

interactions, but rather technical and is therefore omitted here. It is based on analyzing the conditions on the rates and densities for the existence of a product measure Eq. (5.11) for the general three–site Hamiltonian.

Instead we present a general consideration why the existence of two fluctuating stationary product measures is impossible for non particle–conserving Hamiltonians. This is not intended to be a mathematical rigorous proof, it is rather a physical consistency check. This consideration is related to the positive rates conjecture, see Refs. [139, 140].

Let us assume that there are two fluctuating stationary densities $\rho_1 \neq \rho_2$ for a non particle–conserving Hamiltonian. Then due to fluctuations there is a finite probability that in the stationary state with density ρ_1 a region of density ρ_2 emerges. As ρ_1 is a stationary density this region has to be suppressed and vanishes again. Consequently the domain walls $\rho_1|\rho_2$ and $\rho_2|\rho_1$ are moving toward each other shortening the domain of ρ_2. But if this is the case ρ_2 cannot be a stationary state, as a region of ρ_1 emerging in a phase of ρ_2 is growing. Hence the assumption of the existence of two fluctuating stationary densities was wrong.

Note that Gacs error correcting model [139, 140] does not represent a counter example for this statement. It is crucial that product measures are considered: For this case no dynamics is able to determine the length of a one–dimensional domain – the domain growth is independent of the domain size, while phase separation requires a faster growth of larger domains.

In Fig. 5.2 the time evolution of a non particle–conserving system is shown. The particle density in the low density region is not stationary and increases until the first shock vanishes. The second shock disappears due to another mechanism, here the diffusion equation of the shock is not fulfilled and consequently the shock dissolves.

The situation is basically different if particle–conserving Hamiltonians are considered. In this case the system is not ergodic and hence a region of different density cannot evolve in the bulk of the system. Consequently several stationary densities are possible.

As non–conserving Hamiltonians do not allow for the existence of two fluctuating phases we only need to investigate particle–conserving Hamiltonians and recover the solution of the investigation of nearest neighbor interactions, the asymmetric simple exclusion process (ASEP) [131]:

$$\begin{aligned} A\varnothing \overset{D_R}{\to} \varnothing A; \qquad \varnothing A \overset{D_L}{\to} A\varnothing \\ D_R \frac{\rho_1}{1-\rho_1} = D_L \frac{\rho_2}{1-\rho_2} \\ \delta_1 = 0; \qquad \delta_2 = \frac{1-\rho_1}{1-\rho_2} D_L; \qquad \delta_2 = \frac{1-\rho_2}{1-\rho_1} D_R; \qquad \delta_4 = 0 \end{aligned} \tag{5.25}$$

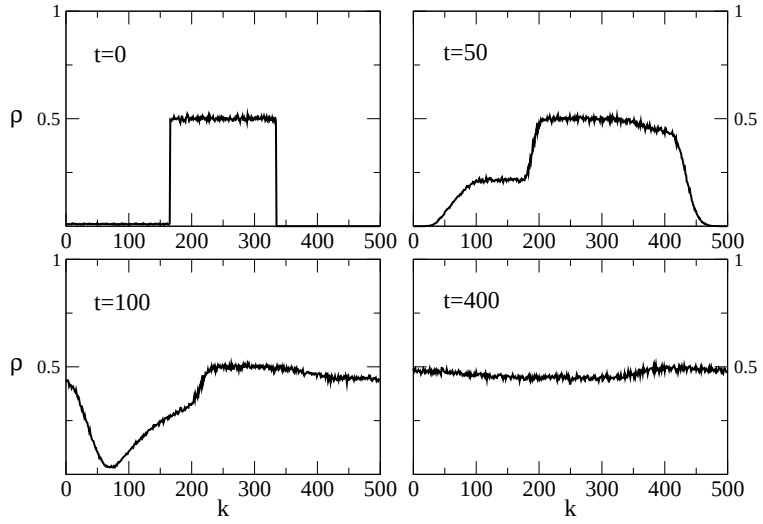

Figure 5.2: Monte Carlo simulation of the model $A\varnothing\varnothing \to AAA$; $AAA \to \varnothing\varnothing A$, the number of sites is 500 and an average over 5000 systems was performed, the boundary conditions are periodic. As initial condition we took a shock measure with steps at site 166 from 0.01 to 1/2 and at site 333 from 1/2 to 0. The left step is not stable because the product measure with $\rho_1 = 0.01$ is not a stationary state and the right step is not stable because there the diffusion equation is not fulfilled.

The inclusion of next–nearest neighbor interaction does not lead to further models in this case.

5.4.3 Shocks from $\rho_1 = 0$ to $\rho_2 \in (0; 1)$

While the existence of two fluctuating stationary states is impossible, the existence of one fluctuating and one non fluctuating phase is easy to construct. The density $\rho_1 = 0$ is stationary if all processes from the empty lattice, $\varnothing\varnothing\varnothing$, are prohibited. This is a violation of the assumption underlying the positive rates conjecture as certain types of fluctuations are absent. Therefore two stationary states are possible, however, the nonfluctuating phase is unstable and the fluctuating phase will always enlarge at the expense of the nonfluctuating one.

For the existence of a product measure $\rho_2 \in (0; 1)$ it is then necessary that as well no process to the empty lattice is present. Apart from these constraints no further processes can be excluded a priori. We restrict ourselves to the case of a shock between $\rho_1 = 0$ to $\rho_2 \in (0; 1)$. The cases of a shock

from $\rho_1 = 1$ to $\rho_2 \in (0;1)$ can be obtained by exchanging particles and holes, and the case of the fluctuating phase to the left can be obtained by a parity transformation.

As argued above, the degrees of freedom are too many for a complete investigation and we classify the systems by the symmetries charge (C), parity (P) and time (T). In this context, charge symmetry is the invariance of the microscopic processes under the exchange of particles and holes ($A \leftrightarrow \varnothing$), i.e., for each process in the model there exists the C-symmetric one with the same rate. Although this picture is quite artificial when applied to particles it is natural in the language of spins where in the absence of an external field the symmetry between the up and down spin is obvious. Parity symmetry is the invariance of the microscopic processes under the exchange of left and right, i.e., for each process in the model there exists the P-symmetric one with the same rate. Time symmetry is the invariance under the transformation of $t \to -t$. A stochastic model is T–invariant if detailed balance with respect to its stationary distribution is fulfilled, [142], i.e., these models are able to reach an equilibrium steady state. This is the case if for all states η_1,η_2 the transition rates $w_{\eta_1 \to \eta_2}$, $w_{\eta_2 \to \eta_1}$ and probabilities of finding the system in the configurations $P(\eta_1)$, $P(\eta_2)$, obey the equation $w_{\eta_1 \to \eta_2} P(\eta_1) = w_{\eta_2 \to \eta_1} P(\eta_2)$, i.e., there is no net current between states. If the stationary state of a system is a product measure, the validity of detailed balance is easily checked or refuted, because the calculation of the probabilities of the system to be in a specific states is trivial and additionally the absence of correlations permits to investigate only the local rates instead of the configurations of the whole lattice.

One has to distinguish between a combined symmetry, for example PT, from an independent symmetry, here expressed by the symbol '$\wedge$', for example $P \wedge T$. While in the former case the system is invariant after applying the symmetries one after each other, in the latter case the system is invariant under the symmetries applied each by themselves.

$C \wedge P \wedge T$ symmetric systems with shock measures

The 56 possible three–site interaction transitions can be arranged in 11 minimal models which obey $C \wedge P \wedge T$ symmetry each (but are not necessarily described by exact diffusive shock measures). If we exclude those which have transitions involving the configurations $\varnothing\varnothing\varnothing$ or AAA only 6 remain. There are 63 combinations which can be build out of 6 elements. We checked all combinations and found that there is only one model which is $C \wedge P \wedge T$

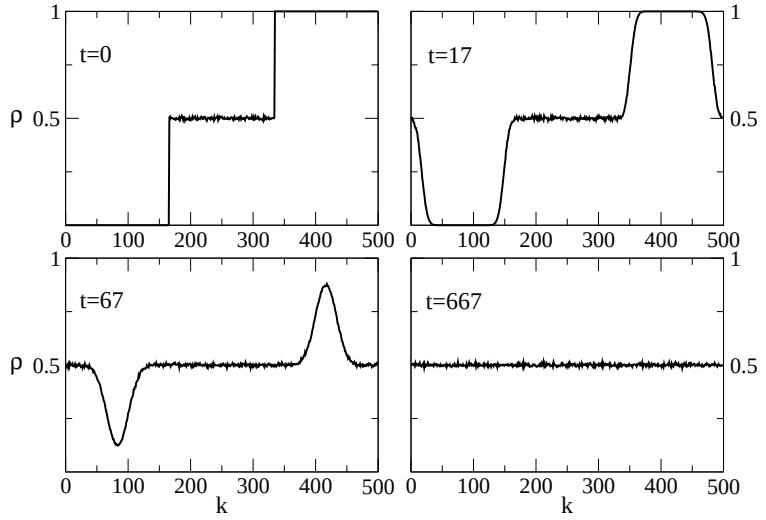

Figure 5.3: Monte Carlo simulation of the $C \wedge P \wedge T$ symmetric model, the number of sites is 500 and an average over 10000 systems was performed. As initial condition we took a shock measure with steps at site 166 from 0 to 1/2 and at site 333 from 1/2 to 1.

symmetric and has an exact diffusive shock measure as solution:

$$\begin{gathered} A\varnothing \xrightarrow{1} \varnothing A; \qquad \varnothing A \xrightarrow{1} A\varnothing; \\ \varnothing\varnothing A \xrightarrow{1} \varnothing AA; \qquad \varnothing AA \xrightarrow{1} \varnothing\varnothing A; \qquad A\varnothing\varnothing \xrightarrow{1} AA\varnothing; \qquad AA\varnothing \xrightarrow{1} A\varnothing\varnothing; \\ \rho_2 = 1/2; \qquad \delta_1 = \delta_4 = 0; \qquad \delta_2 = 2; \qquad \delta_3 = 1. \end{gathered} \tag{5.26}$$

In this model diffusion is combined with branching processes which are only possible to a neighboring lattice site if the subsequent site is empty and its reversal, the coalescence process.

Due to the $C \wedge P$ symmetry this model has the property that both the shock from 0 or 1 to 1/2 and the shock from 1/2 to 0 or 1 is stable. Hence double shocks $0|\frac{1}{2}|0$ and $0|\frac{1}{2}|1$ are possible. We calculated the time evolution of an initial double shock $(0|\frac{1}{2}|1)$ in a periodic system by a Monte Carlo simulation as shown in Fig. 5.3. As calculated the shock moves with a drift of 1 and such that always the fluctuating phase penetrates the non–fluctuating phase. The shock $1|0$ between site 500 and 0 evolves into two steps, $1|\frac{1}{2}$ and $\frac{1}{2}|0$, since these shocks drift into the nonfluctuating phase and split up. As a consequence of the periodic boundary conditions the two shock fronts moving into the non–fluctuating phase coalesce after finite time and

the non–fluctuating phase vanishes. This is a consequence of the stability of the fluctuating phase as argued in section 5.4.2. A detailed discussion of the reaction of shock fronts will be given in 5.5.

$C \wedge P$ symmetric systems with shock measures

There are 17 minimal models obeying $C \wedge P$ symmetry, if we exclude those which have transitions involving the configurations $\varnothing\varnothing\varnothing$ and AAA only 8 remain. Thus in this case 255 combinations have to be checked, but no additional model besides the $C \wedge P \wedge T$ model can be found.

$P \wedge T$ symmetric systems

There are 18 minimal models obeying $P \wedge T$ symmetry, if we exclude those which have transitions involving the configurations $\varnothing\varnothing\varnothing$ only 13 remain. Thus in this case 8191 combinations have to be checked. We found 14 models, as presented in the appendix. Due to the P symmetry in each of these models downward shocks are also stable.

In Fig. 5.4 we show a Monte Carlo simulation of the model D (see appendix) with $\omega = 1/2$ on a ring. As predicted two aspects can be observed: First, both the upward and the downward shock are stable. Second, the fluctuating phase spreads into the nonfluctuating one until the latter finally vanishes. We remind that due to the superposition of shocks the ensemble average does not exhibit a sharp step although each single realization does.

$C \wedge T$ symmetric systems

There are 16 minimal models obeying $C \wedge T$ symmetry, if we exclude those which include the configurations $\varnothing\varnothing\varnothing$ or AAA only 9 remain. Thus in this case 511 combinations have to be checked. Besides the $C \wedge P \wedge T$ model we find the following two models:

$$\varnothing A\varnothing \xrightarrow{1} \varnothing AA; \qquad \varnothing AA \xrightarrow{1} \varnothing A\varnothing; \qquad A\varnothing\varnothing \xrightarrow{1} A\varnothing A; \qquad A\varnothing A \xrightarrow{1} A\varnothing\varnothing;$$
$$\rho_2 = 1/2; \qquad \delta_1 = \delta_2 = \delta_3 = \delta_4 = 0. \tag{5.27}$$

In this model only branching to the right is possible in the presence of another zero at the nearest neighboring site and the corresponding coalescence processes. The domain wall $0|\frac{1}{2}$ is not fluctuating even though the domain is.

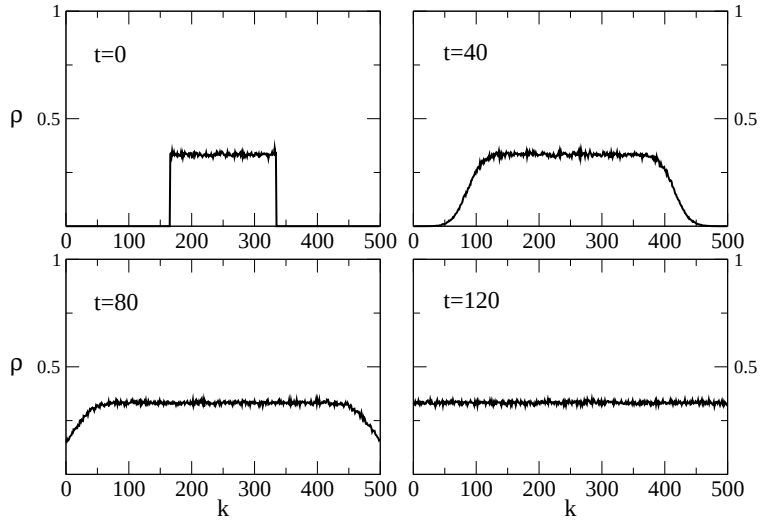

Figure 5.4: Monte Carlo simulation of the $P \wedge T$ symmetric model D with $\omega = 1/2$, the number of sites is 500 and an average over 5000 systems was performed. As initial condition we took a shock measure with steps at site 166 from 0 to 1/3 and at site 333 from 1/3 to 0.

The second model is a combination of branching and coalescence processes to both directions

$$\begin{array}{llll} \varnothing\varnothing A \xrightarrow{1} \varnothing AA; & \varnothing AA \xrightarrow{1} \varnothing\varnothing A; & A\varnothing\varnothing \xrightarrow{1} AA\varnothing; & AA\varnothing \xrightarrow{1} A\varnothing\varnothing; \\ A\varnothing\varnothing \xrightarrow{1} \varnothing AA; & \varnothing AA \xrightarrow{1} A\varnothing\varnothing; & \varnothing A\varnothing \xrightarrow{1} A\varnothing A; & A\varnothing A \xrightarrow{1} \varnothing A\varnothing; \\ & \rho_2 = 1/2; & \delta_1 = \delta_4 = 0; & \delta_2 = \delta_3 = 2. \end{array} \tag{5.28}$$

The domain wall performs an unbiased diffusion with diffusion constant $D = 2$.

For these two $C \wedge T$ models a downward shock has not necessarily to be stable as it is the case for the models which are P symmetric. Indeed, a downward shock is *not* stable in the two models because otherwise the space reflected versions of the processes would show a stable upward shock and would constitute additional $C \wedge T$ models.

Some further models

Here we present some models which do not belong to the classes presented above.

The following model is the totally asymmetric exclusion process combined with activated Langmuir kinetics used in chapter 4 to show hysteresis in driven diffusive systems:

$$\begin{aligned} A\varnothing &\xrightarrow{1} \varnothing A; \\ A\varnothing A &\xrightarrow{\omega_a} AAA; \qquad AAA \xrightarrow{\omega_d} A\varnothing A; \\ \rho_2 &= \frac{\omega_a}{\omega_a+\omega_d}; \qquad \delta_1=\delta_2=\delta_4=0; \qquad \delta_3=(1-\rho_2). \end{aligned} \tag{5.29}$$

The simplest model with a fluctuating shock front not included in nearest neighbor interaction models is

$$A\varnothing\varnothing \to \varnothing\varnothing A; \qquad \delta_4=(1-\rho_2)^2, \tag{5.30}$$

where particles are only allowed to hop over a vacancy to the right. This model is PT symmetric, because reversing the direction of the process is equal to exchanging left and right.

Another simple model is

$$\begin{aligned} A\varnothing\varnothing &\xrightarrow{1} AAA; \qquad AAA \xrightarrow{\omega} \varnothing\varnothing A; \\ \rho_2 &= \frac{\sqrt{\omega}-1}{\omega-1}; \qquad \delta_1=\delta_2=\delta_3=0; \qquad \delta_4=\omega\rho_2^2. \end{aligned} \tag{5.31}$$

This model is again PT symmetric by the same argument as in the model presented above. In this case one has to pay attention to the rates when reversing the time direction, the time reversed process is:

$$AAA \xrightarrow{\omega} A\varnothing\varnothing; \qquad \varnothing\varnothing A \xrightarrow{1} AAA. \tag{5.32}$$

For $\omega = 1$ the density is $\rho_2 = \frac{1}{2}$.

5.5 Reactions of domain walls

Up to now we have only investigated whether the shock fronts are stable and if so how they move. The movement of the shocks can be used to describe the dynamics of the systems as their positions are sufficient to characterize the state of the system. This has been used for example in chapter 4 where the dynamics with many degrees of freedom could be reduced to an effective one particle system. In order to describe a system completely by the position of the domain walls we additionally have to investigate how the domain walls affect each other.

A special case would be if the domain walls do not interact at all. This means that their rates do not change in the presence of another wall – certainly the possibility of mutual annihilation has to be included as a phase may vanish if two boundaries meet. In this case one could interpret the dynamics as the motion of annihilating random walkers. For those systems a direct link to free fermion system has been discussed in Ref. [91] and thus, for the unaffected movement of domain walls a description by free fermions could be possible. To this end one may apply the Jordan–Wigner [144] transformation which converts spin–1/2 operators into fermionic creation and annihilation operators.

The significance of the Jordan–Wigner transformation in this context is that some Hamiltonians of spin–1/2 systems transform into fermion Hamiltonians which include only bilinear expressions of the fermionic operators – this can be regarded as a system of free fermions. For these Hamiltonians additional techniques for calculating the dynamical properties are available. Interestingly the dynamics of all particle models showing stable shock fronts with two–site interactions can be represented by the free motion of domain walls without interactions [131]. For the BCRW and the AKGP this is directly related to the free fermion character of these systems.

It is the purpose of this section to investigate potential relations of the three–site interactions models found above to fermion systems, since a link between the domain wall motion and free fermion behavior would be interesting. We first discuss the dynamics of domain walls in detail and then turn to the transformation into fermion systems.

Dynamics of domain walls

When investigating the interaction of domain walls, the situation simplifies again by the fact that within the domains the probabilities are given by a product measure. By this two domain walls may only influence each other if the distance is smaller than three lattice sites and thus only operators acting on a small range have to be included.

The first model to be considered is the $C \wedge P \wedge T$ model. In Fig. 5.3 on the one hand it is shown how a domain wall $1|0$ splits into two domain walls $1|\frac{1}{2}$ and $\frac{1}{2}|0$ and on the other hand how two domain walls $\frac{1}{2}|0$ and $0|\frac{1}{2}$ coalesce. These two cases are now studied in detail analytically.

If the system is characterized simply by the position of the domain walls without further correlations it will be sufficient to describe the dynamics by states

$$|k,l;\rho_1,\rho_2,\rho_3\rangle = \cdots \otimes |\rho_1\rangle \otimes \cdots |\underset{k}{\rho_1}\rangle \otimes |\underset{k+1}{\rho_2}\rangle \otimes \cdots \otimes |\underset{l-1}{\rho_2}\rangle \otimes |\underset{l}{\rho_3}\rangle \otimes \cdots . \quad (5.33)$$

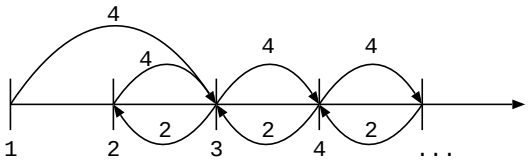

Figure 5.5: The difference $l-k$ of the two shock fronts in the state $|k,l\rangle$ perform a biased random walk.

In order to describe the evolution of the step $1|0$ we define

$$|k,l\rangle \equiv |k,l;1,\frac{1}{2},0\rangle\,. \tag{5.34}$$

In the following the densities are omitted for the sake of simplicity. By applying the Hamiltonian of the $C \wedge P \wedge T$ model on this state one gets

$$\frac{\partial}{\partial t}|k,l\rangle = \begin{cases} 4\,|k-1,l+1\rangle - 4\,|k-1,k\rangle & l-k=1 \\ 2\,|k-1,l\rangle + 2\,|k,l+1\rangle - 4\,|k,l\rangle & l-k=2 \\ 2\,|k-1,l\rangle + |k+1,l\rangle + 2\,|k,l+1\rangle + |k,l-1\rangle - 6\,|k,l\rangle & \\ & l-k\geq 3. \end{cases} \tag{5.35}$$

Thus the time evolution of the system can be completely described by the movement of the domain walls, no additional correlations evolve. Starting from $1|0$ both domain walls simultaneously move by one lattice site creating a fluctuating domain of two sites with density $\frac{1}{2}$. The time evolution of a state in which the domain walls are separated by a lattice site is given by the separate movement of both domain walls by one lattice site. A state in which the domain walls are separated by two or more lattice sites evolves simply by the rates $\delta_2 = 2$ and $\delta_3 = 1$ as calculated before. The time evolution of the distance of the domain walls $l-k$ is illustrated in Fig. 5.5. Once the domain walls are separated it is not possible that they coalesce again as the $l-k=1$ is an isolated point. Thus the movements of the domain walls are not independent, a repulsive interaction is present.

Next, the interaction of the shock fronts $\frac{1}{2}|0$ and $0|\frac{1}{2}$ shall be investigated. To this end we now define

$$|k,l\rangle \equiv |k,l;\frac{1}{2},0,\frac{1}{2}\rangle\,, \tag{5.36}$$

and test again whether the dynamics can be described in terms of the $|k,l\rangle$. Applying the Hamiltonian on the state $|k-1,k+1\rangle$ shows that additional

correlations appear and that consequently the time evolution cannot be described simply by the location of the domain walls.

Nevertheless it is instructive to analyze the appearance of the correlations in detail in order to reveal the link to free fermion systems. The correlations can be compensated by including the process $A\varnothing A \leftrightharpoons AAA$. By this the C symmetry is broken (the $\rho = 1$ phase is not stable anymore), but it is still a $P \wedge T$ model.

Choosing the rate for the forward and backward reaction to be 2 one gets:

$$\frac{\partial}{\partial t}\left|k,l\right\rangle = \begin{cases} 0 & l-k=1 \\ 4\left|\tfrac{1}{2}\right\rangle + \left|k-1,l\right\rangle + \left|k,l+1\right\rangle - 6\left|k,l\right\rangle & l-k=2 \\ \left|k-1,l\right\rangle + \left|k,l+1\right\rangle + 2\left|k+1,l\right\rangle + 2\left|k,l-1\right\rangle - 6\left|k,l\right\rangle & \\ & l-k\geq 3, \end{cases} \tag{5.37}$$

where $\left|\frac{1}{2}\right\rangle = \left|k,l\right\rangle\left|_{k-l=1}\right.$ is the product measure with density $\rho = \frac{1}{2}$. This state is stationary which is recovered by the vanishing time derivative for $k-l=1$. The time evolution of the system can be described completely by the movement of the shocks and their dynamics is independent of each other until they meet, then both are annihilated.

Consequently this system is a candidate for the description by free fermions. However, by including the process $A\varnothing A \leftrightharpoons AAA$ we get the model C of the appendix which is the BCRW – only a two–site interaction model. The transformation of the BCRW into a free fermion system is known [91, 131].

As a second example the model J of the appendix is chosen as it is one of the simplest models. Again we define

$$\left|k,l\right\rangle \equiv \left|k,l;\rho,0,\rho\right\rangle, \tag{5.38}$$

and apply the Hamiltonian. The description by the states $\left|k,l\right\rangle$ is only closed if we set the parameter of the model $w=1$ for which $\rho = 1/2$ and some of the rates vanish. One gets

$$\frac{\partial}{\partial t}\left|k,l\right\rangle = \begin{cases} 0 & l-k=1 \\ 4\left|\tfrac{1}{2}\right\rangle + \left|k-1,l\right\rangle + \left|k,l+1\right\rangle - 6\left|k,l\right\rangle & l-k=2 \\ \left|k-1,l\right\rangle + \left|k,l+1\right\rangle + 2\left|k+1,l\right\rangle + 2\left|k,l-1\right\rangle - 6\left|k,l\right\rangle & \\ & l-k\geq 3, \end{cases} \tag{5.39}$$

Next the time evolution of a state

$$\left|k,l\right\rangle \equiv \left|k,l;0,\frac{1}{2},0\right\rangle \tag{5.40}$$

is investigated.

We find

$$\frac{\partial}{\partial t}|k,l\rangle = \begin{cases} 0 & l-k=1 \\ |k+1,l\rangle + |k,l-1\rangle + 2\,|k-1,l\rangle + 2\,|k,l+1\rangle - 6\,|k,l\rangle & \\ & l-k\geq 3. \end{cases} \tag{5.41}$$

For $k-l=2$ it turns out that the time evolution of this state cannot be described by a superposition of shock measures, i.e. additional correlations emerge. Thus no independent movement of the shock fronts is possible in this case. This suggests that this is not a free fermion model.

5.6 Conclusions

In this chapter we have investigated exact diffusive shock measures in one–dimensional reaction diffusion systems with next nearest neighbor interactions and open boundaries. We distinguish the following three cases:

1. The connection of two non–fluctuating phases, the two densities are 0 and 1. The conditions that both states are stable exclude many models and we find many next nearest neighbor models as solution generalizing the Glauber Ising model at zero temperature.

We restricted ourselves to the case of completely ordered connected phases as initial conditions. It would be interesting to investigate how a system evolves out of random initial conditions. In this scenario coarsening of the ordered domains or the emergence of a third stationary state which is fluctuating is possible.

2. The connection of two fluctuating phases, both densities are between 0 and 1. It is argued that in general non–conservative models cannot have two fluctuating product measures as solution, in agreement with the positive rates conjecture. Consequently only conservative models have to be investigated and we recover the ASEP as the most general solution. Hence, the inclusion of three–site interactions does not lead to models not known from the investigation of nearest neighbor interactions.

3. The connection of a non–fluctuating phase to a fluctuating phase, one density 0 or 1 and one between 0 and 1. In this case numerous models exist and we classify the systems with respect to their symmetry. There is only one model which is $C \wedge P \wedge T$ invariant, and this is as well the only model which is $C \wedge P$ invariant. Two additional models are found that are $C \wedge T$ invariant and 14 models are found that are $P \wedge T$ invariant.

We stress that the mechanisms of exact shock measures are *not* suitable to construct a (one–species) model which shows phase separation on a

ring. On the one hand, although models with one fluctuating phase and one non–fluctuating phase allow for stable up– and downward–shocks, the non–fluctuating phase will always vanish on a ring because the two shock fronts always enlarge the active region. On the other hand conservative models, which in principle allow for shocks between two fluctuating phases, are unable to show both up– and downward–shocks. This is a consequence of the collective velocity $v_c(\rho)$ which describes the movement of the center of mass of a disturbance in a region of a certain density ρ. In order that a shock is stable a disturbance has to tend toward the shock, $v_c(\rho_1) > v_s > v_c(\rho_2)$, where v_s is the shock velocity. Obviously this equation can only hold either for the upward– or the downward–shock. Note that this consideration only holds for short–ranged, homogeneous one–species models, it is known that phase separation is possible in models with defects [145] or several species of particles [96, 102].

Although it is shown that double shocks $0|\rho|0$ are possible we argue that this cannot be used to construct models which show phase separation in one–dimensional, short–ranged periodic systems with a single species.

We have also investigated the influence of shock fronts on each other. A case of special interest is when the fronts move independently, except for the possibility of mutual annihilation. In the $C \wedge P \wedge T$ model this cannot be observed, it turns out that it has to be combined with an additional process violating C symmetry. But by this the BCRW which is a two–site interaction model is recovered for which the independence of shock fronts is known.

We conclude that there is no direct connection of models whose time evolution is given by exact diffusive shock measures and free fermion systems.

5.7 Appendix: $P \wedge T$ models

The 14 $P \wedge T$ models are:

Model A:

$$\begin{aligned} A\varnothing A &\xrightarrow{\omega_a} AAA; \qquad AAA \xrightarrow{\omega_d} A\varnothing A \\ \rho &= \frac{\omega_a}{\omega_a + \omega_d}; \delta_1 = \delta_2 = \delta_3 = \delta_4 = 0 \end{aligned} \tag{5.42}$$

The shock position is fixed without fluctuations in this model, but the model is not ergodic.

Model B:

$$\begin{aligned} A\varnothing &\xrightarrow{1} \varnothing A; \qquad \varnothing A \xrightarrow{1} A\varnothing; \\ \varnothing\varnothing A &\xrightarrow{\omega} \varnothing AA; \qquad \varnothing AA \xrightarrow{1} \varnothing\varnothing A; \\ A\varnothing\varnothing &\xrightarrow{\omega} AA\varnothing; \qquad AA\varnothing \xrightarrow{1} A\varnothing\varnothing; \\ \rho_2 = \frac{\omega}{\omega+1}; &\qquad \delta_1 = \delta_4 = 0; \qquad \delta_2 = \frac{1}{1-\rho_2}; \qquad \delta_3 = 1 \end{aligned} \tag{5.43}$$

In the case $\omega = 1$ this model is C–invariant and we recover the $C \wedge P \wedge T$ model.

Model C:

$$\begin{aligned} A\varnothing &\xrightarrow{1} \varnothing A; \qquad \varnothing A \xrightarrow{1} A\varnothing \\ A\varnothing &\xrightarrow{\omega} AA; \qquad \varnothing A \xrightarrow{\omega} AA; \\ AA &\xrightarrow{1} A\varnothing; \qquad AA \xrightarrow{1} \varnothing A; \\ \rho_2 = \frac{\omega}{\omega+1}; &\qquad \delta_1 = \delta_4 = 0; \qquad \delta_2 = \frac{1}{1-\rho_2}; \qquad \delta_3 = 1; \end{aligned} \tag{5.44}$$

This model is a purely two–site interaction model and known as the branching coalescing random walk. It can be obtained by combining model A and B.

Model D:

$$\begin{aligned} \varnothing\varnothing A &\xrightarrow{1} \varnothing A\varnothing; \qquad A\varnothing\varnothing \xrightarrow{1} \varnothing A\varnothing; \\ \varnothing A\varnothing &\xrightarrow{1} \varnothing\varnothing A; \qquad \varnothing A\varnothing \xrightarrow{1} A\varnothing\varnothing; \\ \varnothing\varnothing A &\xrightarrow{\alpha\omega} \varnothing AA; \qquad \varnothing AA \xrightarrow{\alpha} \varnothing\varnothing A; \\ A\varnothing\varnothing &\xrightarrow{\alpha\omega} AA\varnothing; \qquad AA\varnothing \xrightarrow{\alpha} A\varnothing\varnothing; \\ \varnothing A\varnothing &\xrightarrow{\omega} A\varnothing A; \qquad A\varnothing A \xrightarrow{1} \varnothing A\varnothing; \\ \varnothing AA &\xrightarrow{\frac{1}{1-\omega}} AA\varnothing; \qquad AA\varnothing \xrightarrow{\frac{1}{1-\omega}} \varnothing AA; \\ \varnothing A\varnothing &\xrightarrow{\frac{\omega^2}{1-\omega}} AAA; \qquad AAA \xrightarrow{\frac{1}{1-\omega}} \varnothing A\varnothing; \\ \alpha = \frac{(1-2\,\omega)}{1-\omega}; &\qquad \omega \leq \frac{1}{2} \\ \rho_2 = \frac{\omega}{\omega+1}; &\qquad \delta_1 = \delta_4 = 0; \qquad \delta_2 = \frac{2}{1-\rho_2}; \qquad \delta_3 = 2 \end{aligned} \tag{5.45}$$

For $\omega = \frac{1}{2}$ we get $\alpha = 0$ and some of the rates vanish.

Model E:

$$\begin{aligned}
\varnothing\varnothing A &\xrightarrow{1} \varnothing A\varnothing; & A\varnothing\varnothing &\xrightarrow{1} \varnothing A\varnothing;\\
\varnothing A\varnothing &\xrightarrow{1} \varnothing\varnothing A; & \varnothing A\varnothing &\xrightarrow{1} A\varnothing\varnothing;\\
\varnothing\varnothing A &\xrightarrow{\omega} \varnothing AA; & \varnothing AA &\xrightarrow{1} \varnothing\varnothing A;\\
A\varnothing\varnothing &\xrightarrow{\omega} AA\varnothing; & AA\varnothing &\xrightarrow{1} A\varnothing\varnothing;\\
\varnothing A\varnothing &\xrightarrow{\omega} A\varnothing A; & A\varnothing A &\xrightarrow{1} \varnothing A\varnothing;\\
\varnothing AA &\xrightarrow{1} AA\varnothing; & AA\varnothing &\xrightarrow{1} \varnothing AA;\\
\varnothing AA &\xrightarrow{\omega} AAA; & AA\varnothing &\xrightarrow{\omega} AAA;\\
AAA &\xrightarrow{1} \varnothing AA; & AAA &\xrightarrow{1} AA\varnothing;\\
\rho_2 = \frac{\omega}{\omega+1}; \qquad \delta_1 = \delta_4 = 0; & \qquad \delta_2 = \frac{2}{1-\rho_2}; & \qquad \delta_3 = 2
\end{aligned} \tag{5.46}$$

Model F:

$$\begin{aligned}
\varnothing\varnothing A &\xrightarrow{1} \varnothing A\varnothing; & A\varnothing\varnothing &\xrightarrow{1} \varnothing A\varnothing;\\
\varnothing A\varnothing &\xrightarrow{1} \varnothing\varnothing A; & \varnothing A\varnothing &\xrightarrow{1} A\varnothing\varnothing;\\
\varnothing A\varnothing &\xrightarrow{\omega(1-2\omega)} \varnothing AA; & \varnothing A\varnothing &\xrightarrow{\omega(1-2\omega)} AA\varnothing;\\
\varnothing AA &\xrightarrow{1-2\omega} \varnothing A\varnothing; & AA\varnothing &\xrightarrow{\frac{1-2\omega}{\omega^2}} \varnothing A\varnothing;\\
\varnothing A\varnothing &\xrightarrow{\omega} A\varnothing A; & A\varnothing A &\xrightarrow{1} \varnothing A\varnothing;\\
\varnothing AA &\xrightarrow{2\omega+1} AA\varnothing; & AA\varnothing &\xrightarrow{2\omega+1} \varnothing AA;\\
\varnothing A\varnothing &\xrightarrow{2\omega^2} AAA; & AAA &\xrightarrow{2} \varnothing A\varnothing;\\
& \omega \le \frac{1}{2};\\
\rho_2 = \frac{\omega}{\omega+1}; \qquad \delta_1 = \delta_4 = 0; & \qquad \delta_2 = \frac{2}{1-\rho_2}; & \qquad \delta_3 = 2
\end{aligned} \tag{5.47}$$

For $\omega = \frac{1}{2}$ some rates vanish.

Model G:

$$\begin{aligned}
\varnothing\varnothing A &\xrightarrow{1} \varnothing A\varnothing; & A\varnothing\varnothing &\xrightarrow{1} \varnothing A\varnothing;\\
\varnothing A\varnothing &\xrightarrow{1} \varnothing\varnothing A; & \varnothing A\varnothing &\xrightarrow{1} A\varnothing\varnothing;\\
\varnothing A\varnothing &\xrightarrow{\omega} \varnothing AA; & \varnothing A\varnothing &\xrightarrow{\omega} AA\varnothing;\\
\varnothing AA &\xrightarrow{1} \varnothing\varnothing A; & AA\varnothing &\xrightarrow{1} \varnothing A\varnothing;\\
\varnothing A\varnothing &\xrightarrow{\omega} A\varnothing A; & A\varnothing A &\xrightarrow{1} \varnothing A\varnothing;\\
\varnothing AA &\xrightarrow{1} AA\varnothing; & AA\varnothing &\xrightarrow{1} \varnothing AA;\\
\varnothing AA &\xrightarrow{2\omega} AAA; & AA\varnothing &\xrightarrow{2\omega} AAA;\\
AAA &\xrightarrow{2} \varnothing AA; & AAA &\xrightarrow{2} AA\varnothing;\\
\rho_2 = \frac{\omega}{\omega+1}; \qquad \delta_1 = \delta_4 = 0; & \qquad \delta_2 = \frac{2}{1-\rho_2}; & \qquad \delta_3 = 2
\end{aligned} \tag{5.48}$$

Model H:

$$\begin{aligned}
\varnothing\varnothing A &\xrightarrow{1} \varnothing A\varnothing; & A\varnothing\varnothing &\xrightarrow{1} \varnothing A\varnothing;\\
\varnothing A\varnothing &\xrightarrow{1} \varnothing\varnothing A; & \varnothing A\varnothing &\xrightarrow{1} A\varnothing\varnothing;\\
\varnothing A\varnothing &\xrightarrow{2\omega(1-\omega)} \varnothing AA; & \varnothing A\varnothing &\xrightarrow{2\omega(1-\omega)} AA\varnothing;\\
\varnothing AA &\xrightarrow{2(1-\omega)} \varnothing A\varnothing; & AA\varnothing &\xrightarrow{2(1-\omega)} \varnothing A\varnothing;\\
\varnothing AA &\xrightarrow{1} A\varnothing A; & A\varnothing A &\xrightarrow{1} \varnothing AA;\\
A\varnothing A &\xrightarrow{1} AA\varnothing; & \varnothing AA &\xrightarrow{1} A\varnothing A;\\
\varnothing AA &\xrightarrow{2\omega} AA\varnothing; & AA\varnothing &\xrightarrow{2\omega} \varnothing AA;\\
\varnothing A\varnothing &\xrightarrow{2\omega^2} AAA; & AAA &\xrightarrow{2} \varnothing A\varnothing;\\
\omega \le 1;&\\
\rho_2 = \frac{\omega}{\omega+1}; \qquad \delta_1 = \delta_4 = 0; & \qquad \delta_2 = \frac{2}{1-\rho_2}; & \qquad \delta_3 = 2
\end{aligned} \tag{5.49}$$

For $\omega = 1$ some of the rates vanish.

Model I:

$$\begin{aligned}
\varnothing\varnothing A &\xrightarrow{1} \varnothing A\varnothing; & A\varnothing\varnothing &\xrightarrow{1} \varnothing A\varnothing;\\
\varnothing A\varnothing &\xrightarrow{1} \varnothing\varnothing A; & \varnothing A\varnothing &\xrightarrow{1} A\varnothing\varnothing;\\
\varnothing A\varnothing &\xrightarrow{\omega} A\varnothing A; & A\varnothing A &\xrightarrow{1} \varnothing A\varnothing;\\
\varnothing AA &\xrightarrow{2} AA\varnothing; & AA\varnothing &\xrightarrow{2} \varnothing AA;\\
\varnothing A\varnothing &\xrightarrow{\omega} AAA; & AAA &\xrightarrow{\frac{1}{\omega}} \varnothing A\varnothing;\\
\varnothing AA &\xrightarrow{\omega(2-\omega)} AAA; & AA\varnothing &\xrightarrow{\omega(2-\omega)} AAA;\\
AAA &\xrightarrow{2-\omega} \varnothing AA; & AAA &\xrightarrow{2-\omega} AA\varnothing;\\
&& \omega &\leq 2;\\
\rho_2 = \frac{\omega}{\omega+1}; \qquad \delta_1 = \delta_4 = 0; & \qquad \delta_2 = \frac{2}{1-\rho_2}; & \qquad \delta_3 = 2
\end{aligned} \tag{5.50}$$

For $\omega = 2$ some of the rates vanish.

Model J:

$$\begin{aligned}
A\varnothing &\xrightarrow{1} \varnothing A; & \varnothing A &\xrightarrow{1} A\varnothing;\\
\varnothing AA &\xrightarrow{1} AA\varnothing; & AA\varnothing &\xrightarrow{1} \varnothing AA;\\
\varnothing A\varnothing &\xrightarrow{\omega} AAA; & AAA &\xrightarrow{\frac{1}{\omega}} \varnothing A\varnothing;\\
\varnothing AA &\xrightarrow{\omega-1} AAA; & AA\varnothing &\xrightarrow{\omega-1} AAA;\\
AAA &\xrightarrow{\frac{\omega-1}{\omega}} \varnothing AA; & AAA &\xrightarrow{\frac{\omega-1}{\omega}} AA\varnothing;\\
&& \omega &\geq 1;\\
\rho_2 = \frac{\omega}{\omega+1}; \qquad \delta_1 = \delta_4 = 0; & \qquad \delta_2 = \frac{1}{1-\rho_2}; & \qquad \delta_3 = 1
\end{aligned} \tag{5.51}$$

For $\omega = 1$ some of the rates vanish.

Model K:

$$\begin{array}{ll}
\varnothing\varnothing A \xrightarrow{1} \varnothing AA; & \varnothing AA \xrightarrow{1} \varnothing\varnothing A; \\
A\varnothing\varnothing \xrightarrow{1} AA\varnothing; & AA\varnothing \xrightarrow{1} A\varnothing\varnothing; \\
\varnothing\varnothing A \xrightarrow{1} A\varnothing\varnothing; & A\varnothing\varnothing \xrightarrow{1} \varnothing\varnothing A; \\
\varnothing\varnothing A \xrightarrow{1} A\varnothing A; & A\varnothing\varnothing \xrightarrow{1} A\varnothing A; \\
A\varnothing A \xrightarrow{1} \varnothing\varnothing A; & A\varnothing A \xrightarrow{1} A\varnothing\varnothing; \\
\varnothing\varnothing A \xrightarrow{1} AA\varnothing; & \varnothing AA \xrightarrow{1} A\varnothing\varnothing; \\
A\varnothing\varnothing \xrightarrow{1} \varnothing AA; & AA\varnothing \xrightarrow{1} \varnothing AA; \\
\varnothing\varnothing A \xrightarrow{1} AAA; & A\varnothing\varnothing \xrightarrow{1} AAA; \\
AAA \xrightarrow{1} \varnothing\varnothing A; & AAA \xrightarrow{1} A\varnothing\varnothing; \\
\varnothing A\varnothing \xrightarrow{1} A\varnothing A; & A\varnothing A \xrightarrow{1} \varnothing A\varnothing;
\end{array} \tag{5.52}$$

$$\rho_2 = \frac{1}{2}; \qquad \delta_1 = 4; \qquad \delta_2 = 2; \qquad \delta_3 = 1; \qquad \delta_4 = 1$$

Model L:

$$\begin{array}{ll}
\varnothing\varnothing A \xrightarrow{1} A\varnothing\varnothing; & A\varnothing\varnothing \xrightarrow{1} \varnothing\varnothing A; \\
\varnothing\varnothing A \xrightarrow{1} A\varnothing A; & A\varnothing\varnothing \xrightarrow{1} A\varnothing A; \\
A\varnothing A \xrightarrow{1} \varnothing\varnothing A; & A\varnothing A \xrightarrow{1} A\varnothing\varnothing; \\
\varnothing\varnothing A \xrightarrow{1} AA\varnothing; & \varnothing AA \xrightarrow{1} A\varnothing\varnothing; \\
A\varnothing\varnothing \xrightarrow{1} \varnothing AA; & AA\varnothing \xrightarrow{1} \varnothing AA; \\
\varnothing\varnothing A \xrightarrow{1} AAA; & A\varnothing\varnothing \xrightarrow{1} AAA; \\
AAA \xrightarrow{1} \varnothing\varnothing A; & AAA \xrightarrow{1} A\varnothing\varnothing; \\
\varnothing A\varnothing \xrightarrow{1} \varnothing AA; & \varnothing A\varnothing \xrightarrow{1} AA\varnothing; \\
\varnothing AA \xrightarrow{1} \varnothing A\varnothing; & AA\varnothing \xrightarrow{1} \varnothing A\varnothing; \\
\varnothing A\varnothing \xrightarrow{1} A\varnothing A; & A\varnothing A \xrightarrow{1} \varnothing A\varnothing; \\
\varnothing AA \xrightarrow{1} AAA; & AA\varnothing \xrightarrow{1} AAA; \\
AAA \xrightarrow{1} \varnothing AA; & AAA \xrightarrow{1} AA\varnothing;
\end{array} \tag{5.53}$$

$$\rho_2 = \frac{1}{2}; \qquad \delta_1 = 4; \qquad \delta_2 = 2; \qquad \delta_3 = 1; \qquad \delta_4 = 1$$

Model M:

$$
\begin{aligned}
&\varnothing\varnothing A \xrightarrow{1} A\varnothing\varnothing; \qquad A\varnothing\varnothing \xrightarrow{1} \varnothing\varnothing A;\\
&\varnothing\varnothing A \xrightarrow{1} A\varnothing A; \qquad A\varnothing\varnothing \xrightarrow{1} A\varnothing A;\\
&A\varnothing A \xrightarrow{1} \varnothing\varnothing A; \qquad A\varnothing A \xrightarrow{1} A\varnothing\varnothing;\\
&\varnothing\varnothing A \xrightarrow{1} AA\varnothing; \qquad \varnothing AA \xrightarrow{1} A\varnothing\varnothing;\\
&A\varnothing\varnothing \xrightarrow{1} \varnothing AA; \qquad AA\varnothing \xrightarrow{1} \varnothing AA;\\
&\varnothing\varnothing A \xrightarrow{1} AAA; \qquad A\varnothing\varnothing \xrightarrow{1} AAA;\\
&AAA \xrightarrow{1} \varnothing\varnothing A; \qquad AAA \xrightarrow{1} A\varnothing\varnothing;\\
&\varnothing A\varnothing \xrightarrow{1} \varnothing AA; \qquad \varnothing A\varnothing \xrightarrow{1} AA\varnothing;\\
&\varnothing AA \xrightarrow{1} \varnothing A\varnothing; \qquad AA\varnothing \xrightarrow{1} \varnothing A\varnothing;\\
&\varnothing AA \xrightarrow{1} \varnothing AA; \qquad \varnothing A\varnothing \xrightarrow{1} AA\varnothing;\\
&\varnothing AA \xrightarrow{1} \varnothing\varnothing A; \qquad AAA \xrightarrow{1} \varnothing A\varnothing;\\
&\varnothing A\varnothing \xrightarrow{1} AAA; \qquad AAA \xrightarrow{1} \varnothing A\varnothing;\\
\rho_2 = \frac{1}{2}; \qquad &\delta_1 = 4; \qquad \delta_2 = 2; \qquad \delta_3 = 1; \qquad \delta_4 = 1
\end{aligned}
\tag{5.54}
$$

Model N:

$$
\begin{aligned}
&\varnothing\varnothing A \xrightarrow{1} A\varnothing\varnothing; \qquad A\varnothing\varnothing \xrightarrow{1} \varnothing\varnothing A;\\
&\varnothing\varnothing A \xrightarrow{1} A\varnothing A; \qquad A\varnothing\varnothing \xrightarrow{1} A\varnothing A;\\
&A\varnothing A \xrightarrow{1} \varnothing\varnothing A; \qquad A\varnothing A \xrightarrow{1} A\varnothing\varnothing;\\
&\varnothing\varnothing A \xrightarrow{1} AA\varnothing; \qquad \varnothing AA \xrightarrow{1} A\varnothing\varnothing;\\
&A\varnothing\varnothing \xrightarrow{1} \varnothing AA; \qquad AA\varnothing \xrightarrow{1} \varnothing AA;\\
&\varnothing\varnothing A \xrightarrow{1} AAA; \qquad A\varnothing\varnothing \xrightarrow{1} AAA;\\
&AAA \xrightarrow{1} \varnothing\varnothing A; \qquad AAA \xrightarrow{1} A\varnothing\varnothing;\\
&\varnothing A\varnothing \xrightarrow{1} A\varnothing A; \qquad A\varnothing A \xrightarrow{1} \varnothing A\varnothing;\\
&\varnothing AA \xrightarrow{1} AA\varnothing; \qquad AA\varnothing \xrightarrow{1} \varnothing AA;\\
&\varnothing A\varnothing \xrightarrow{1} AAA; \qquad AAA \xrightarrow{1} \varnothing A\varnothing;\\
\rho_2 = \frac{1}{2}; \qquad &\delta_1 = 4; \qquad \delta_2 = 2; \qquad \delta_3 = 1; \qquad \delta_4 = 1
\end{aligned}
\tag{5.55}
$$

Bibliography

[1] M. Paessens and M. Henkel. *J. Phys.*, A36:8983, 2003.

[2] M. Henkel, M. Paessens, and M. Pleimling. *Europhys. Lett.*, 62:664, 2003.

[3] M. Henkel, M. Paessens, and M. Pleimling. *Phys. Rev.*, E69:056109, 2004.

[4] M. Paessens and G. M. Schütz. *J. Phys.*, A37:4709, 2004.

[5] A. Rákos, M. Paessens, and G. M. Schütz. *Phys. Rev. Lett.*, 91:0238302, 2003.

[6] L.F. Cugliandolo. *cond-mat*, 0210312, 2002.

[7] A. J. Bray. *Adv. Phys*, 43:357, 1994.

[8] M. E. Cates and M. R. Evans, editors. *Soft and Fragile Matter.* IOP Press, Bristol, 2000.

[9] C. Godrèche and J.M. Luck. *J. Phys. Cond. Matt.*, 14:1589, 2002.

[10] D.S. Fisher and D.A. Huse. *Phys. Rev.*, B38:373, 1988.

[11] D.A. Huse. *Phys. Rev.*, B40:304, 1989.

[12] A. Picone and M. Henkel. *J. Phys.*, A35:5575, 2002.

[13] C. Yeung, M. Rao, and R.C. Desai. *Phys. Rev.*, E53:3073, 1996.

[14] M. Henkel. *Nucl. Phys.*, B641:405, 2002.

[15] M. Henkel, M. Pleimling, C. Godrèche, and J.-M. Luck. *Phys. Rev. Lett.*, 87:265701, 2001.

[16] L.F. Cugliandolo and J. Kurchan. *J. Phys.*, A27:5749, 1994.

[17] L.F. Cugliandolo, J. Kurchan, and G. Parisi. *J. Physique*, I4:1641, 1994.

[18] A. Garriga. *J. Phys. Cond. Matt.*, 14:1581, 2002.

[19] A. Pérez-Madrid, D. Reguera, and J.M. Rubí. *J. Phys. Cond. Matt.*, 14:1651, 2002.

[20] T.S. Grigera and N.E. Israeloff. *Phys. Rev. Lett.*, 83:5038, 1999.

[21] D. Hérisson and M. Ocio. *Phys. Rev. Lett.*, 88:257202, 2002.

[22] L. Bellon and S. Ciliberto. *Physica*, D168-169:352, 2002.

[23] A.J. Bray, K. Humayun, and T.J. Newman. *Phys. Rev.*, B43:3699, 1991.

[24] H.K. Janssen, B. Schaub, and B. Schmittmann. *Z. Phys.*, B73:539, 1989.

[25] T.J. Newman and A.J. Bray. *J. Phys*, A23:4491, 1990.

[26] J.G. Kissner and A.J. Bray. *J. Phys*, A26:1571, 1993.

[27] A. Coniglio, P. Ruggiero, and M. Zanetti. *Phys. Rev.*, E50:1046, 1994.

[28] P. Calabrese and A. Gambassi. *Phys. Rev.*, E65:066120, 2002.

[29] P. Calabrese and A. Gambassi. *Phys. Rev.*, B66:212407, 2002.

[30] P. Calabrese and A. Gambassi. *Phys. Rev.*, E66:066101, 2002.

[31] P. Calabrese and A. Gambassi. *Phys. Rev.*, E67:036111, 2003.

[32] N. Fusco and M. Zannetti. *Phys. Rev.*, E66:066113, 2003.

[33] A. Picone, M. Henkel, and J. Richert. *J. Phys.*, A36:1249, 2003.

[34] L.F. Cugliandolo and D.S. Dean. *J. Phys.*, A28:4213, 1995.

[35] L.F. Cugliandolo and D.S. Dean. *J. Phys.*, A28:L453, 1995.

[36] R. Kühn W. Zippold and H. Horner. *Eur. Phys. J.*, B13:531, 2000.

[37] C. Godrèche and J.M. Luck. *J. Phys.*, A33:9141, 2000.

[38] S.A. Cannas, D.A. Stariolo, and F.A. Tamarit. *Physica*, A294:362, 2001.

[39] F. Corberi, E. Lippiello, and M. Zanetti. *Phys. Rev.*, E65:046136, 2002.

[40] W. Wernsdorfer, K. Hasselbach, A. Benot, B. Barbara, B. Doudin, J. Meier, J.-Ph. Ansermet, and D. Mailly. *Phys. Rev.*, B55:11552, 1997.

[41] S. Mangin, A. Sulpice, G. Marchal, C. Bellouard, W. Wernsdorfer, and B. Barbara. *Phys. Rev.*, B60:1204, 1999.

[42] M.A. Abramowitz and I.A. Stegun. *Handbook of Mathematical Functions*. Dover, New York, 1965.

[43] S. Ludwig and D.D. Osheroff. *Phys. Rev. Lett.*, 91:105501, 2003.

[44] K. Brendel and G.T. Barkema et H. van Beijeren. *Phys. Rev.*, E67:026119, 2002.

[45] S.W. Sides, P.A. Rikvold, and M.A. Notvotny. *Phys. Rev.*, E95:2710, 1999.

[46] G. Korniss, P.A. Rikvold C.J. White, and M.A. Notvotny. *Phys. Rev.*, E63:016120, 2000.

[47] G. Korniss, P.A. Rikvold, and M.A. Notvotny. *Phys. Rev.*, E66:056127, 2002.

[48] A.P. Mehta, A.C. Mills, K. Dahmen, and J.P. Sethna. *Phys. Rev.*, E65:046139, 2002.

[49] A. Chatterjee and B.K. Chakrabarti. *Phys. Rev.*, E67:046113, 2003.

[50] V.R. Vieira V. Turkowski and P.D. Sacramento. *cond-mat*, 0305139, 2003.

[51] M. Saiko N.K. Karapetyants, A.A. Kilbas and S.G. Samko. *J. Integral Equations Appl.*, 12:421, 2000.

[52] A. Buhot and J.P. Garrahan. *Phys. Rev. Lett.*, 88:225702, 2002.

[53] L. Berthier, P.C.W. Holdsworth, and M. Sellitto. *J. Phys.*, A34:1805, 2001.

[54] C. Chatelain. *J. Phys.*, A36:10739, 2003.

[55] G. Baéz, H. Larralde, F. Levyraz, and R.A. Méndez-Sánchez. *Phys. Rev. Lett.*, 90:135701, 2003.

[56] G. Parisi, F. Ricci-Tersenghi, and J.J. Ruiz-Lorenzo. *Eur. Phys. J.*, B11:317, 1999.

[57] F. Corberi, E. Lippiello, and M. Zanetti. *Phys. Rev.*, E68:046131, 2003.

[58] C. Godrèche and J.M. Luck. *J. Phys.*, A33:1151, 2000.

[59] E. Lippiello and M. Zannetti. *Phys. Rev.*, E61:3369, 2000.

[60] L. Berthier, J.L. Barrat, and J. Kurchan. *Eur. Phys. J.*, B11:635, 1999.

[61] F. Corberi, E. Lippiello, and M. Zanetti. *Phys. Rev. Lett.*, 90:099601, 2003.

[62] F. Corberi, E. Lippiello, and M. Zanetti. *Eur. Phys. J.*, B24:359, 2001.

[63] A. Barrat. *Phys. Rev.*, E57:3629, 1998.

[64] M. Henkel and M. Pleimling. *Phys. Rev.*, E68:065101(R), 2003.

[65] R.J. Baxter. *Exactly solved models in statistical mechanics*. Academic Press, London, 1982.

[66] L. Berthier, L.F. Cugliandolo, and J.L. Iguain. *Phys. Rev.*, B63:051302, 2001.

[67] T. Tomé and M.J. de Oliveira. *Phys. Rev.*, A41:4251, 1990.

[68] J.F.F. Mendes and E.J.S. Lage. *J. Stat. Phys.*, 64:653, 1991.

[69] J.P. Sethna, O. Perkovic, and K.A. Dahmen. *cond-mat*, 9704059, 1997.

[70] P.A. Rikvold, G. Brown, S.J. Mitchell, and M.A. Novotny. *Springer Lecture Notes in Physics*, volume 593, chapter Nanostructured Magnetic Materials and their Applications, page 164. Springer, Heidelberg, 2002.

[71] H. Fujisaka, H. Tutu, and P.A. Rikvold. *Phys. Rev.*, E63:036109, 2001.

[72] T. Yasui, H. Tutu, M. Yamamoto, and H. Fujisaka. *Phys. Rev.*, E66:036123, 2002.

[73] T. Yasui, H. Tutu, M. Yamamoto, and H. Fujisaka. *Phys. Rev.*, E67:019901(E), 2003.

[74] M. Rao, H.R. Krishnamurthy, and R. Pandit. *Phys. Rev.*, B42:856, 1990.

[75] D. Dhar and P. Thomas. *J. Phys.*, A25:4967, 1992.

[76] H. Jang and M.J. Grimson. *Phys. Rev.*, E63:06619, 2001.

[77] H. Jang, M.J. Grimson, and C.K. Hall. *Phys. Rev.*, B67:094411, 2003.

[78] H. Jang, M.J. Grimson, and C.K. Hall. *Phys. Rev.*, E68:046115, 2003.

[79] I.R. Pimentel, T. Temesvári, and C. DeDominicis. *Phys. Rev.*, B65:224420, 2002.

[80] W.H. Press, S.A. Teukolsky, W.T. Vetterling, and B.P. Flannery. *Numerical Recipes*. University Press, Cambridge, 2nd edition, 1992.

[81] H. Hinrichsen. *Adv. Phys.*, 49:815, 2000.

[82] E. Carlon, M. Henkel, and U. Schollwöck. *Phys. Rev.*, E63:036101, 2001.

[83] G.T. Barkema and E. Carlon. *Phys. Rev.*, E68:036113, 2003.

[84] G. Ódor. *Phys. Rev.*, E67:016111, 2003.

[85] J. Kockelkoren and H. Chaté. *Phys. Rev. Lett.*, 90:125701, 2003.

[86] G. Ódor. *Phys. Rev.*, E62:R3027, 2000.

[87] M. Henkel and H. Hinrichsen. *cond-mat*, 0402433, 2004.

[88] M.J. Howard and U.C. Täuber. *J. Phys.*, A30:7721, 1997.

[89] M. Doi. *J. Phys.*, A9:1465, 1976.

[90] S. Trimper, U.C. Täuber, and G.M. Schütz. *Phys. Rev.*, E62:6071, 2000.

[91] G. M. Schütz. *C. Domb and J. Lebowitz: Phase Transitions and Critical Phenomena*, volume 19, chapter 1, pages 1–251. Academic, London, 2001.

[92] B. Houchmandzadeh. *Phys. Rev.*, E66:052902, 2002.

[93] W.R. Young, A.J. Roberts, and G. Stuhne. *Nature*, 412:328, 2001.

[94] *Table of Integrals, Series, and Products*. Academic, 1980.

[95] M. R. Evans, D. P. Foster, C. Godrèche, and D. Mukamel. *J. Stat. Phys.*, 80:69, 1995.

[96] M. R. Evans, Y. Kafri, H. M. Koduvely, and D. Mukamel. *Phys. Rev. Lett.*, 80:425, 1998.

[97] P. F. Arndt, T. Heinzel, and V. Rittenberg. *J. Phys.*, A31:L45, 1998.

[98] O. M. Braun, B. Hu, A. Filippov, and A. Zeltser. *Phys. Rev.*, E58:1311, 2002.

[99] R. Barlovic, L. Santen, A. Schadschneider, and M. Schreckenberg. *Eur. Phys. J.*, 5:793, 1998.

[100] Y. Kafri, E. Levine, D. Mukamel, G. M. Schütz, and J. Török. *Phys. Rev. Lett.*, 89:035702, 2002.

[101] D. Helbing, D. Mukamel, and G. M. Schütz. *Phys. Rev. Lett.*, 82:10, 1999.

[102] Y. Kafri, E. Levine, D. Mukamel, G. M. Schütz, and R.D. Willmann. *Phys. Rev.*, E68:035101(R), 2003.

[103] N. Rajewsky, T. Sasamoto, and E. Speer. *Physica*, A279:123, 2000.

[104] T. Sasamoto and D. Zagier. *J. Phys.*, A34:5033, 2001.

[105] G.M. Schütz. *J. Phys.*, A36:R339, 2003.

[106] C. T. MacDonald, J. H. Gibbs, and A. C. Pipkin. *Biopolymers*, 6:1, 1968.

[107] E. Carlon, A. Drzewinski, and J.M.J. van Leeuwen. *Phys. Rev.*, E64:010801, 2002.

[108] M. Paessens and G. M. Schütz. *Phys. Rev.*, E66:012806, 2002.

[109] A. Parmeggiani, T. Franosch, and E. Frey. *Phys. Rev. Lett.*, 90:086601, 2003.

[110] R. D. Willmann, G. M. Schütz, and D. Challet. *Physica*, A316:430, 2002.

[111] R.D. Willmann. *PhD Thesis*. Bonn, 2004.

[112] V. Popkov, A. Rákos, R. D. Willmann, A. B. Kolomeisky, and G. M. Schütz. *Phys. Rev.*, E67:066117, 2003.

[113] M. R. Evans, R. Juhász, and L. Santen. *Phys. Rev.*, E68:026117, 2003.

[114] J.S. Hager, J. Krug, V. Popkov, and G.M. Schütz. *Phys. Rev.*, E63:053110, 2001.

[115] K. Binder, M. Paczuski, and M. Barma. *Phys. Rev.*, E49:1174, 1994.

[116] V. Popkov and G. M. Schütz. *Europhys. Lett.*, 48:257, 1999.

[117] A. Kolomeisky, G. M. Schütz, E. B. Kolomeisky, and J. P. Straley. *J. Phys.*, A31:6911, 1998.

[118] K. P. N. Murthy and K. W. Kehr. *Phys. Rev.*, A40:2082, 1989.

[119] P. A. Ferrari, C. Kipnis, and E. Saada. *Ann. Prob.*, 19:226, 1991.

[120] E.D. Andjel, M. Bramson, and T.M. Ligget. *Prob. Theory Rel. Fields*, 78:231, 1988.

[121] M.E.J. Newman and G.T. Barkema. *Monte Carlo methods in statistical physics*. Clarendon Press, Oxford, 1999.

[122] M.C. Cross and P.C. Hohenberg. *Rev. Mod. Phys.*, 65:851, 1994.

[123] R. Welch and D. Kaiser. *PNAS*, 26:14907, 2001.

[124] V. Hunyadi, Z. Rácz, and L. Sasvári. *Phys. Rev.*, E69:066103, 2004.

[125] V. Popkov and M. Salerno. *Phys. Rev.*, B62:352, 2000.

[126] R.A. Fisher. *Ann. Eugen.*, 7:355, 1937.

[127] J.M. Burgers. *The Non Linear Diffusion Equation*. Reidel, Boston, 1974.

[128] D. ben Avraham. *Phys. Lett.*, A247:53, 1998.

[129] C. Pigorsch and G.M. Schütz. *J. Phys.*, A33:7919, 2000.

[130] V. Belitsky and G.M. Schütz. *El. J. Prob.*, 7:11, 2002.

[131] K. Krebs, F.H. Jafapour, and G. M. Schütz. *New Journal of Physics*, 5:145.1, 2003.

[132] G.M. Schütz. *J. Stat. Phys.*, 79:243, 1995.

[133] M. Alimohammadi, M. Khorrami, and A. Aghamohammadi. *Phys. Rev.*, E64:056116, 2001.

[134] M. Mobilia and P.A. Bares. *Phys. Rev.*, E64:045101(R), 2001.

[135] M. Balázs. *J. Stat. Phys.*, 105:511, 2001.

[136] M. Balázs. *math.PR*, page 0401053, 2004.

[137] M. Khorrami, A. Aghamohammadi, and M. Alimohammadi. *J. Phys.*, A36:345, 2003.

[138] M. Henkel and H. Hinrichsen. *J. Phys.*, A34:1561, 2001.

[139] L.F. Gray. *J. Stat. Phys.*, 103:1, 2001.

[140] P. Gacs. *J. Stat. Phys.*, 103:45, 2001.

[141] J.A. Cuesta and A. Sánchez. *cond-mat*, page 0306354, 2003.

[142] N.G. van Kampen. *Stochastic processes in physics and chemistry*. Elsevier, Amsterdam, 2001.

[143] T. Antal and G.M. Schütz. *Phys. Rev.*, E62:83, 2000.

[144] P. Jordan and E. Wigner. *Z. Phys.*, 47:631, 1928.

[145] K. Mallik. *J. Phys.*, A29:5375, 1996.

Acknowledgements

I would like to express my gratitude to Gunter M. Schütz for the supervision of this thesis – he introduced me into the topic, gave many useful suggestions and was open to discussions.
Ulf-G. Meißner is thanked for taking the part of the second referee.

Malte Henkel is acknowledged for warm hospitality at the Université Henri Poincaré, Nancy where I could spend six nice and productive months during which he took the rôle of the supervisor.

I thank the whole group "Theory II" for help and companionship.
In particular Attila Rákos is acknowledged for countless valuable discussions.
Helga Paffen is thanked for administrative support, the good coffee during the morning chats which helped considerably to get the days started.

Richard Willmann is acknowledged for listening to all those unready ideas (not all of them where concerning science) running through my mind and for a pleasant atmosphere in our office.

Stefanie Pfaff supported me mentally; without her patience and sympathy I would not have been able to concentrate on the work to this extend – thank you so much!

I am deeply grateful to my parents, Margret and Willi Paeßens, who not only raised my interest in science but also provided support in every way.

Summary / Zusammenfassung

Summary

In this work non–equilibrium phenomena in statistical models with more than nearest neighbor interactions are examined. The investigated models belong to three different types of non–equilibrium, i.e. systems undergoing aging, absorbing phase transitions and systems being intrinsically out of equilibrium.

The behavior of the mean spherical model after a temperature quench from the disordered phase into the ordered phase in an external magnetic field is calculated. For a sufficiently small external field, the kinetics of the magnetization reversal transition from the metastable to the ground state is comparable to the aging behavior in the case without external field. For an oscillating external magnetic field the absence of a dynamic phase transition is demonstrated.

The bosonic pair contact process with diffusion shows unusual behavior of the second moment of the probability distribution for which a phase transition from a constant asymptotic value to exponential divergence is found. The control parameter of this transition is the ratio of reaction and diffusion rates which gives insight into the role of diffusion in this process. The divergence of the second moment can lead to a negative correlation time while the correlation length is positive.

Coupling conservative diffusion system to reaction dynamics leads to interesting behavior if the rates are tuned adequately. The general conditions for ergodicity breaking in those systems are derived and an example is constructed. For this example hysteresis is demonstrated. The behavior, including the exact steady state phase diagram, of this non–equilibrium many particle system is well described by an effective equilibrium one–particle problem.

The motion of domain walls in reaction diffusion systems is investigated for three site interactions. A variety of models is found and they show phenomena like double shocks or additional symmetries not possible for two–site interaction models. While the two–site interaction models leading to exact shock measures are connected by the transformability to free fermion systems, this is not valid for the three site interaction models.

Zusammenfassung

Diese Arbeit behandelt Nichtgleichgewichts–Phänomene in statistischen Modellen mit Wechselwirkungen die über nächste Nachbarn hinaus gehen. Die betrachteten Modelle basieren auf verschiedenen Arten des Nichtgleichgewichts – Alterung, absorbierende Phasenübergänge und Systeme, die sich nach Konstruktion außerhalb des Gleichgewichts befinden.

Das Verhalten des Sphärischen Modelles, nachdem es von der ungeordneten Phase in die geordnete Phase abgeschreckt wurde, wird für den Fall eines externen Magnetfeldes berechnet. Für ausreichend kleine Felder ist die Dynamik der Magnetisierungsumkehrung von dem metastabilen in den stabilen Grundzustand vergleichbar zu dem Alterungsverhalten bei Abwesenheit des Feldes. Für ein oszillierendes externes Magnetfeld wird die Abwesenheit eines dynamischen Phasenübergangs gezeigt.

Der bosonische Paarkontaktprozess mit Diffusion zeigt ungewöhnliches Verhalten für das zweite Moment der Wahrscheinlichkeitsverteilung, für welches ein Phasenübergang zwischen konstantem asymptotischen Verhalten zu exponentieller Divergenz gefunden wird. Der Kontrollparameter dieses Übergangs ist das Verhältnis von Reaktions- zu Diffusionsraten. Dies liefert Einblick in die Rolle der Diffusion bei diesem Prozess. Die Divergenz des zweiten Momentes weist auf eine negative Korrelationszeit hin, während die Korrelationslänge positiv ist.

Interessantes Verhalten kann beobachtet werden, wenn konservative Diffusionssysteme an Reaktionsdynamiken mit adäquaten Raten gekoppelt werden. Die allgemeinen Bedingungen unter denen Ergodizitätsbrechung zu erwarten ist, werden für solche Systeme hergeleitet und ein Beispiel hierfür konstruiert. Für dieses Beispiel wird Hysterese demonstriert. Das Verhalten dieses Nichtgleichgewichts–Vielkörperproblem kann durch ein effektives Gleichgewichts–Einteilchenproblem beschrieben werden, dieses Bild liefert auch das exakte Phasendiagramm.

Die Bewegung von Domänengrenzen in Reaktions–Diffusions–Systemen mit Dreipunktwechselwirkung wird untersucht. Eine Reihe von Modellen wird gefunden; diese zeigen Phänomene, die nicht für Zweipunktwechselwirkungen möglich sind, wie zum Beispiel Doppelschocks oder zusätzliche Symmetrien. Während die Zweipunktwechselwirkungsmodelle, die zu exakten Schockmaßen führen, gemeinsam haben, dass sie sich in Freie–Fermion–Modelle transformieren lassen, gilt dieses nicht im Falle der Dreipunktwechselwirkung.